NTNU – Trondheim
Norwegian University of
Science and Technology

Residual Gas Mobility in Ormen Lange

Elisabeth Undeland

Petroleum Engineering
Submission date: May 2012
Supervisor: Jon Kleppe, IPT

Norwegian University of Science and Technology
Department of Petroleum Engineering and Applied Geophysics

Preface

This report has been prepared as a result of the course TPG4915 Petroleum Engineering – Reservoir Technology, Master Thesis at the Norwegian University of Science and Technology (NTNU), Department of Petroleum Engineering and Applied Geophysics, during the spring of 2012. The Master's thesis is mandatory in the 10th term for all MSc. petroleum-students, and it constitutes 30 out of 30 ECTS (European Credit Transfer System) credits for the spring term. The objective of the master thesis is to give the student the opportunity to specialize within a given subject related to reservoir technology, by gathering knowledge from literature review and combine it with already gained knowledge from previous courses and new knowledge gained through experiments and analysis. It is required to complete the master thesis as an independent project work and prepare a project report in accordance with accepted standards.

This master thesis is a continuance of the report "Physics Residual Gas Mobility" [21] written in the course TPG4535 Reservoir Technology and Petrophysics, Specialization Project in the autumn of 2011. In the project report the topic is introduced and the physics behind residual gas mobility described through a literature review. This Master's thesis will continue the study that was introduced in the project report, focusing on residual gas as a result of aquifer influx in gas-reservoirs. Simulation runs will be conducted on the already existing Ormen Lange Hydrodynamic Aquifer Model to evaluate residual gas mobility and its interaction with the aquifer and other variables. To make the thesis as readable and understandable as possible some of the work done in the project report[21] will be reproduced in this Master's thesis.

The topic of the work is "Mobility of Residual Gas Ormen Lange". The assignment has been prepared in close co-operation between the student, Norske Shell AS and the Department of Petroleum Engineering and Applied Geophysics at NTNU.

I would like to thank my supervisor at NTNU, Jon Kleppe for helpful guidance and contribution. I would also like to thank Reservoir Engineers Arjen Cense, Michael Krassnitzer and Knut Terje Noraberg in X-Border Asset, Norske Shell, for providing me with technical assistance throughout the project. I would direct a special thanks to main supervisor during this project, Reservoir Engineer Gerbert de Bruijn, for his initiative and enthusiasm in preparing this thesis and support in making the final report. I would also like to thank all my other colleagues in Norske Shell for their guidance and support. The same goes to AS Norske Shell, who throughout the winter and spring has provided me with unlimited amount of information and excellent working facilities.

Trondheim, May 2012

Executive Summary

The topic of this report is "Mobility of Residual Gas in Ormen Lange" and it has been prepared as a part of the course TPG4915 Petroleum Engineering - Reservoir Engineering, Master Thesis at the Norwegian University of Science and Technology (NTNU). The work has been performed on Ormen Lange, a natural gas field on the Norwegian continental shelf, operated by A/S Norske Shell.

Substantial volumes of residual gas are present in the Ormen Lange field as a result of the hydrodynamic aquifer flow[9]. Total residual gas volume in 2007 is 80±30 Bcm gas depending on the residual gas saturation, Sgr. Depending on scenario 15±6 Bcm of the residual gas is recovered in 2040, and the recovery factor of residual gas is 15±5%. In general, with increasing residual gas saturation, residual gas volume increases and the recovery factor of the residual gas zones decreases.

The main challenge and purpose of this project has been to understand the physics of residual gas during depletion, and to assess the potential recovery from the residual gas in different parts of the reservoir. A literature study aiming to identify the main driving parameters with respect to residual gas mobility has been conducted and used as a basis for subsequent simulation work.

The need to understand the charge history of the field became important in 2008 when an appraisal well in the northern part of the field encountered only residual gas saturations in the crest of the structure and in the middle of the Direct Hydrocarbon Indicator (DHI). Core analyses, well logs and geological interpretation obtained during drilling and gas production in Ormen Lange so far allows the assessment of residual gas, and gives indications of where it resides in the reservoir. Residual gas saturations (Sgr) in the range of 0.21 to 0.41 have been observed in water-flood core measurements.

Recovery of residual gas depends on the final reservoir pressure. The recovery from the residual gas zone in the south, where the reservoir is well depleted, is good compared to the north where the pressure depletion is limited. Applying the base case residual gas saturation value of 0.3 and assuming no mobility threshold above residual gas saturation (critical gas saturation is equal to residual gas saturation), the total recovery in 2040 of residual gas is 19%, see Figure 1. Future development plans will increase total residual gas recovery, as the pressure will be further depleted.

In the South where an acting aquifer is present, recovery from residual gas highly depends on the strength of the aquifer. Earlier breakthrough of water with a potential stronger aquifer results in earlier shut-in of the wells, hence higher abandonment pressure and lower recovery of residual gas in the south.

The critical gas saturation is one of the parameters that has been extensively investigated in this project. The critical gas saturation is the saturation at which a continuous gas flow can be first observed, coinciding with a non-zero gas relative-permeability. Most literature indicates that residual gas requires approximately 5% increase of gas saturation units in order to reach critical gas saturation. The implementation of the latter mobility threshold for residual gas in Ormen Lange reduces the total residual gas recovery by 2%. The flow rate of the remobilized gas depends on how fast the gas relative permeability increases during secondary drainage. Hence changing the slope of the gas relative permeability curve, Ng, and the endpoint value, krg, also affects the ultimate recovery of residual gas.

Kortfattet Sammendrag

Temaet for denne rapporten er "Residuell Gass Mobilitet i Ormen Lange". Rapporten har blitt skrevet som en del av Master oppgaven i faget TPG4915 Petroleum Engineering - Reservoir Engineering, ved det Norske Tekniske og Naturvitenskapelig Universitet (NTNU). Arbeidet har blitt utført på Ormen Lange, et naturlig gass felt på den norske kontinental sokkel operert av A/S Norske Shell.

Store volumer residuell gass finnes i Ormen Lange som resultat av den hydrodynamiske akvifer strømmen[9]. Totale residuelle gass volumer i 2007 er 80±30 Gm^3 avhengig av den residuelle gass metningen. 15±6 Gm^3 av den residuelle gassen er utvunnet i 2040, avhengig av hvilke forutsetninger som er satt. Generelt, ettersom den residuelle gass metningen (Sgr) øker, øker det residuelle gass volumet og utvinningen av residuell gass minker.

Hoved utfordringen i dette prosjektet har vært å forstå hvordan residuell gass oppfører seg etter hvert som reservoar trykket synker under produksjon, og å vurdere utvinningsgraden av residuell gass for de ulike delene av reservoaret. Et litteratur studie ble først utført for å kartlegge de viktigste parameterne med hensyn til residuell gass mobilitet, og dette ble brukt som en base for videre simulerings-studier.

I 2008, etter at en avgrensningsbrønn i den nordre delen av reservoaret påviste residuell gass i reservoar-kammen og i midten av den direkte hydrokarbon indikatoren (DHI), ble det behov for en forbedret forståelse av fyllings-historien til reservoaret. Kjerneprøver, brønnlogger og geologisk tolkning oppnådd gjennom boring og produksjon i Ormen Lange så langt tillater evalueringen av residuell gass, og gir indikasjoner på hvor i reservoaret den residuelle gassen befinner seg. Residuelle gass metninger fra 0.21 til 0.41 har blitt observert i eksperimenter med vannflømming.

Utvinningen av residuell gass er avhengig av trykkfallet i reservoaret. Utvinningen av residuell gass i den sørlige delen av reservoaret, hvor trykket synker betraktelig under produksjon, er god i forhold til den nordre delen av reservoaret hvor trykkfallet er begrenset. For den gjennomsnittlige residuelle gassmetningen, 0.3, uten noen mobilitet-terskel over residuell metning (kritisk gassmetning er lik den residuelle gassmetningen), er total utvinning av residuell gass i 2040 19%, se Figur 1. Framtidens utviklingsplaner vil øke utvinningen av residuell gas, ettersom reservoartrykket vil bli videre senket.

I sør er en aktiv akvifer tilstede og utvinningen av residuell gass er avhengig av styrken på akviferen. Tidligere vanngjennombrudd med sterkere akvifer resulterer i tidligere stenging av brønnene i sør, derav høyere sluttrykk og lavere utvinning av residuell gass i den denne delen av reservoaret.

Kritisk gassmetning er en av parameterne som har blitt grundig utforsket i dette prosjektet. Den kritiske gassmetningen er metningen hvorav en kontinuerlig strømning av gass kan bli observert for første gang. Denne metningen sammenfaller med en relativ gass permeabilitet høyere enn null. I litteraturen er det rapportert at den kritiske gassmetningen er om lag 5% høyere enn den residuelle gassmetningen. Implementeringen av denne mobilitets-terskelen (5% høyere enn Sgr) for residuell gass i Ormen Lange reduserer utvinningen av residuell gass med 2%. Strømnings-raten av den mobiliserte gassen avhenger av hvor hurtig den relative permeabiliteten til gassen stiger. Dermed vil utvinningen av residuell gass også være påvirket av endringer i stigningstallet til relativ gass permeabilitets kurven, Ng, og endepunkts verdien på kurven, krg.

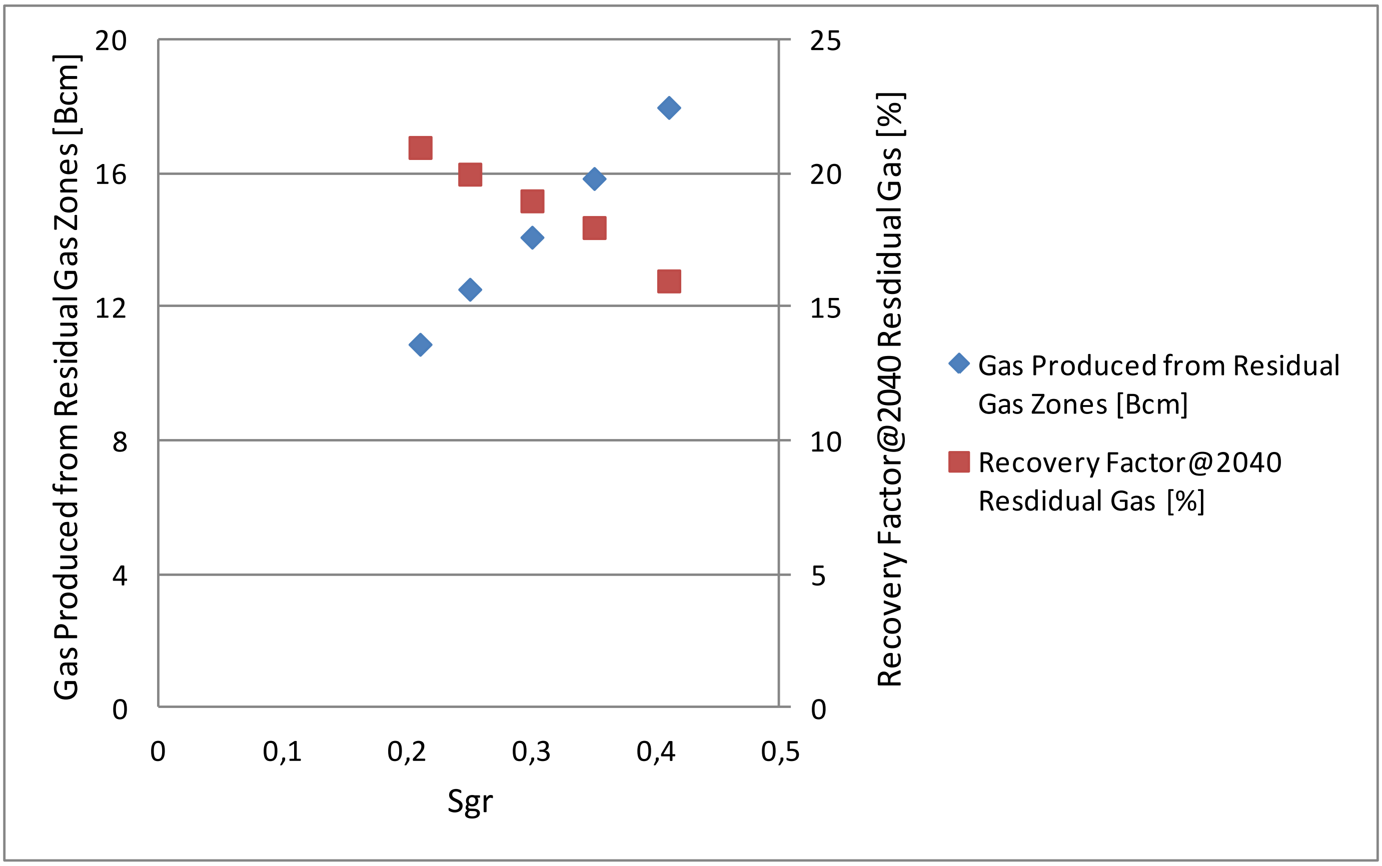

Figure 1 Recovery from residual gas versus residual gas saturation

Table of contents

Preface I

Executive Summary III

Kortfattet Sammendrag V

Table of contents IX

List of Figures XI

List of Tables XV

1. Ormen Lange 1

  1.1 Ormen Lange Field Overview 1

  1.2 Evolution of Fluid Fill in Ormen Lange 6

2. Literature Review 11

  2.1 Impact of Rock Type 11

  2.2 Identification of the Remobilization Process for Residual gas 12

  2.3 Literature Review on the Gas Remobilization process from Sgr by Expansion 15

3. Conventional Relative Permeability Hysteresis Models 19

  3.1 Land trapping model 19

  3.2 Killough Hysteresis Model 21

  3.3 Corey-correlation 21

4. Modeling Approaches Residual Gas Mobility Ormen Lange 23

  4.1 Initialization of Hydrodynamic Aquifer with Scanning-Curves 23

  4.2 Initialization of Hydrodynamic Aquifer without Scanning-Curves 26

  4.3 Production mode/Forecast (From 2007→) 26

  4.4 Capillary Pressure 27

5. Initialization of Simulation Model Including Sensitivities 29

  5.1 Initialization of the Hydrodynamic Aquifer Model without Scanning-Curves 29

  5.2 Comparison of Initialization with and without Scanning-curves 31

6. Forward Simulation Including Sensitivities 33

  6.1 Recovery from Residual Gas 33

  6.2 Residual Gas Physics – Discussion of Results 36

  6.3 Effect of krg and Ng on Recovery of Residual Gas 49

7. Aquifer Strength Sensitivity 55

  7.1 Stronger Analytical Aquifer 55

  7.2 Zero Analytical Aquifer 59

  7.3 Impact of Sgr on water-breakthrough 63

8. Conclusions 73

  8.1 Literature 73

  8.2 Simulation 73

9. Recommendations 75
9.1 Laboratory 75
9.2 Simulation 75
10. Nomenclature 76
11. References 77

List of Figures

Figure 1 Recovery from residual gas versus Sgr VII
Figure 2 Location and Map of Ormen Lange field showing Top Egga Member (grey contours), DHI (red polygon), volume reporting segments (green polygons), well and subsea template locations 2
Figure 3 Structural Elements in the Ormen Lange Region and location on the Norwegian continental shelf 3
Figure 4 Current production forecast versus PDO, main difference GIIP and compression assumptions. 6
Figure 5 Ormen Lange – (left) Map showing regional context for Ormen Lange, (bottom) Petroleum system 7
Figure 6 After the primary drainage process is completed, all gas residing in the north 8
Figure 7 Bounding imbibition situation in the north, primary drainage occurring in the south 8
Figure 8 Due to a slowing aquifer in recent times the interaction with the gas in the South will change, creating the residual gas zone. 8
Figure 9 Primary Drainage, gas migrating into the reservior, reaching maximum Sgi/Swc (Conceptual picture) 9
Figure 10 Bounding Imbibition, taking the gas saturation down to residual (Conceptual picture) 9
Figure 11 Secondary Drainage, gas expanding → Remobilization (Conceptual picture) 10
Figure 12 Residual gas as a function of initial gas saturation (adapted from M.H. Holtz[22]) 11
Figure 13 During drainage capillary forces act against the displacement and larger pores are more easily invaded (conceptual picture) 14
Figure 14 Drainage Pc curve; effect of gravity on gas saturation in a spherical cluster (adapted from A.E. Zweers et al[2]) 15
Figure 15 Gas/brine relative permeability curves shape according to the manner Sg varies: injection (left) or depletion from Sgr (right) (adapted from Fishlock et al.[19]) 16
Figure 16 Average In-Situ Brine Saturation Versus Pressure, illustration through ISSM measurements of secondary mobility threshold under depletion (Cable et al.[7]) 17
Figure 17 Measured In-Situ Brine Saturation (Cable et al.[7]) 17
Figure 18 Shape of the krg curve used in the new formalism. 18
Figure 19 Residual Gas versus initial gas saturations Land correlation 20
Figure 20 Parameters in evaluation of trapping and relative permeability hysteresis models (Adapted from J.E. et al[12]) 20
Figure 21 Primary Drainage/ Bounding Imbibition as used in initialization of the hydrodynamic aquifer model (conceptual picture) 24
Figure 22 Residual gas versus initial gas saturation 24
Figure 23 North-south cross section of the Ormen Lange field before initialization of the HDA. Saturation shown by color; the lower gas-saturations in the transition zone show that it is important to use scanning curves when modeling residual gas saturations 25
Figure 24 Bounding Imbibition, Secondary drainage (conceptual picture) 26
Figure 25 Imbibition capillary pressure data from porous plate and centrifuge experiments. Strongly water wet system, very limited forced imbibition. (Spontaneous imbibition green, forced imbibition red) 27
Figure 26 Imbibition relative permeability curves for 3 cases; I1-I3 29
Figure 27 Initial residual gas volume per segment (Egga+Subegga) for tree cases; I1-I3 30
Figure 28 Imbibition relative permeability curves for initialization with scanning curves. Drainage curves in pink; imbibition curves in green. 31
Figure 29 Comparison of gas-saturation after initialization with (right) and without (left) use of scanning-curves. 32

Figure 30 Critical gas saturation in secondary drainage for residual gas (blue) varies from 0.35 (left upper corner) to 0.45 (right lower corner) 33
Figure 31 Recovery from residual gas (Sgr = 0.30) vs critical gas-saturation 35
Figure 32 Difference map of gas recovery per segment: the difference between CGS = Sgr = 0.30 and CGS = 0.4 is shown. 36
Figure 33 Saturationmap@2007, location of grid-block 35.72.3 → no potential gas-inflow from surrounding grid-blocks containing mobile gas 37
Figure 34 Saturationmap@2007, location of grid-blocks (30.78.3 and 22.46.5) → potential gas-inflow from surrounding grid-block containing mobile gas 38
Figure 35 Pressure maps Ormen Lange before and after production (2007→2040) 39
Figure 36 OL charts remaining GIP/km2 before and after production (2007→2040) 40
Figure 37 Bounding Imbibition and Secondary Drainage Sgr = 0.35, CGS= 0.45 41
Figure 38 Secondary drainage gas relative permeability Grid Block 35.72.3 CGS=0.45 41
Figure 39 CGS, Sgr, pressure, accumulation of gas and accumulation of water versus time grid-block 35.72.3 42
Figure 40 PV/Z versus time grid-block 35.72.3 43
Figure 41 Secondary drainage gas relative permeability grid-block 30.78.3 and 22.45.6 43
Figure 42 Pressure and Sgr versus time for grid-block 30.78.3 and 22.46.5 44
Figure 43 PV/Z versus time grid-block 30.78.3 and 22.46.5 45
Figure 44 Accumulation of gas and water versus time grid-block 22.46.5 45
Figure 45 Accumulation of gas and water versus time grid-block 30.78.3 46
Figure 46 Location of Grid-block 29.8.1 and 29.9.1 in the South 47
Figure 47 Secondary drainage gas relative permeability grid-block 29.9.1 and 29.8.1 48
Figure 48 Sgr and pressure versus time for two different grid-blocks (29.8.1 and 29.9.1) 49
Figure 49 Accumulation of gas and water versus time for two different grid-blocks (29.8.1 and 29.9.1) 49
Figure 50 Relative permeability bounding imbibition and secondary drainage, Sgr=CGS=0.30, changing krg 50
Figure 51 Relative permeability secondary drainage, Sgr=CGS=0.30, changing Ng 51
Figure 52 Pressure and accumulation of gas grid-block 32.70.10 for two different values of krg 51
Figure 53 Recovery of residual gas versus krg 52
Figure 54 Pressure and accumulation of gas grid-block 32.70.10 for two different values of Ng 53
Figure 55 Recovery of residual gas versus Ng 53
Figure 56 Saturation and pressure versus time in grid-block 13.23.6 56
Figure 57 Accumulation of gas and water in grid-block 13.23.6 56
Figure 58 Relative permeability curves used under production. High (0.3) krw in blue, low (0.03) krw in red, krg remains constant 57
Figure 59 Initial (@2007) gas saturations in the South 58
Figure 60 Gas saturation @2040 extra strong aquifer krw=0.3 58
Figure 61 Gas saturation @2040 extra strong aquifer krw=0.03 59
Figure 62 RF @2040 Segment 5 Sgr=0.35 for 3 different scenarios (Zero, normal, strong aquifer) 59
Figure 63 Cumulative gas production and average gas pressure segment 5 Sgr = 0.35 60
Figure 64 Saturation and pressures versus time in grid-block 13.23.6 61
Figure 65 Accumulation of gas and water versus time in grid-block 13.23.6 61
Figure 66 Gas-saturation@2040; left figure no analytical aquifer, mid figure normal, right side strong aquifer 62
Figure 67 Imbibition relative permeability for constant krw, Sgr = 0.21→0.41 63
Figure 68 Recovery factor of residual gas from segment 3-5 versus residual gas versus Sgr for segment 3, 4 and 5, krw independent of Sgr 64

Figure 69 Sg @2007 in segment 4 and 5 (transition zone) for 2 different Sgr cases 65
Figure 70 Abandonment pressure for the 3 different Sgr-cases (0.21→0.41) independent krw 66
Figure 71 Charts remaining GIP/km2 @2040 for the 3 different cases (Sgr 0.21→0.41) krw independent 67
Figure 72 Imbibition relative permeability for dependent krw, Sgr = 0.21→0.41 68
Figure 73 Water relative permeability end point, green dots from recent SCAL on D7. 68
Figure 74 Water-breakthrough in 6305/7-D3 for the two models in chapter 7.3.1 and 7.3.2 69
Figure 75 Water-breakthrough in 6305/7-D2 for the two models in chapter 7.3.1 and 7.3.2 69
Figure 76 Average gas pressure segment 5 for the two relative permeability models in chapter 7.3.1 and 7.3.2 70
Figure 77 RF residual gas @2040 in segment 5 when Sgr is independent (weak color)/dependent (strong color) of Sgr 71
Figure 78 Abandonment pressure @2040 for the 3 different cases (Sgr 0.21→0.41) dependent on krw 71
Figure 79 Charts remaining GIP/km2 @2040 for the 3 different cases (Sgr 0.21→0.41) dependent on krw 72

List of Tables

Table 1 Summary of the results available in the literature concerning CGS............................16
Table 2 Different realizations for *initialization* without hysteresis..29
Table 3 Residual Gas Volumes in Bcm per segments for the different Sgr values....................30
Table 4 Comparison of GIP distribution with/without scanning-curves, gas-volumes in Bcm. ...32
Table 5 Four different cases for Sgr equals 0.35 in *production mode/forecast*........................33
Table 6 Recovery Factors @1.1.2040 Case F1...34
Table 7 Recovery Factors Residual Gas Total Field @1.1.2040 Case F1-F4............................34

1. Ormen Lange

This chapter provides an introduction to the Ormen Lange field with a brief review of location, facilities, subsurface, development and production. In addition, a high level description of the origin and concept behind the Ormen Lange hydrodynamic aquifer model is given, since this model is used in the simulation study performed during this project.

1.1 Ormen Lange Field Overview

1.1.1 Location

Ormen Lange is a natural gas field on the Norwegian continental shelf. It is located 120 kilometers northwest of Kristiansund, in the Møre Basin illustrated in Figure 3. The Ormen Lange gas accumulation, illustrated with the red spot in Figure 3, covers an area of approximately 350 km^2 and is defined over much of the area by seismic direct hydrocarbon indication observations, see Figure 2. Ormen Lange is located in water depths ranging from 700m to 1100m in the far northern sector. The Storegga slide, a huge submarine slide that occurred 8000 years ago, removed more than 600m of the overburden in the northern part of the field. As a result of the slide, water depth and sea bottom conditions vary greatly over the field. Using the fluid contact information from wells and the seismic interpreted flat spot, the field has been divided into 5 principle segments from North to South[25], see Figure 2.

The Ormen Lange field covers three licensees: PL208 (Blocks 6305/4 & 6305/7), PL209 (Block 6305/5) and PL250 (Block 6305/8).

Operator and licensees (name and %-interest) for the Ormen Lange field:

A/S Norske Shell	17.04%
Dong E&P Norge AS	10.34%
ExxonMobil E&P Norway AS	7.23%
Petoro AS	36.48%
Statoil Hydro	28.91%

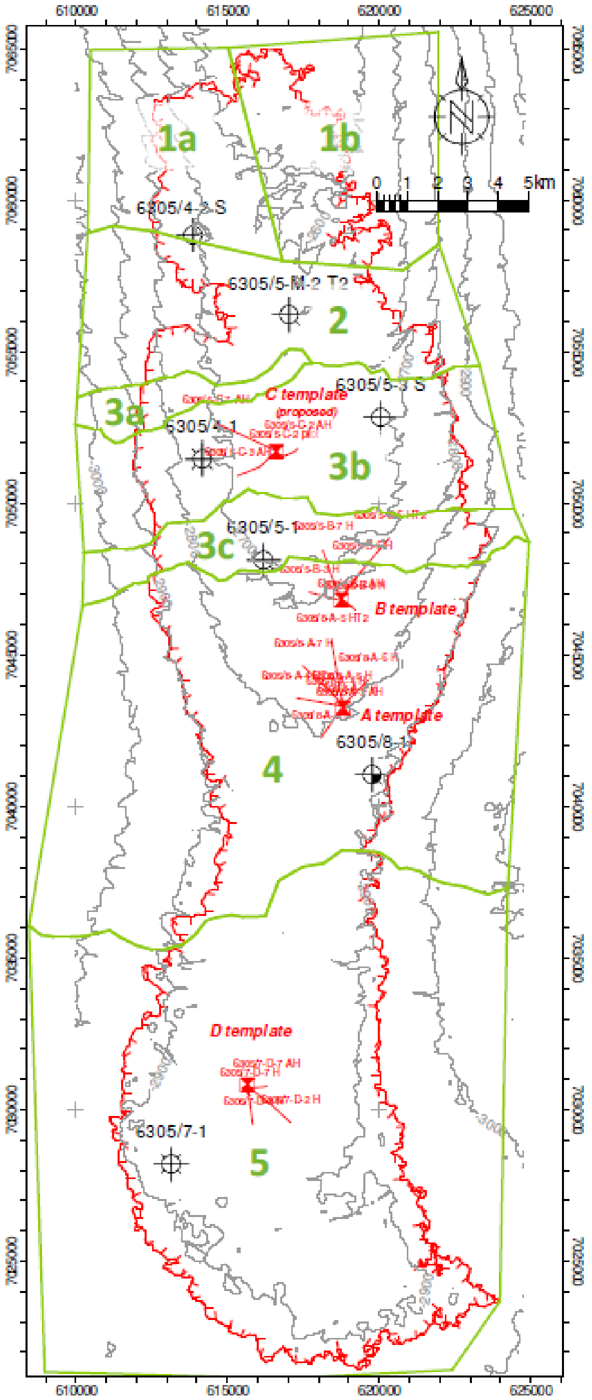
610000
615000
620000
625000
7065000
7060000
7055000
7050000
7045000
7040000
7035000
7030000
7025000
0
1
2
3
4
5km
1a
1b
6305/4-1 S
6305/5-M-2 T2
2
C template
(proposed)
6305/5-3 S
3a
6305/4-1
3b
6305/5-1
3c
B template
A template
6305/8-1
4
D template
6305/7-1
5

Figure 2 Location and Map of Ormen Lange field showing Top Egga Member (grey contours), DHI (red polygon), volume reporting segments (green polygons), well and subsea template locations

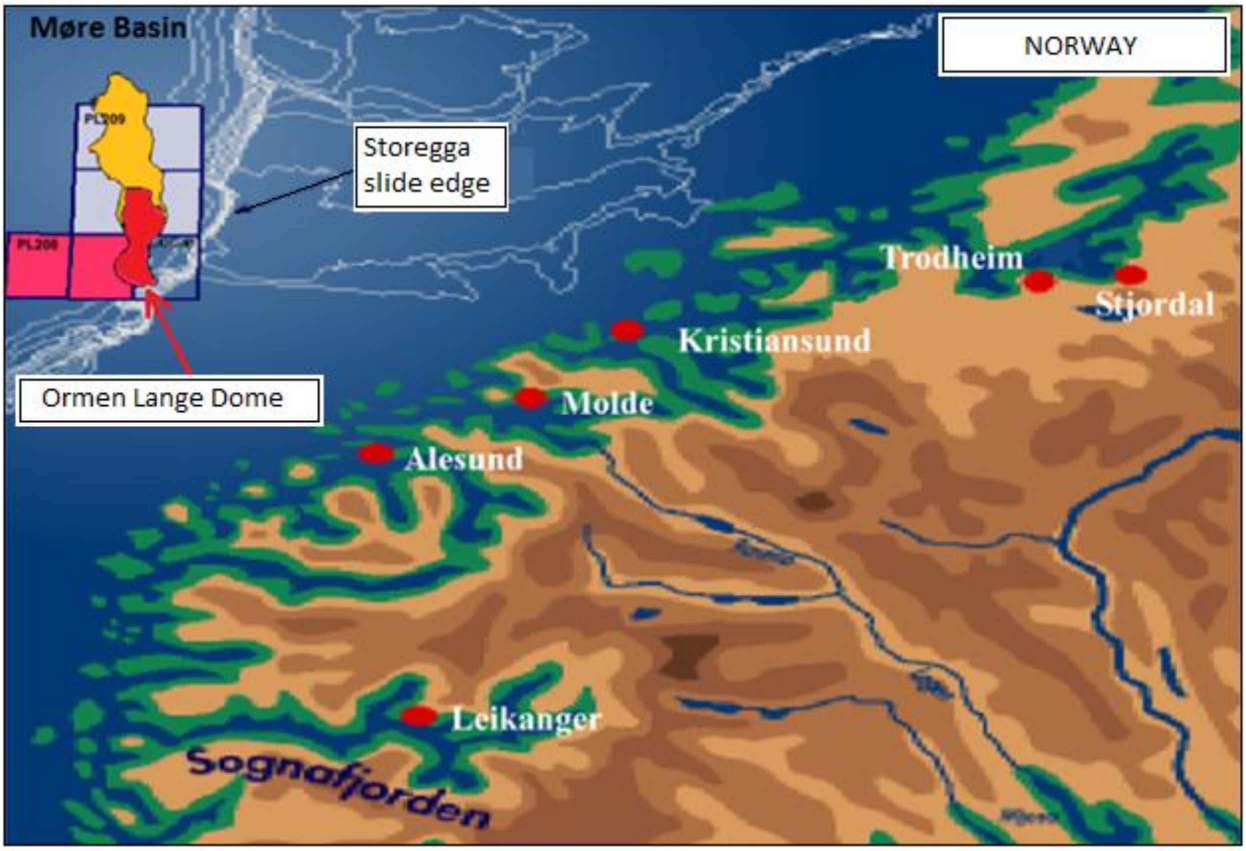

Figure 3 Structural Elements in the Ormen Lange Region and location on the Norwegian continental shelf

1.1.2 Facilities

The facilities (Nyhamna plant, Mangled pipeline, in-field pipeline and well templates) were delivered on schedule and have performed to expectation[24].

A future compression solution is being developed. The current reference case is a combination of onshore compression by 2016 plus an infield compression solution by 2021. The in-field compression solution consists of either a two train subsea compression or a slim version of floating compression. Maturation of subsea compression is dependent on the outcome of an ongoing pilot of subsea compression technology. Earliest timing for concept selection for the in-field compression solution is in 2012[24].

1.1.3 Subsurface

The main reservoir sandstones of the Egga Member (Våle Formation) form the primary development target. Figure 2 provides the Ormen Lange Top Egga structure map together with well and drilling centre locations. Appraisal well penetrations confirm the presence of a reservoir in the underlying Våle Heterolithics and Jorsalfare Formations, with varying reservoir quality and fluid fill. With additional appraisal and development drilling, it is now believed that the reservoir quality deteriorates in the north-eastern part of the field.

In the PDO[25], the field was described as a stratigraphic trap with the sand edge being aligned almost perfectly with the DHI (Direct Hydrocarbon Indicator) to explain the gas distribution. A DHI observed on multiple seismic cubes was taken as the field outline, within which full saturation of producible hydrocarbons was assumed. The Field Development Plan was defined with the information available from just four exploration and appraisal wells. With additional well penetrations, the DHI has been proven not to be a reliable method for fluid saturation prediction since seismic cannot distinguish between gas saturation above 5%. The significantly shallower FWL found in several wells in the north largely accounts for a 33% lower mobile GIIP in the 2011 update of 354 Bcm[26] relative to the original 532Bcm expectation estimate from the PDO[24].

Work during 2010 and 2011 has progressed understanding of the complex fluid fill history of the field. Currently the concept of a hydrodynamic aquifer is taken as the reference case for the explanation of fluid distributions in Ormen Lange. This is based on data observations and greater understanding of the hydrodynamic concept through isopotential mapping[27,28] and forward simulation modeling[9].

1.1.4 Development to 2012

On 27th October 2005 the "West Navigator" drill-ship spudded the first Ormen Lange development well. Initially the rig was contracted for 8 development wells, with the option of adding another 4 wells. The Ormen Lange Production License subsequently took the opportunity to extend the agreement to end-2012, and further extension is now under consideration.

1.1.4.1 Mid Field A & B Templates (Main Production Area):

Development drilling started at the A Template, see Figure 2. First gas was produced from three wells on the A Template (A2AH, A3H, A7H) at the end of September 2007. With the addition of three more producers (A6H, B2H & B3H) the field was ramped up to 57MMSm3/d during Q4 2008. Four development wells were brought on stream (A4H T2, A5H T2, B7H & B6H T2) in 2009, taking the field up to, and exceeding, the plateau rate of 70MMSm3/d.

1.1.4.2 Southern (D) Template:

In spring 2007 license approval was given to proceed with construction, installation & development of the Southern (D) Template area. The template was installed in the spring of 2009, with a tieback to the main production area in mid-2009. The pilot hole 6305/5-D7H reached TD in February 2010. Approximately 2 bar depletion was measured in the pilot hole, demonstrating a limited degree of communication with the A and B template production areas in segment 4.

D7AH and D2H came on stream during August/September 2010, with both wells capable of producing at 10MMSm3/d. Total field production during Q3 2010 increased by approximately 7MMsm3/d. D3H was brought on stream July 2011, together with D1H and D8H. During 2011 overall production from the D-wells added more than 9MMsm3/d of incremental production to Ormen Lange.

1.1.4.3 Northern (C) Template:

During Q1 2009, a follow-up two well appraisal program was approved focusing on the "Mid-North" and "Far-North" (segments 3 & 2 as per PDO 2003 definition[25]) with the purpose of delineating the hydrocarbon distribution in light of encountering a shallow FWL in 2008. The first of these appraisal wells (5-3-S T2) found an 8-9m gas column (with a FWL) and showed 2-

3 bar pressure depletion, proving limited connectivity of segment 3 volumes to the A/B template wells in segment 4[24]. A second well (M-2 T2) found the Egga formation completely water bearing, see Figure 2.

The third well (5-4-2) was drilled in the north-western segment of the field. The well targeted an observed seismic brightening, indicating potential gas bearing sand in an upside scenario. The well was found water bearing, and presence of residual gas is highly likely. However, exact saturations could not be determined due to lack of critical data. Post drill evaluation concluded that even in the best case scenario, further Far North development is not economically viable[24].

In September 2011 a pilot hole from the C template reached reservoir with expected results. The pilot hole measured gas down to 2706 m TVSS in the Jorsalfare formation. Reservoir pressure in the Egga demonstrated pressure baffling with segments 3C and segment 4. The pilot-hole results supported the base plan to proceed with three production wells from the C template (C2, C7 and C6), see Figure 2, and a fourth well that will target a combination of Egga and Sub-Egga (C5)[24].

1.1.5 Production and Pressure History

Production performance to date has been exceeding or meeting the PDO 2003[25] with successful and timely delivery of capacity through production wells and high availability of the integrated production system. Compared to the PDO, pressure decline in the A and B template areas is steeper, but lowering of Nyhamna plant pressure has kept the production rates high. Pressure communication between the central production area and the southern field is more limited compared to the PDO expectation. Due to limited pressure depletion in the D7 pilot hole after producing 37 Bcm from the central production area dedicated wells are required in the Southern segment. Pressure communication between the central production area and the north is also subjected to pressure baffles. In September 2011 the C template pilot hole confirmed pressure baffling and is in support of the C template wells that are currently being drilled.

Figure 4 provides the current mid case production forecast (Ormen Lange FDR 2011[24]) together with the production profile from the PDO. The effect of having a 33% lower mobile GIIP in the 2011 update compared to the PDO expectation is significant towards the end of field life from 2015.

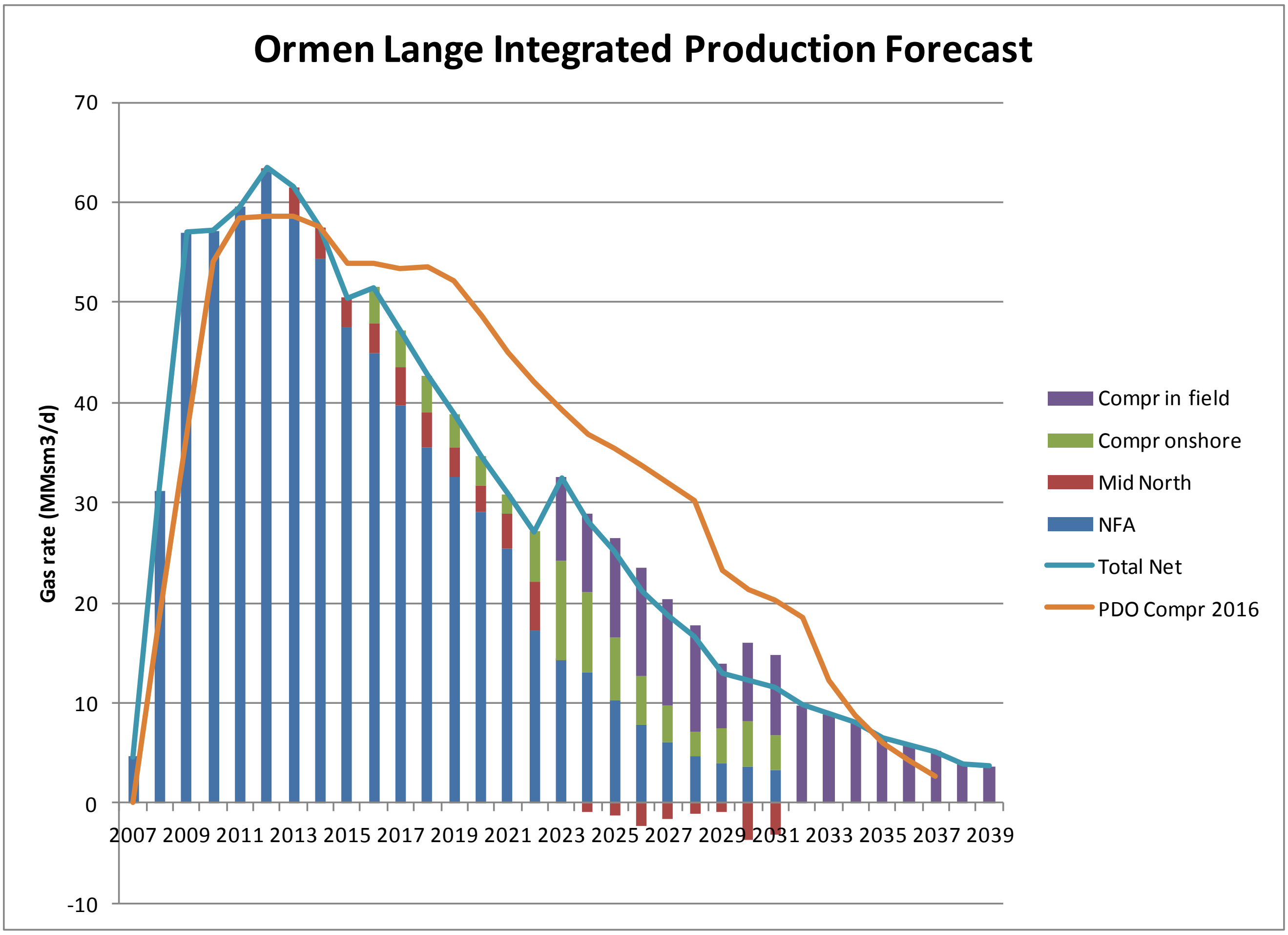

Figure 4 Current production forecast versus PDO, main difference GIIP and compression assumptions.

1.2 Evolution of Fluid Fill in Ormen Lange

Key data that provide insight into the fluid distribution in Ormen Lange are:

- Presence of residual gas between the present-day FWL and the seismic DHI.
- Formation pressure data indicating over-pressured water consistently increasing in the northern direction
- Production history and well test data indicating communication/baffling across the field.
- Similar gas and water (i.e. 9Kppm salinity) composition across the field.

The gas charge into the Ormen Lange structure has occurred in parallel with the formation of the dome itself throughout the Miocene, see Figure 5. The hydrodynamic conditions created the stepping northwards of the paleo-FWL delineated by seismic direct hydrocarbon indicator (as mentioned in chapter 1.1.3). An increase of overpressure during the latest glaciations 3 million years ago increased the rate of water expulsion from the basin shales in the north of the field, and resulted in a continuous flow of water from the north to the south.

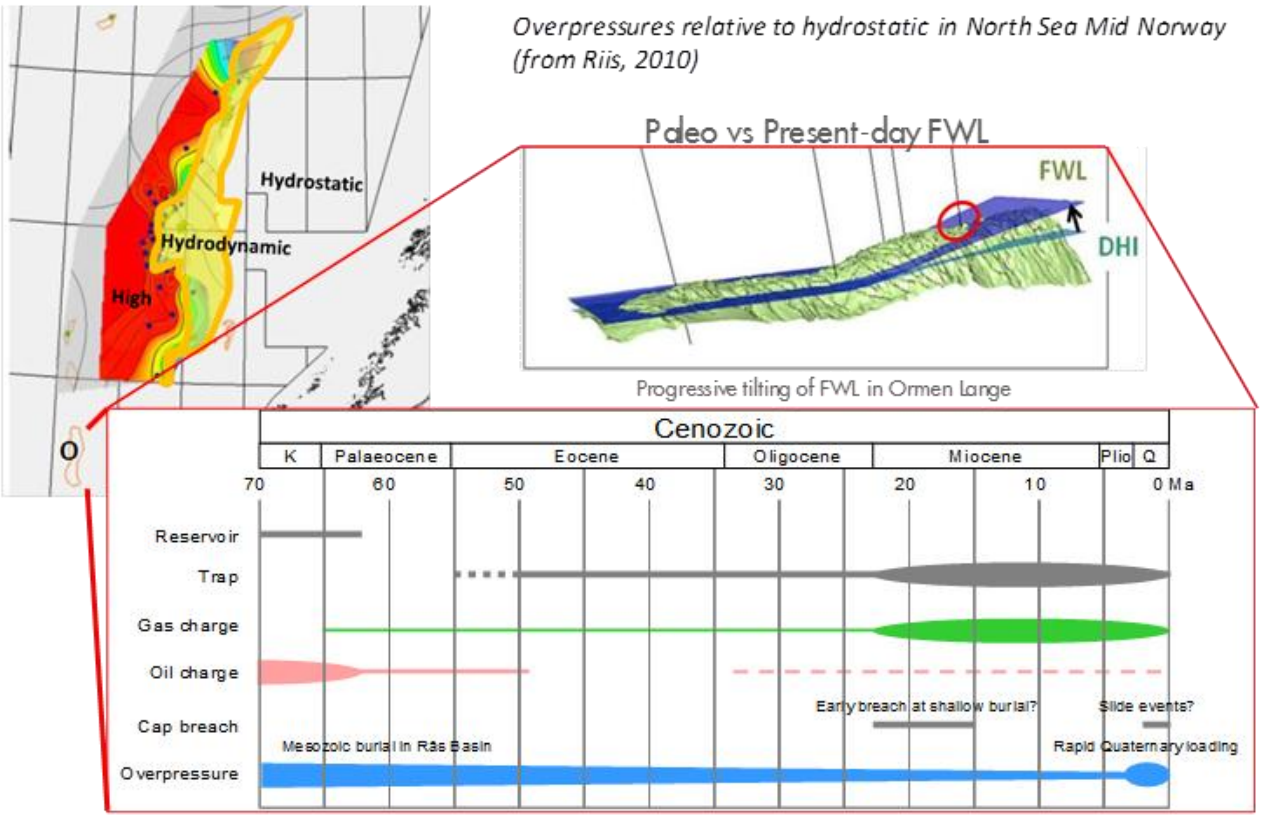
Overpressures relative to hydrostatic in North Sea Mid Norway (from Riis, 2010)
Hydrostatic
Hydrodynamic
High
O
Paleo vs Present-day FWL
FWL
DHI
Progressive tilting of FWL in Ormen Lange
Cenozoic
K
Palaeocene
Eocene
Oligocene
Miocene
Plio
Q
70
60
50
40
30
20
10
0 Ma
Reservoir
Trap
Gas charge
Oil charge
Cap breach
Overpressure
Early breach at shallow burial?
Slide events?
Mesozoic burial in Rås Basin
Rapid Quaternary loading

Figure 5 Ormen Lange – (left) Map showing regional context for Ormen Lange, (bottom) Petroleum system

It is the combination of charge, structuration and different stages of basin overpressure that is responsible for the stepping of the DHI and the present FWL in the Ormen Lange field.

1.2.1 Conceptual Fluid Fill Model – Ormen Lange

Hydrodynamic equilibrium was established by circulating water through the aquifer at a rate of 10m3/day using one pseudo injection and one pseudo production well at the opposite ends of the Ormen Lange full field simulation model effectively mimicking the potentiometric gradients mapped from the iso-potential mapping exercise. Steady state conditions are reached after approximately 0.2 million years i.e. when the hydrocarbon column reaches pressure equilibrium and gas pressures lines up on the same gradient.

As can be seen in Figure 8 the residual gas resides in two different parts of the reservoir. There is a residual gas zone in the North, where the aquifer has pushed the gas from the crest of the structure into the South of the field leaving a northward-thickening prism of residual gas behind. In the South, a 14 m residual gas zone is observed, penetrated by well 6305/7-1. The residual gas zone in the South is related to a change in hydrodynamic aquifer flow rate due to the Storegga slide (10000 years ago). Due to lower overburden pressure in the North after the landslide, the aquifer rate decreased, thus changing the interaction with the gas in the South.

This is captured in the full field simulation model by decreasing the aquifer rate from 10m3/day to 0.82 m3/day during the last 10000 years of initialization.

The saturation change under initialization of hydrodynamic aquifer flow and under production in Ormen Lange is illustrated in Figure 6-Figure 8. It is assumed that the primary drainage process is completed when initialization of the hydrodynamic (HD) aquifer begins. The situation before the aquifer starts to flow, with 100% water (blue) in the South and initial gas saturation, Sgi (green), in the North is showed in Figure 6[9]. Figure 7[9] shows the situation when the HD aquifer created by de-watering of the over-pressured shale in the north starts to displace the gas southwards. The northern part of the reservoir goes into a bounding imbibition process, while a primary drainage process will occur in the south. Due to a slowing aquifer in recent times the gas will recede due to lower pressure, creating the residual gas zone in the south, see Figure 8.

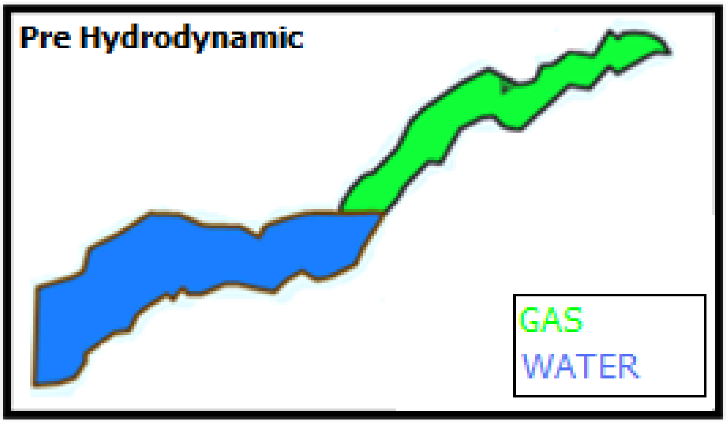
Pre Hydrodynamic
GAS
WATER

Figure 6 After the primary drainage process is completed, all gas residing in the north

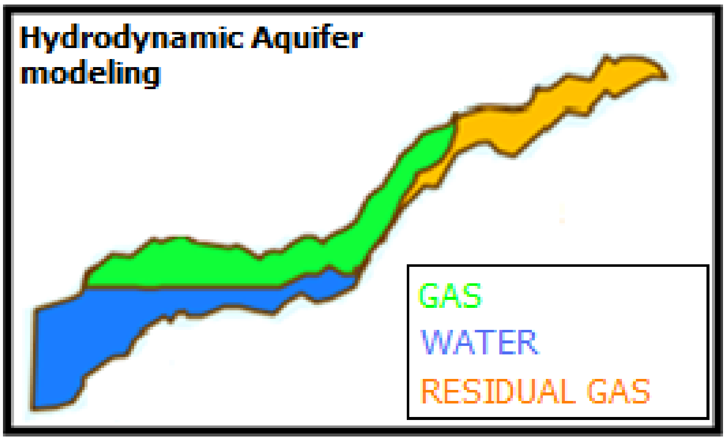
Hydrodynamic Aquifer modeling
GAS
WATER
RESIDUAL GAS

Figure 7 Bounding imbibition situation in the north, primary drainage occurring in the south

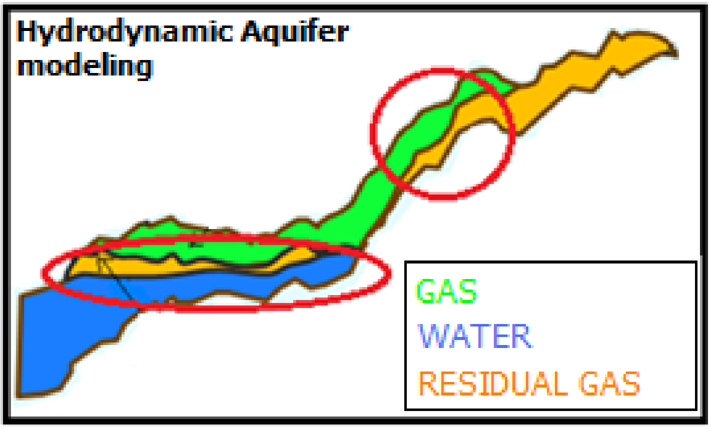
Hydrodynamic Aquifer modeling
GAS
WATER
RESIDUAL GAS

Figure 8 Due to a slowing aquifer in recent times the interaction with the gas in the South will change, creating the residual gas zone.

1.2.2 Fluid fill at the pore level

To understand how residual gas can become mobilized during pressure depletion of the reservoir, we need to zoom in at the pore level. The reservoir was initially water-saturated. At some point gas started to migrate from the source to the reservoir rock, reaching the highest historically achieved gas saturation, see Figure 9. Water is covering the water wet sand grains; gas is residing in the middle of the pores. The initial gas saturation and gas relative permeability is high.

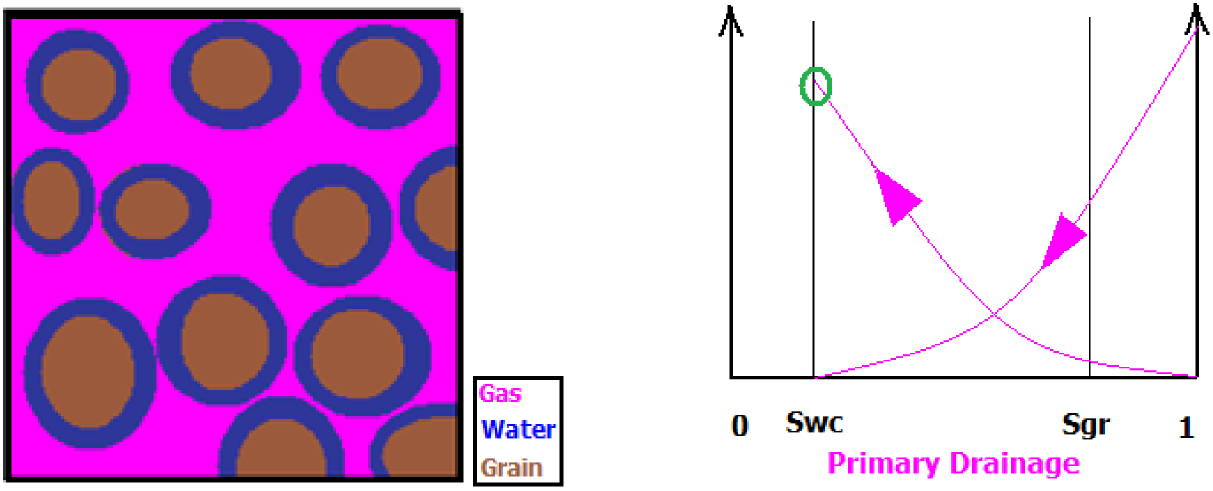

Figure 9 Primary Drainage, gas migrating into the reservior, reaching maximum Sgi/Swc (Conceptual picture)

During hydrodynamic aquifer flow water displaces the gas, see Figure 10. Parts of the reservoir is going through a bounding imbibition process, ending up at residual gas saturation, Sgr. The gas is snapped of and is residing in the middle of the pores. The Southern part of the reservoir will experience a primary drainage process at this stage. A lower relative permeability for water under imbibition compared to drainage is expected since high trapped gas saturation will occupy all of the largest pore sizes (being non wetting) effectively blocking the water phase mobility.

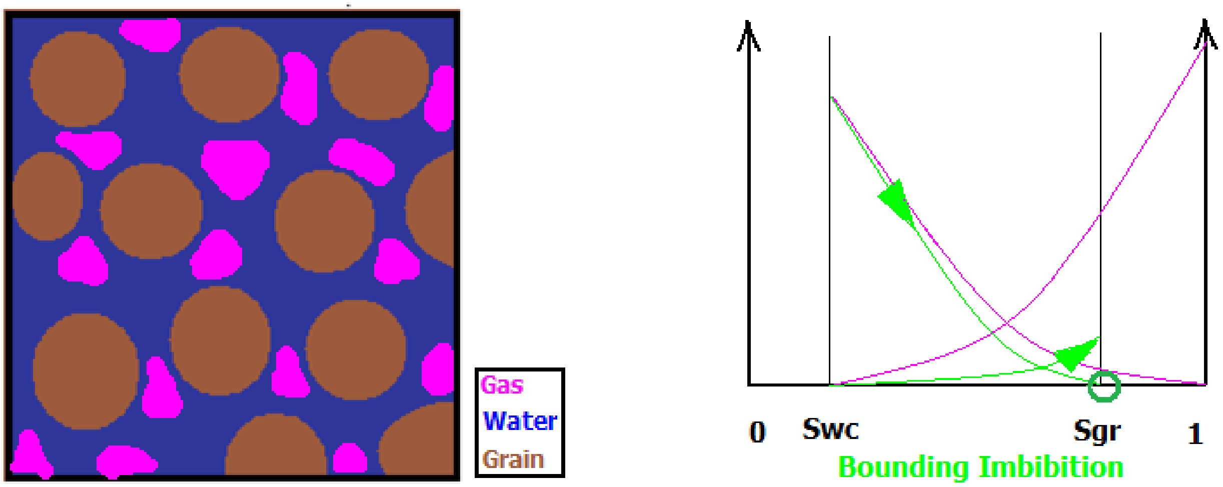

Figure 10 Bounding Imbibition, taking the gas saturation down to residual (Conceptual picture)

While depleting the reservoir, residual gas bubbles that undergoes pressure decline will start to expand, going into a secondary drainage process, see Figure 11. A gas saturation threshold above residual to reconnect the gas phase is expected. The trapped gas remains immobile until the mobility threshold is reached. Once mobile, the high mobility of gas makes the saturation remain close to the gas saturation at which the gas remobilized[8]. In the following the recovery processes related to the latter is described in further detail.

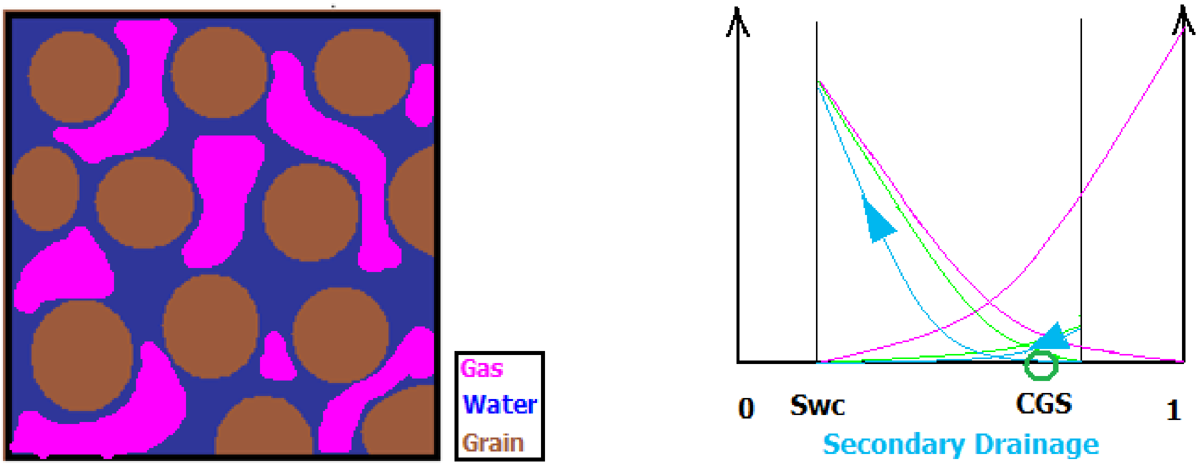

Figure 11 Secondary Drainage, gas expanding → Remobilization (Conceptual picture)

2. Literature Review

Residual gas saturation controls the volume of gas trapped in that portion of the reservoir that has experienced water encroachment. As water moves into a rock volume filled with gas, the water displacement of the gas is incomplete. The water fills pores and pore throats, causing capillary pressure and relative permeability effects to stop the flow of gas and allow only water to pass through the rock volume. This stoppage results in gas being trapped behind the encroaching waterfront as residual gas. The volume and location of the residual gas are controlled by the distribution of the petro-physical properties. Knowledge about volumes and recovery of residual gas is important when predicting the recovery factor for water-drive gas-reservoirs. Remobilization of residual gas will occur when a saturation coinciding with a non-zero relative permeability is achieved. The results from the experiments done in the literature[6,7,19] suggest that there are differences in gas relative permeability curves, depending on the manner in which the gas saturation increases from its waterflood residual value. When the gas saturation increases during gas injection, the gas almost immediately becomes mobile, assuming little hysteresis between the imbibition and secondary-drainage relative permeability-curves[7,19]; but when the gas saturation increases by expansion, an appreciable increase is required before gas can flow at detectable levels[7,19]. The saturation required for remobilization under internal gas drive (gas liberation during depressurization) is in this work referred to as critical gas saturation (CGS). Recovery of residual gas throughout the reservoir will depend on rock type, pressure-communication and aquifer-strength.

2.1 Impact of Rock Type

2.1.1 Residual Gas Saturation, Sgr

Rock and pore type can have a strong effect on the value of Sgr, and variations in rock type can also significantly affect Sgr. For a given rock-type Sgr increases with an increase in clay content and cementation, and decreases with an increase in sorting and grain size, as seen in Figure 12[22]. Residual gas is a capillary phenomenon; the rock characteristics that appear to increase Sgr also increase pore network complexity, hence porosity is decreasing and pore throat size is decreasing. Figure 12 also illustrates that for a given rock-type, a higher initial gas saturation results in higher residual gas saturation.

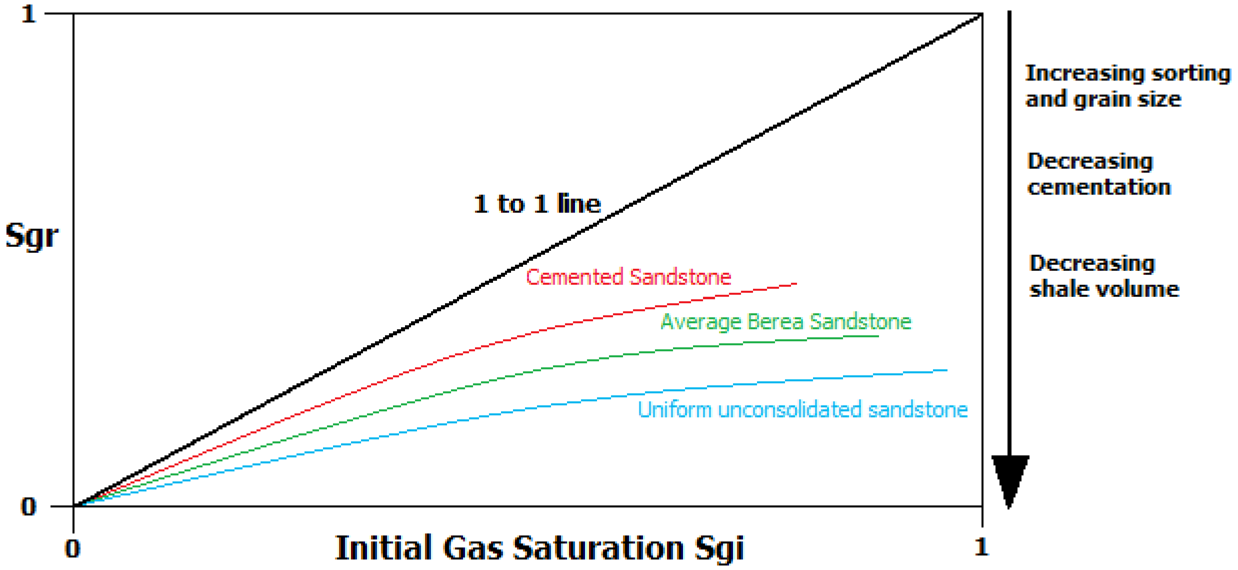

Figure 12 Residual gas as a function of initial gas saturation (adapted from M.H. Holtz[22])

2.1.2 Internal/External Gas Drive

The origin of the onset of gas mobility above residual gas saturation has been discussed by Fishlock et al[19]. When gas is injected for a secondary drainage process, it tends to follow the preferential pathways in terms of hydraulic resistance leading to a very efficient reconnection process of the residual gas (viscous forces overcome the capillary forces). When the gas saturation is growing by expansion, there is a local quasistatic equilibrium between viscous and capillary forces that leads to the saturation of pores which are not involved in the reconnection process. It makes the relative permeability curves to be process dependent parameters, and this has to be considered for the recovery processes based on depletion. However, the results also show that this difference is rock-dependent and may thus be much smaller for a particular reservoir rock. Some results in the literature support the view that differences are larger for more permeable rocks[30]. A comparison of the two gas drive processes has been performed by McDougall et al[20]. Their results suggest that pore size distribution, coordination number (connectivity of network) and bubble density are the main factors that condition how large the difference between gas relative permeability is for internal and external drive.

The variation of critical gas saturation with pore structure diminishes at higher depletion rate. The significance to field application of depletion is that near the production well the pore structure has little influence on the critical gas saturation, while at low depletion rate in the reservoir (far from well) the pore structure may be an important factor for the critical saturation.

2.2 Identification of the Remobilization Process for Residual gas

2.2.1 Origin of Residual Gas

The general process of build-up of critical gas saturation for any initial reservoir condition (virgin oil/gas, watered out oil/gas) can be divided into three stages:

1. Formation of gas bubbles
2. Growth of gas bubbles/clusters and
3. Merging of gas clusters creating a network of gas channels allowing upward migration of subsequently liberated gas →Remobilization.

When residual gas is initially present, the process will start at the second stage; upon pressure decline in a watered-out gas-reservoir, gas bubbles grow to such an extent that they break through the pore throats and form gas channels. Buoyancy forces promote growth in vertical direction – i.e., upward migration of gas.

At what pressure remobilization will occur depends on the pressure at it was first trapped. If the reservoir-pressure at which gas-trapping by encroaching water occurred is subsequently lowered, this gas will expand to saturation greater than residual and a portion of the gas will be mobilized. If the reservoir pressure increases, the gas will be compressed and occupy a saturation less than residual. In this case the pressure must be lowered below the previous minimum before any gas can be mobilized. This pressure is defined as "entrapment pressure".

Flow of the remobilized gas is assumed to be dependent on the relative magnitude of gravity, viscous and heterogeneous capillary forces[31]. A set of dimensionless numbers is usually defined to quantify these relative magnitudes. The capillary number Ca is the typical ratio of the viscous pressure drop at pore scale to the capillary pressure, while the "Bond number" quantifies that of the typical hydrostatic pressure drop over a pore to the capillary pressure:

$$Ca = \frac{\Delta Pvisc}{\Delta Pcap} = \frac{\mu_w v}{\gamma} \qquad (2.1)$$

$$Bo = \frac{\Delta Pgrav}{\Delta Pcap} = \frac{\Delta \rho g K}{\gamma} \qquad (2.2)$$

Where μ_w is the viscosity of the wetting fluid, v is the filtration or Darcy velocity, K is the permeability, γ is the surface tension, $\Delta\rho$ is the density difference in the two fluids, and g is the acceleration due to gravity in the direction of flow.

2.2.2 Spherical growth of Gas Bubble

When a trapped gas bubble grows due to expansion as a result of pressure decline, it will fill out the pore in which it was originated[2]. Subsequently the gas will enter pore-necks which connect the pore with surrounding pores. Consequently the curvature of the gas/water interface changes and the pressure difference over the gas/water interface increases until the capillary pressure corresponding with the pore-neck diameter has been reached and gas breaks through into a next pore. Indeed, the capillary pressure, which is the difference between the pressures in the non-wetting and in the wetting phase at a point of the interface, is defined by the well-known Young–Laplace[31] law:

$$p_c = p_{nw} - p_w = \gamma\left(\frac{1}{R_1} + \frac{1}{R_2}\right) \qquad (2.3)$$

Where γ is the surface tension between the liquids and R_1 and R_2 are the two principal radii of curvatures for the interface.

If several pores surround the bubble, it will selectively grow into the pore with the widest neck. The two-pore bubble has more surrounding pore necks from which it selects again the widest for growth into a third and so on, thus forming a gas cluster, see Figure 13. The way the cluster of gas-filled pores is growing is fully determined by the distribution of pore-neck sizes and there will be no preferential direction of growth if the rock is homogeneous.

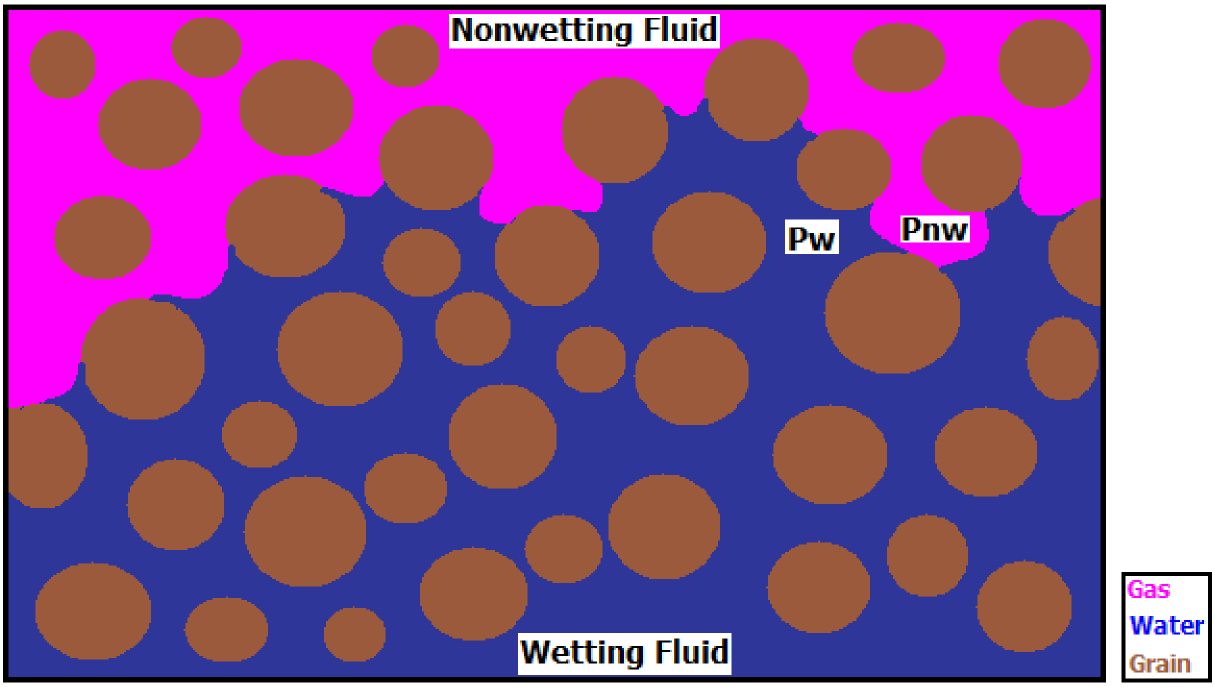

Figure 13 During drainage capillary forces act against the displacement and larger pores are more easily invaded (conceptual picture)

2.2.3 Influence of gravity

In the foregoing section the growth of a gas bubble/cluster was discussed ignoring possible effects due to gravity. However, the spherical growth has its limit due to buoyancy effects acting on gas surrounded by the water[2]. The pressure difference between the gas and the water across the gas/water interface is at the top of the cluster $2\Delta\rho g r$ larger than at the bottom. Consequently, following the Pc curve, the gas saturation at the top of the cluster can be larger than at the bottom, see Figure 14[2].

During growing of the cluster, initially both the gas saturation at the top and at the bottom of the cluster will decrease. At the same time, the pressure difference $2\Delta\rho g r$ will increase. This will cause the decrease of gas saturation at the top of the cluster to lag behind the decrease at the bottom, i.e. the gas saturation at the top will be higher than at the bottom of the cluster. Due to buoyancy, at some critical radius the cluster will stop growing radially and will expand only upwards (gravity domination). The effect of gravity increases with decreasing pressure decline rates, and is significant in field operations.

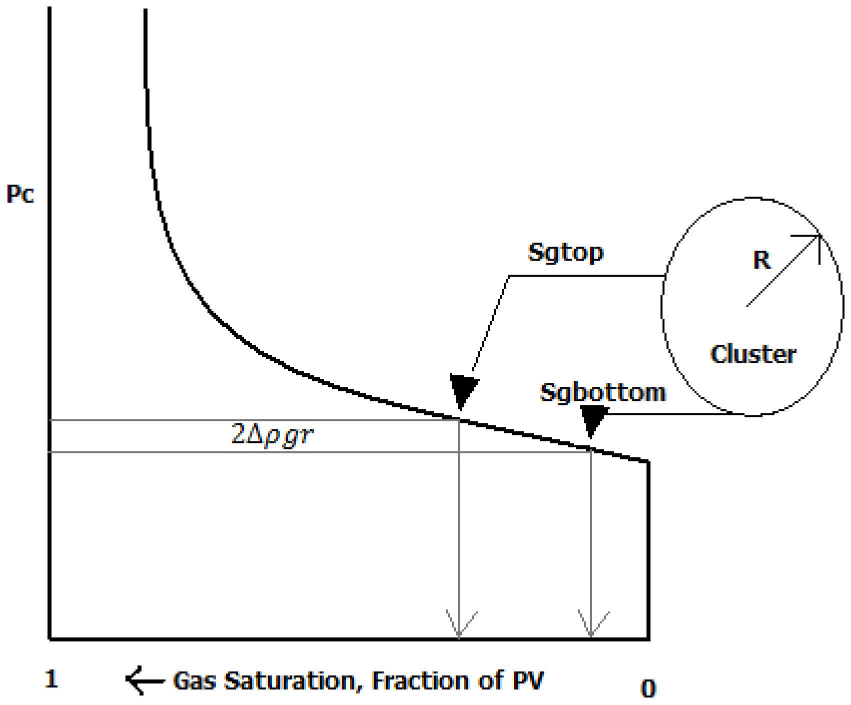

Figure 14 Drainage Pc curve; effect of gravity on gas saturation in a spherical cluster (adapted from A.E. Zweers et al[2])

2.3 Literature Review on the Gas Remobilization process from Sgr by Expansion

The literature associated to the relative permeability curves under depletion is mainly related to cases where gas is not initially present within the porous medium. It concerns applications related to late field depressurization in oil reservoirs (at Swi or after waterflooding) and heavy oil solution gas drive recovery[3]. There are few experimental investigations on the trapped gas behavior under depletion, but they are of good quality and well documented.

The oldest reference was published by Fishlock et al.[19] (1988). A comparative study between secondary drainage relative permeability obtained under injection and depletion is proposed in order to get more insight on the production of waterflood gas condensate reservoirs by blowdown, see Figure 15[19]. The gas/brine relative permeability curves were measured on sandstone cores from the Clashach quarry in Scotland, using two different protocols. The reference relative permeability curves obtained under injection were standards, in agreement with other works[4] and the formalisms widely implemented in the reservoir codes which state a reversibility between imbibition and secondary drainage krg curve[5,6]. The depletion experiments were conducted after establishment of a trapped gas saturation using two different core permeabilities and two depletion rates, and all exhibit the existence of a remobilization threshold (ΔSg) in order to reach critical gas saturation. ISSM was used (In Situ Saturation Monitoring) which enabled cross checking the mass balance and plotting the saturation profiles. All the results are gathered in Table 1, showing remobilization threshold values (ΔSg) ranging between 0.07 and 0.15 (fraction).

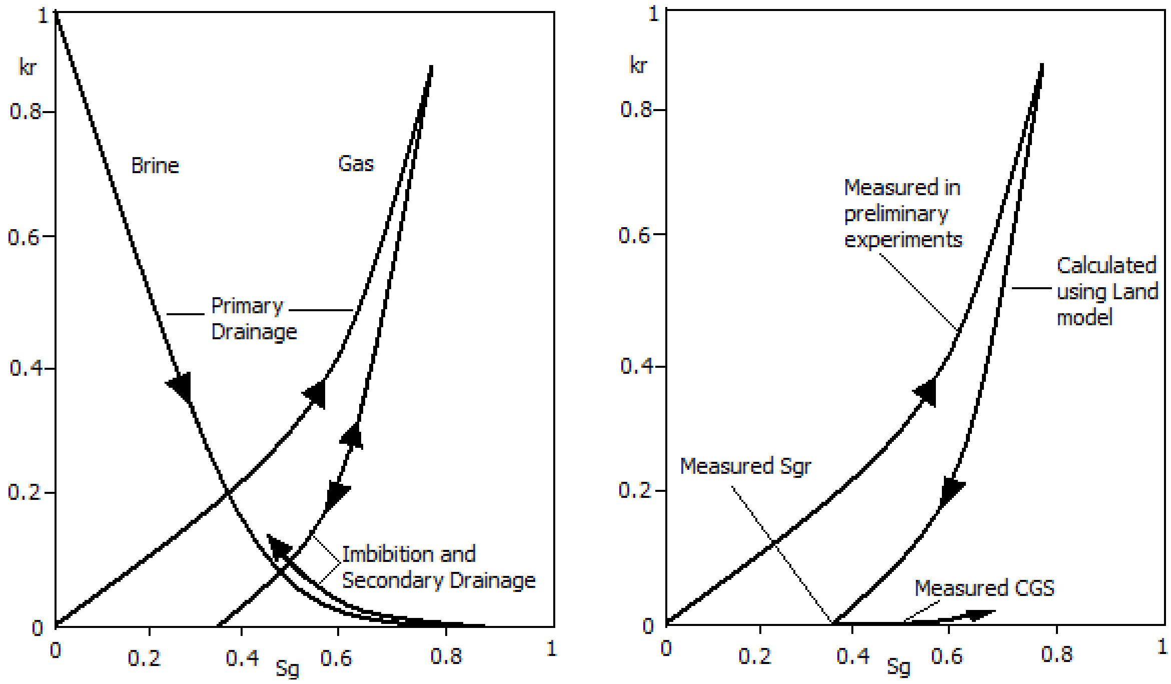

Figure 15 Gas/brine relative permeability curves shape according to the manner Sg varies: injection (left) or depletion from Sgr (right) (adapted from Fishlock et al.[19])

The second reference was published by Cable et al.[7] in the context of the production potential of a transition zone containing trapped gas at elevated saturation values, see Table 1. The experiments were conducted on reservoir cores in a very careful manner with ISSM at high spatial resolution, see Figure 16 and Figure 17. The results indicated that even with high trapped gas saturation values, a mobility threshold around 0.03 exists and needs to be overcome before gas can be mobilized.

Two depressurization experiments were undertaken from uniform trapped gas saturation of 0.47 PV and 0.41 PV. Both depressurization experiments saw gas mobilization and production. Critical gas saturation was just 0.03 PV higher than the trapped gas saturation, which is an expansion of 6%-7%. The first depressurization experiment underwent pressure decline from 117 barg to 34 barg and 70% of the initial trapped gas was recovered. Measured relative permeability curves were estimated from low rate steady state flooding. Gas and brine relative permeabilities were extremely low; around 0.01 at the saturation where krg/krw=1.

Author	Rock Type	K mD	Phi %	DP/dt bar/hr	Sgr	CGS	ΔSg (CGS-Sgr)
Fishlock et al	**Clashach**	1280	20.0	34	0.35	**0.5**	0.15
	Sandstone	1280	20.0	3.4	0.35	**0.49**	0.14
	Low Clay	240	11.6	4	0.39	**0.46**	0.07
Cable et al	**Res. Sands**	3.2	20.4	0.5	0.47	**0.5**	0.03
	High Clay	3.2	20.4	0.5	0.41	**0.44**	0.03

Table 1 Summary of the results available in the literature concerning CGS.

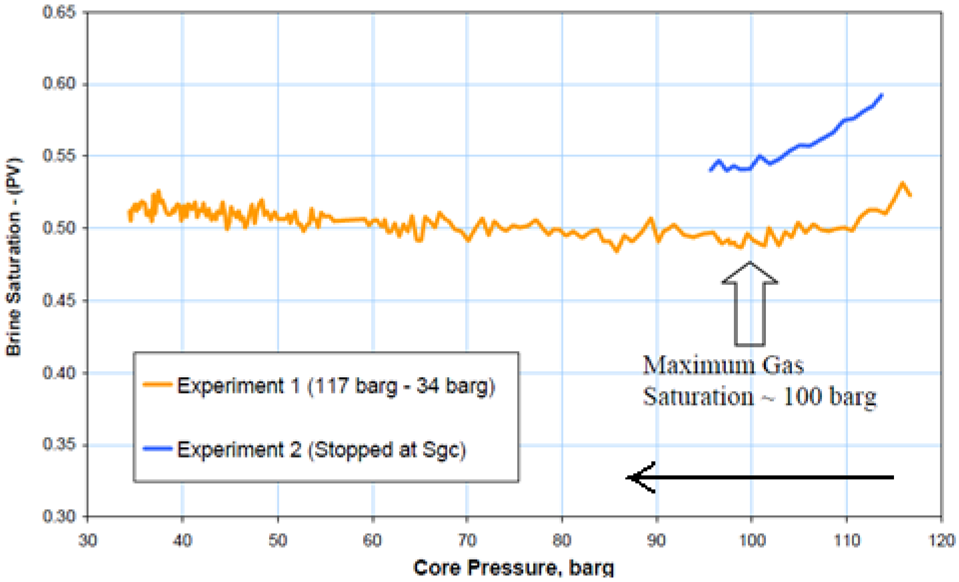

Figure 16 Average In-Situ Brine Saturation Versus Pressure, illustration through ISSM measurements of secondary mobility threshold under depletion (Cable et al.[7]).

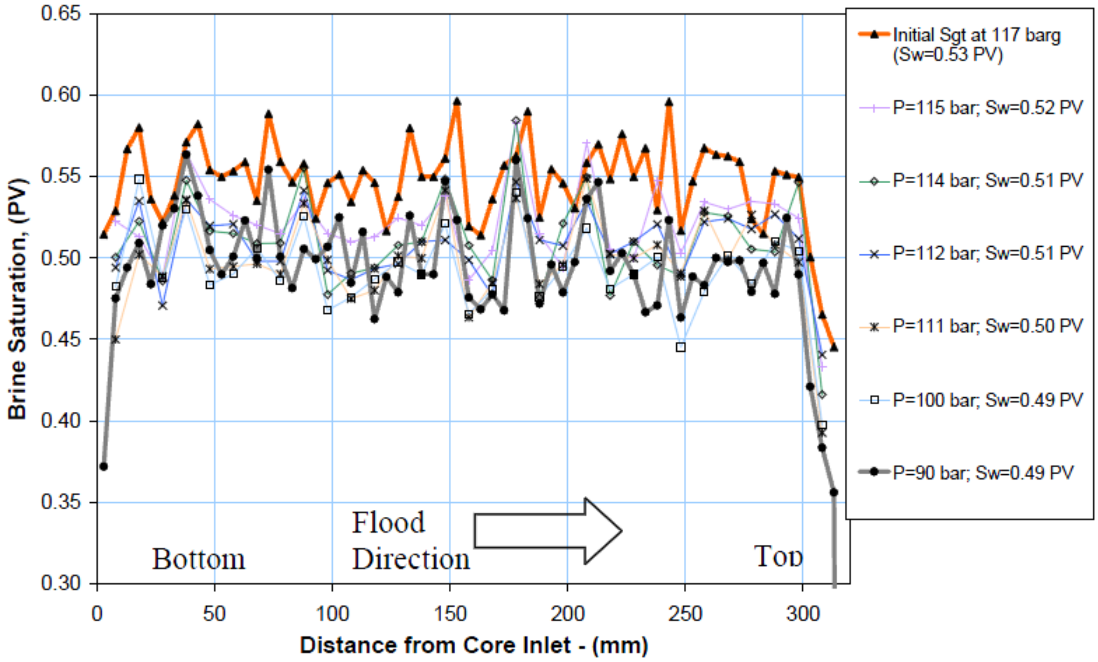

Figure 17 Measured In-Situ Brine Saturation (Cable et al.[7])

2.3.1 Field study - Gas storage

Natural gas storage in deep aquifers is extensively used worldwide to meet gas demand. The storage reservoirs are subjected to annual gas cycling (gas injection in summer and gas withdrawal in winter). In recent years, the development of multi-cycling to optimize the value of stored gas, has caused the need to improve the pressure history matching of numerical models. It has been observed that the simulated pressure tends to systematically overestimate the measured pressure independent of the gas storage site considered. A study done by GDF Suez[8], identifies the hysteresis relative permeability formalism as the main error driver of the history mismatch. A comparison between simulated and observed pressure data indicated that the most important errors occurred at the end of the gas withdrawal period. This behavior was observed in a systematic manner, and several attempts were conducted to improve the reservoir parameter values using an assisted history matching tool with poor success. They therefore suggested that the origin of this mismatch was due to one of the constitutive laws implemented in the model, rather than inadequate parameters.

During the gas withdrawal period, the gas is first trapped by the aquifer at the edge of the underground gas storage (UGS) and at high pressure. The high depletion rates will increase this local trapped saturation due to expansion. Using conventional relative permeability hysteresis curves, this additional gas is immediately mobilized as soon as the saturation becomes higher than the local trapped value, thus available for pressure support in the free gas region of the UGS. This behavior corresponded to the mismatch observed between observed and simulated pressure data.

A modified hysteresis model was successfully developed, implemented and tested to improve the forecast of the pressure regime during the withdrawal period of several UGS reservoirs in aquifer. It permitted to better reproduce the remobilization of the trapped gas by expansion during the production and therefore better predict the pressure support by free gas. From a reservoir engineering point of view, the main learning from this work was the importance of studying the effective physical mechanisms taking place in the reservoir.

The output of the new formalism developed by GDF Suez is illustrated in Figure 18 with the scanning curves in red and green (first drainage and imbibition at Swi in purple and orange). The processes have been numbered to make the link with reservoir behavior:

1. Primary Drainage up to initial gas-saturation, Sgi
2. Bounding Imbibition down to Sgr.
3. Corresponds to the gas trapped by inflow of aquifer.
4. The trapped gas remained immobile until the mobility threshold is reached by gas-expansion during depletion.
5. Gas is injected and can eventually go further on the first drainage curve.

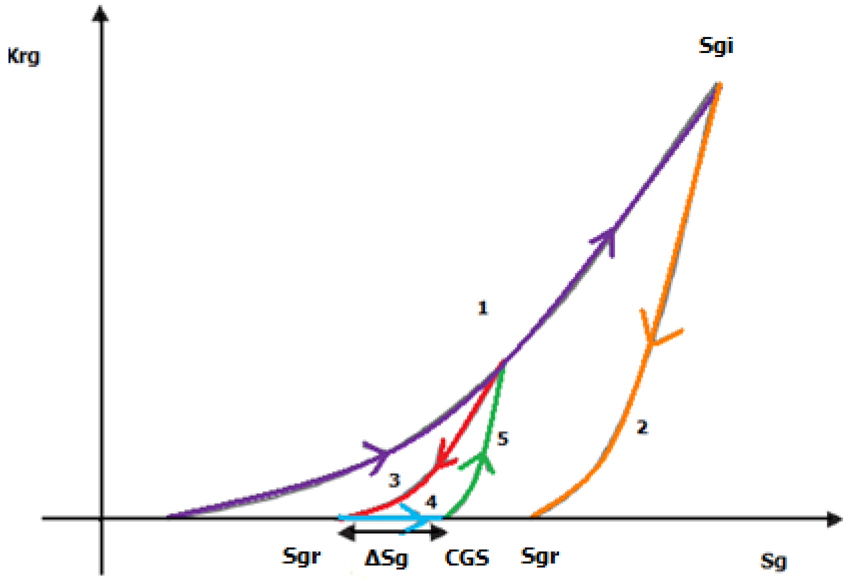

Figure 18 Shape of the krg curve used in the new formalism.

3. Conventional Relative Permeability Hysteresis Models

The two-phase hysteresis models that are typically used in reservoir simulators are those by Land, Carlson and Killough. Killough hysteresis model is used in this study. The Killough[16] model requires a bounding drainage curve and either:

1. A water-flood curve as input (bounding imbibiton).
2. A calculated water-flood curve using Land's model[10] (trapped gas table).

An empirical trapping model typically relates the trapped hydrocarbon saturation to the maximum initial hydrocarbon saturation; that is, the hydrocarbon saturation at flow reversal. In the context of waterflooding, a trapping model defines the ultimate residual gas saturation as a function of the initial water saturation. The most widely used trapping model is that of Land[11,12,13]. It is a single-parameter model, and constitutes the basis for a number of relative permeability models.

3.1 Land trapping model

Land pioneered the definition of a "flowing saturation", and proposed to estimate the imbibition relative permeability at a given actual saturation as the drainage relative permeability evaluated at a modeled flowing saturation.

Land's trapping model was developed for trapped gas saturation as a function of the initial saturation based on published experimental data from water-wet sandstone cores[10,11]. Most relative permeability models that incorporate hysteresis[12,13] are based on the trapping model proposed by Land. The trapped non-wetting phase saturation is computed as:

$$S_{gr}(S_{gi}) = \frac{S_{gi}}{1+CS_{gi}}, \tag{3.1}$$

where S_{gi} is the initial gas saturation and C is the Land trapping parameter. The land coefficient is computed from the bounding drainage and imbibition curves:

$$C = \frac{1}{S_{gr,max}} - \frac{1}{S_{gi,max}}, \tag{3.2}$$

where $S_{gi,max}$ is the maximum historically achieved gas saturation and $S_{gr,max}$ is the maximum trapped gas saturation, associated with the bounding imbibition curve. All these parameters are shown in Figure 20. The value of the Land trapping parameter is dependent on the rock type and fluids. Figure 19 shows the relationship between Sgi and Sgr for different land-correlations.

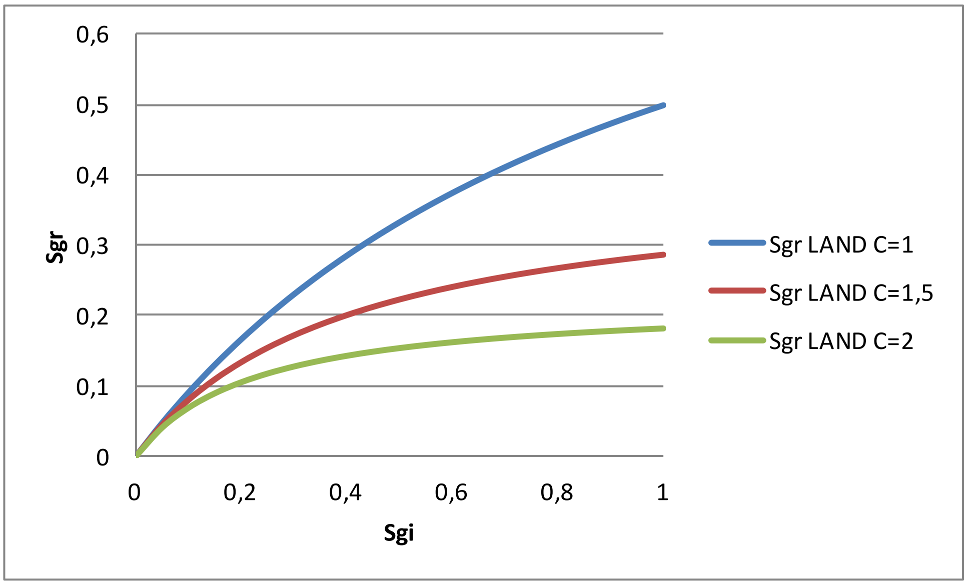

Figure 19 Residual Gas versus initial gas saturations Land correlation

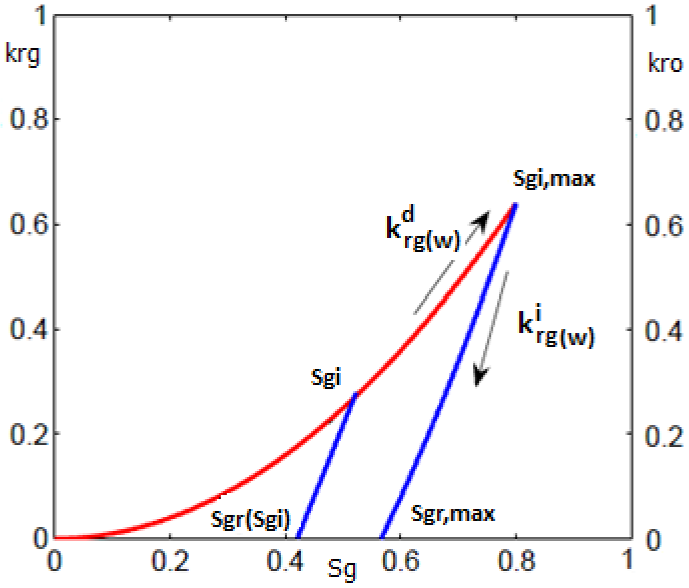

Figure 20 Parameters in evaluation of trapping and relative permeability hysteresis models (Adapted from J.E. et al[12])

3.2 Killough Hysteresis Model

Killough used Land's trapping model[15] to derive a relative permeability hysteresis model; an interpolative model for defining the intermediate scanning curves, intermediate imbibition relative permeability curves between the bounding drainage and imbibition relative permeability curves. His model allows for the use of empirical or analytical curves if experimental data if there is no experimental data available.

The non-wetting phase relative permeability along a scanning curve is computed as:

$$k_{rg}^{i}\left(S_g\right) = \frac{k_{rg(o)}^{i}(S_{g,norm}) * k_{rg(w)}^{d}(S_{gi})}{k_{rg(w)}^{d}(S_{gi,max})} \tag{3.3}$$

where S_{gi} is the initial gas saturation, $S_{gi,max}$ is the maximum gas saturation from the bounding imbibition curve, as in Figure 20, and $S_{g,norm}$ is the normalized gas saturation computed as:

$$S_{g,norm} = S_g + \frac{\left(S_g - S_{gr,max}\right)\left(S_{gr,max} - S_g\right)}{\left(S_{gi} - S_{gr,max}\right)} \tag{3.4}$$

In equation (3.3) $k_{rg(w)}^{i}$ and $k_{rg(w)}^{d}$ represent the relative permeability values on the bounding imbibition and drainage curves, respectively. These variables are shown in Figure 20.

3.3 Corey-correlation

If Swc is the irreducible water saturation, and Sgr is the residual gas saturation after water flooding, we can calculate the normalized water saturation value:

$$S_{wn}(S_w) = \frac{S_w - S_{wc}}{1 - S_{wc} - S_{gr}} \tag{3.5}$$

The Corey correlations of the relative permeability of gas and water are then;

$$k_{rg} = K_{rg}\left(1 - S_{wn}(S_w)\right)^{n_g} \tag{3.6}$$

$$k_{rw} = K_{rw}\left(S_{wn}(S_w)\right)^{n_w} \tag{3.7}$$

Sensitivity of Ng (Corey correlations of the relative permeability of gas) on recovery of residual gas is reported in chapter 6.3.

4. Modeling Approaches Residual Gas Mobility Ormen Lange

This chapter reviews the relative permeability and capillary pressure data used under initialization and production in the Hydro Dynamic Aquifer Model (HDA). It aims to explain the hysteresis-concept, and how the modeling of residual gas saturation under depletion in Ormen Lange is done. An explanation of why initialization of the model was done without scanning-curves between bounding drainage and imbibition is also given throughout the chapter.

4.1 Initialization of Hydrodynamic Aquifer with Scanning-Curves

The hysteresis is implemented in the model by keeping track of the minimum historically achieved water saturation and the maximum historically achieved gas saturation for each grid block. These two properties determine how much gas is trapped, and hence which scanning curve is to be used for the relative permeability. Under primary drainage the actual saturations are equal to the historically achieved maximum saturations, and hence the primary drainage bounding curve is used. For bounding imbibition and secondary drainage the historically achieved extreme saturations differ from the actual saturations, and hence a derived scanning curve is used. If the historically achieved extreme saturations are equal to the absolute extremes, (connate water or maximum gas saturation) then the bounding imbibition curves are used.

For the Killough model, primary drainage, bounding imbibition, and trapping tables can be defined as described in chapter 3.3. For initialization a bounding imbibition curve measured by Norske Hydro[1] on Ormen Lange material is used, with some modifications due to recent SCAL results. Recommended end point values from the work done by Norske Hydro work was 0.15 for krw (Sgr=0.25) and 0.7 for krg (Sgi=0.75). Relative permeability curves from these centrifuge experiments were evaluated by curve fitting of saturation normalized relative permeability data by use of Corey exponents. Recommended values for Ng and Nw in bounding imbibition was 2.4 and 4.0.

Recent SCAL performed on plug material from well 6305/7-D-7H[18] shows residual gas saturations (Sgr) in the range of 0.21-0.41. The new experiments display higher krg and lower krw than earlier found. Therefore a new range has recently been created, with krw(Sgr) varying from 0.03 to 0.20 and krg(Sgi) ranging from 0.5 to 1.36. Results and impact of the experiments are discussed in further chapters.

The bounding imbibition curve (for initialization of the model) used in this work has, for good quality reservoir rock (Egga), a krg value of 0.7, krw 0.15, Sgr varying from 0.21-0.41, Ng 2.4 and Nw 4.0. Due to lower quality rock in Sub-Egga krw for these zones has been set to 0.05. Primary drainage relative permeability curves are created by decreasing the Corey-number, thus increasing the relative permeability for gas and water in this process compared to imbibition relative permeability curve. In primary drainage a value of 2.0 and 3.0 for Ng and Nw is used respectively (Sgr=0). Note that these values for Ng and Nw are not measured, but modified in order to create a primary drainage relative permeability curve that lays over the bounding imbibition relative permeability curve. This is illustrated in Figure 21, where a sketch of the curves for initialization with hysteresis (Egga) is provided.

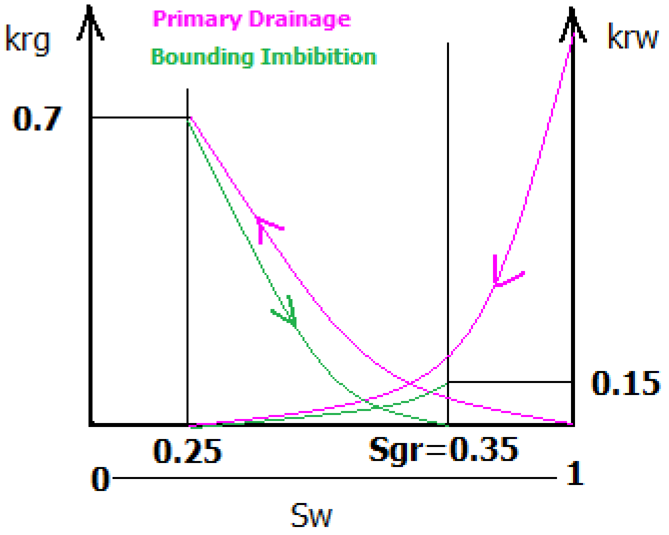

Figure 21 Primary Drainage/ Bounding Imbibition as used in initialization of the hydrodynamic aquifer model (conceptual picture)

Using Killough, MoReS (the Shell proprietary simulation software) creates scanning curves between primary drainage and bounding imbibition with equal spacing between each curve. When no trapping tables are defined, they are created internally from the bounding imbibition and primary drainage tables, using a specific Land correlation in MoReS.

In Figure 22 data on residual gas for Ormen Lange is plotted against initial gas saturation[14]. Land's trapping model with different trapping constants C is also included. The data are from reservoir condition water-floods. Data on the trapped gas saturation from a BP Amoco study on well 6305/7-1 is included. These data together with the 6305/5-1 data seems to fit a Land's model with trapping constant C of 1.5-2.0. One of the experiments on 6305/8-1 also fits in here while the two other 6305/8-1 data sets indicate a trapping constant of 1.0. An explanation for this difference could be that the cores are taken from different zones in the reservoir.

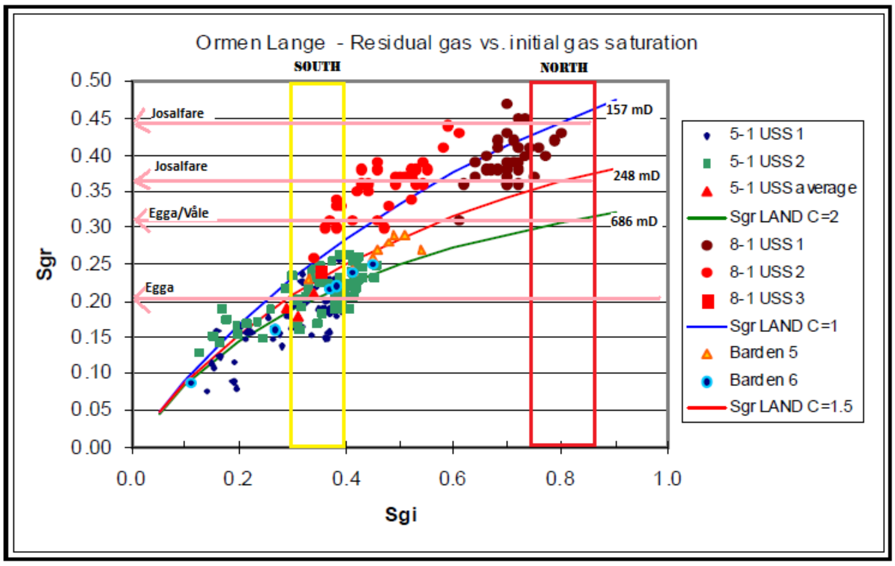

Figure 22 Residual gas versus initial gas saturation

The effect of using scanning curves under initialization of the Hydrodynamic Aquifer[9] (HDA) is only expected to have effect in the transition zone, where the gas-saturation will be lower than 1-Swc. This is the case for grid-blocks in the South and the in the saddle (segment 4 and 5), see Figure 23, where the gas-saturation is ranging from 0.20 to 1-Swc. Hence, by implementing hysteresis and scanning curves, these blocks will end up at lower residual saturation than the blocks with gas-saturation 1-Swc. However, since the gas saturation in most of the grid-blocks in the reservoir initially is almost at 1-Swc (defined in the relative permeability model), simplification can be done by initializing the HDA without scanning-curves. This simplification enables a straight forward method for implementation of secondary drainage curves for modeling of residual gas saturation under depletion, with a saturation threshold required for remobilizing. Implementation of a remobilization threshold above residual value for all the different scanning curves would significantly complicate implementation of the relative permeability model. This study mainly looks into understanding the order of magnitude of potential contributions from residual gas and simplification by excluding the scanning curves is therefore accepted.

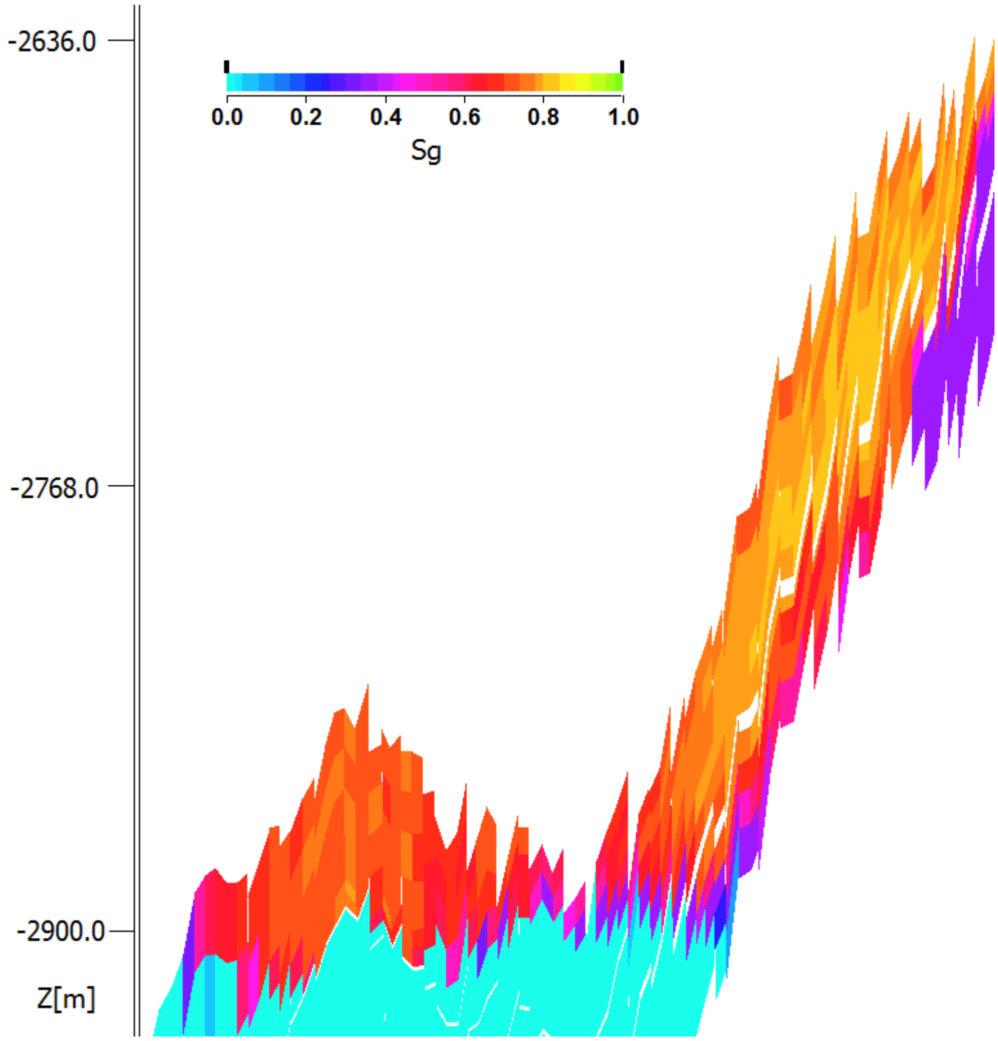

Figure 23 North-south cross section of the Ormen Lange field before initialization of the HDA. Saturation shown by color; the lower gas-saturations in the transition zone show that it is important to use scanning curves when modeling residual gas saturations

4.2 Initialization of Hydrodynamic Aquifer without Scanning-Curves

To simplify the modeling, only the bounding imbibition curve from Figure 21 was used during "initialization", where the hydrodynamic equilibrium is established through 1/2million years of simulation prior to production. This implies that the drainage curve is retracing the imbibition curve and the other way around. Simplification by disregarding hysteresis under imbibition is a pessimistic approach, as more gas will be trapped using the bounding imbibition curve only. All grid-blocks going through a complete imbibition process, independent of initial gas saturation, will end up with the same residual gas-saturation. A comparison of residual gas-volumes by using the two different methods is provided in Chapter 5.1.

4.3 Production mode/Forecast (From 2007→)

Also in production mode, while the reservoir is depleted, the behavior of the gas saturation will depend on its history. The residual gas going into a secondary drainage process is expected to follow a different relative permeability curve than for primary drainage. This behavior is not captured in the previous Ormen Lange hydrodynamic aquifer model[9]. From the literature reviewed we now understand that such simplification by disregarding hysteresis and the existence of a gas saturation threshold under depletion may result in errors when estimating recovery.

The saturation threshold for residual gas to remobilize is observed in the literature to range from 3% to 15%[3,7,19]. The secondary drainage relative permeability curve for residual gas used in this work is shown in blue in Figure 24. The imbibition curve in Figure 24 is the same as under initialization of the hydrodynamic aquifer, and this curve will be retraced under drainage for gas with higher gas saturation than residual; a grid-block with gas-saturation higher than 0.35 will go back on the original imbibition curve in a secondary drainage cycle. A grid-block with gas saturation of 0.35 or lower will follow the specified secondary drainage curve, reaching CGS in order to remobilize. The value of CGS for residual gas has been varied from 0.35 to 0.45.

The relative permeability curve for any secondary imbibition process is assumed to retrace the secondary drainage curve, for both gas and water.

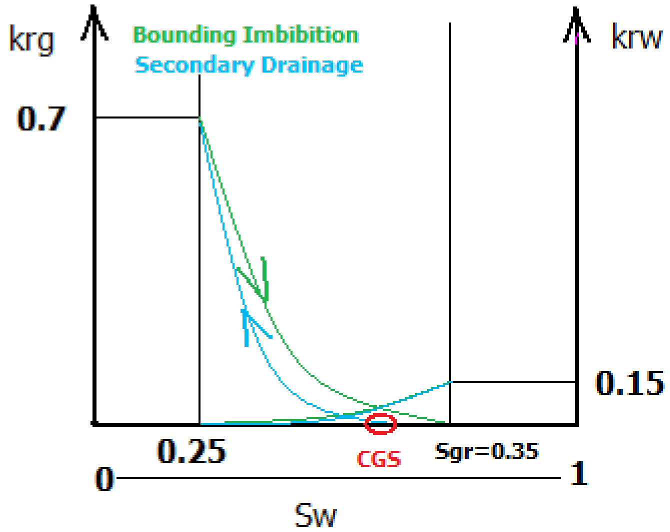

Figure 24 Bounding Imbibition, Secondary drainage (conceptual picture)

4.4 Capillary Pressure

Average drainage capillary pressure models for principle rock classes (Egga and Sub Egga) have been used to implement hydrostatic initialisation using flat contacts prior to Hydro Dynamic Aquifer (HDA) initialisation. The capillary pressure curves are based on saturation height functions from the OL simulation model[17].

Results from spontaneous and forced imbibition experiments displaces a very flat curve under spontaneous imbibition (water-wet system), and very small amounts of water produced in centrifuge and porous plate imbibitions experiments (i.e. limited forced imbibition). Imbibition experiments covered core material ranging from 80-1000 mD as shown in Figure 25.

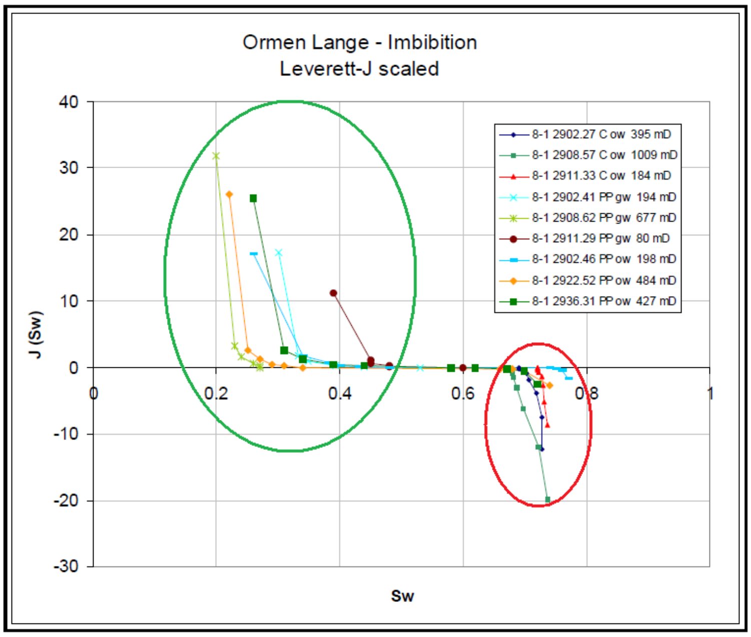

Figure 25 Imbibition capillary pressure data from porous plate and centrifuge experiments. Strongly water wet system, very limited forced imbibition. (Spontaneous imbibition green, forced imbibition red)

It is known that the relationship between capillary pressure and saturation, in two-phase flow problems demonstrates hysteresis effects. However, for this problem we assume that capillary pressure hysteresis can be considered a second order effect because of the very short transition zone. We ignore contact angle hysteresis, and assume no wettability change. Thus, the bounding imbibition and the secondary drainage capillary hysteresis curves are identical.

5. Initialization of Simulation Model Including Sensitivities

In this chapter some of the results from initialization of the model, with different values of Sgr, will be displayed. The main purpose of this chapter is to show the great amount of residual gas that initially resides in Ormen Lange, and the variation of residual gas volume in the different segments from North to South. It also quantifies the impact on residual volume by implementing scanning curves.

5.1 Initialization of the Hydrodynamic Aquifer Model without Scanning-Curves

For initialization without hysteresis scanning-curves 3 different relative permeability models have been implemented, see Table 2. The relative permeability curve for water is the same for all cases, see Figure 26. All the values are within the new range of Sgr, based on most recent lab-results (see chapter 4.1.1). Sgr is the only value altered in the different models. The variation in residual gas saturation as a function of rock-quality is, for simplicity, ignored resulting in the same Sgr value for all grid-blocks in each case (I1-I3), no differentiation between clean sand and Heterolithics.

Relative Permeability curves for Initialization of HDA						
Case	krg	krw_egga	krw_subegga	Ng	Nw	Sgr
I1	0.7	0.15	0.05	2.4	4.0	0.25
I2	0.7	0.15	0.05	2.4	4.0	0.30
I3	0.7	0.15	0.05	2.4	4.0	0.35

Table 2 Different realizations for *initialization* without hysteresis

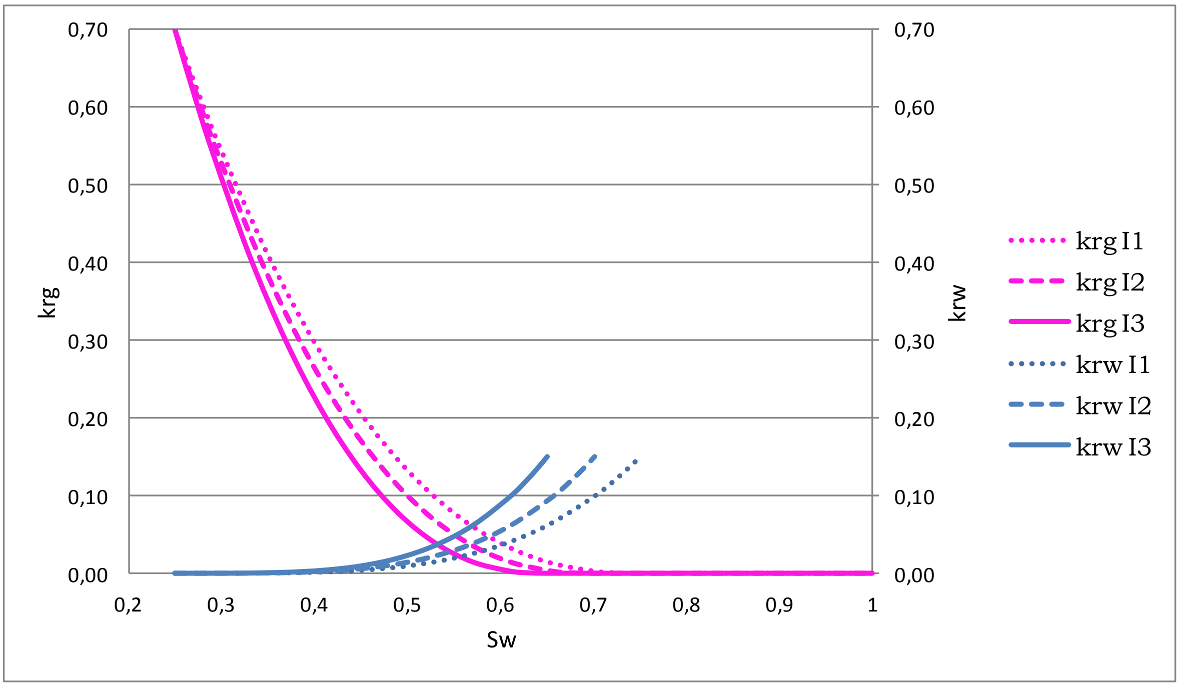

Figure 26 Imbibition relative permeability curves for 3 cases; I1-I3

Table 3 provides the initial residual gas volumes per segment for the three cases, divided into Egga and Subegga. 0.3 is the new average vale for residual gas saturation in Ormen Lange.

This value has been updated from the previous average of 0.25 as a result of recent lab experiments done on core-material from the 6305/7-D7 well[32].The new average value results in 13Bcm additional residual gas in the total field compared to I1. Figure 27 provides initial residual gas volumes for the total field (Egga and Subegga) per segment for all cases. For the segment definition, see Figure 2. The main observation is that, for the relative permeability model in Figure 26, the residual gas volume in the field increases almost linearly with Sgr. This is different when scanning curves are used.

Segment	Sgr=0.25		Sgr=0.30		Sgr=0.35	
	Subegga	Egga	Subegga	Egga	Subegga	Egga
1a	2,05	4,28	2,41	4,97	2,74	5,61
1b	1,66	2,86	1,97	3,38	2,25	3,89
2	5,44	9,52	6,45	11,22	7,41	12,76
3a	1,23	0,62	1,41	0,71	1,59	0,81
3b	7,44	4,21	8,85	4,81	9,93	5,43
3c	2,61	0,94	3,18	1,12	3,54	1,26
4	1,19	1,68	1,77	2,38	2,67	4,71
5	0,04	16,09	0,00	20,41	0,00	24,50
Sum	21,66	40,20	26,03	49,00	30,12	58,96
Total	61,86		75,04		89,09	

Table 3 Residual Gas Volumes in Bcm per segments for the different Sgr values

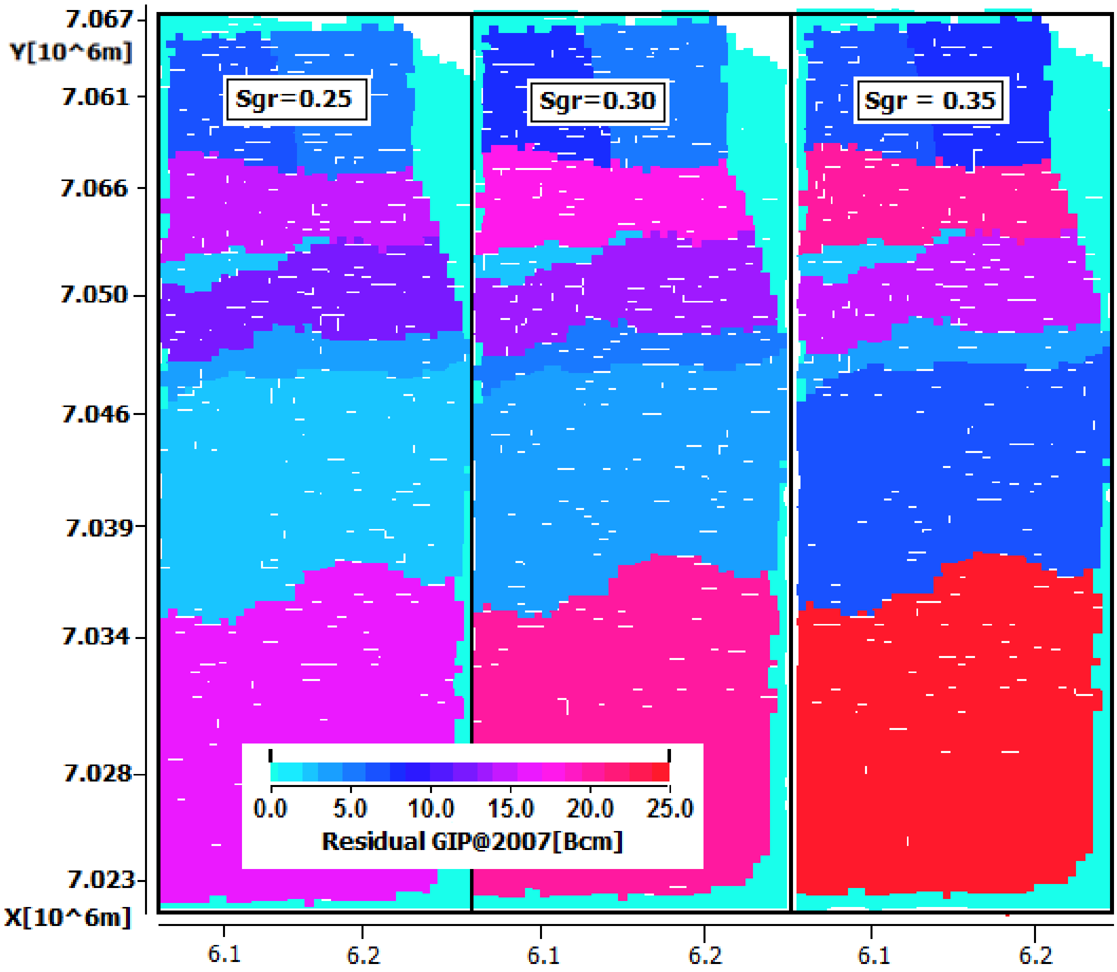
7.067
Y[10^6m]
7.061
7.066
7.050
7.046
7.039
7.034
7.028
7.023
X[10^6m]
Sgr=0.25
Sgr=0.30
Sgr = 0.35
0.0
5.0
10.0
15.0
20.0
25.0
Residual GIP@2007[Bcm]
6.1
6.2
6.1
6.2
6.1
6.2

Figure 27 Initial residual gas volume per segment (Egga+Subegga) for tree cases; I1-I3

From the above figure and tables it is clear that most of the residual gas resides in segment 5. This residual gas zone can be explained by the slowing aquifer-rate after the Storegga-slide; gas receded from the south towards the north creating a residual gas zone (see chapter 2.1). Most of the gas in the north is flushed away by the aquifer, leaving a great amount of residuals in segment 1 and 2. Also in the mid-north (Segment 3) some of the gas has been pushed towards the south by the aquifer, leaving residual gas behind.

5.2 Comparison of Initialization with and without Scanning-curves

The relative permeability model I3 has been used to compare residual gas volumes after initialization with and without scanning curves. The relative permeability model for initialization with hysteresis scanning curves is shown in Figure 28. The scanning curves are created automatically, with a specific Land correlation in MoReS, see chapter 4.

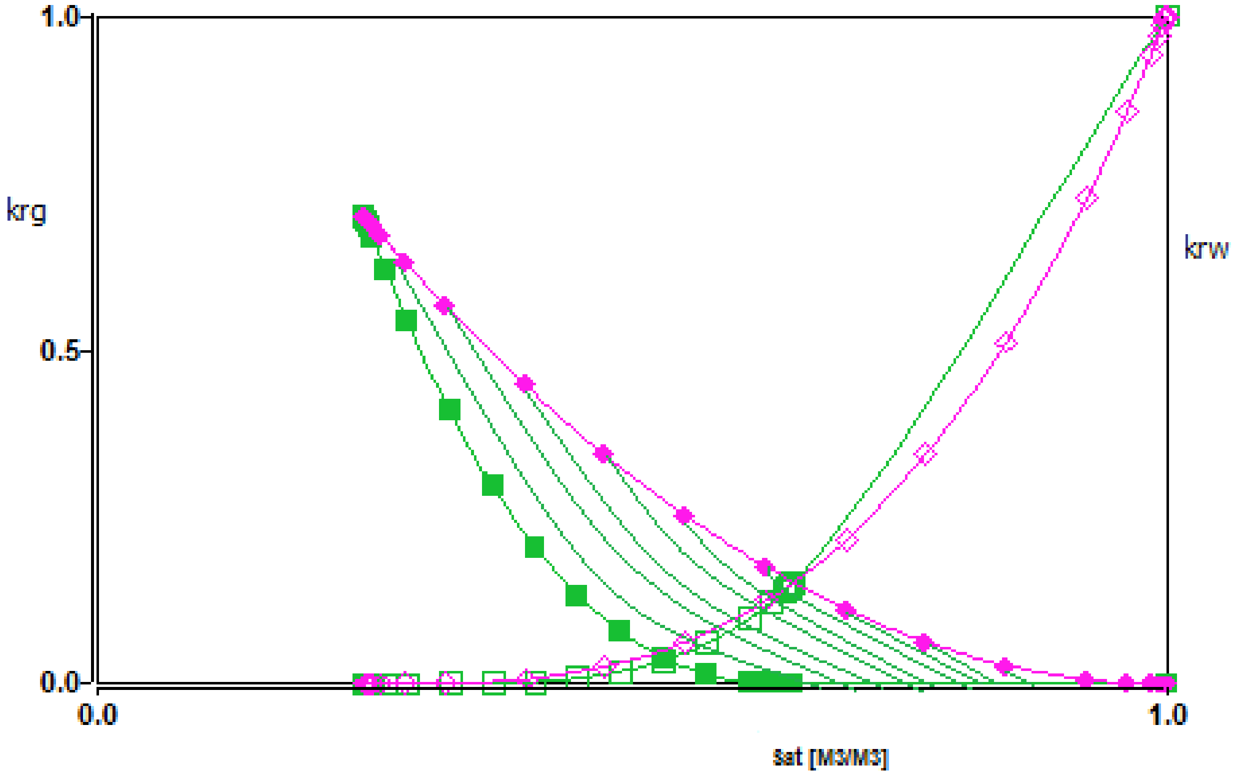

Figure 28 Imbibition relative permeability curves for initialization with scanning curves. Drainage curves in pink; imbibition curves in green.

The residual volumes after initialization with scanning curves are approximately 20% lower compared to the other model. The reason is explained in chapter 4.1; the effect of residual gas saturation being dependent on the initial gas saturation. Figure 29 provides the top-layer gas-saturations in Egga for both methods. It can be seen that by disregarding scanning-curves all the trapped gas ends up with saturations close to the bounding imbibition residual gas value (0.35 in purple). By use of scanning-curves, shown in the right side picture in Figure 29, the gas-saturation in this area is more correctly calculated, resulting in less residual gas volume.

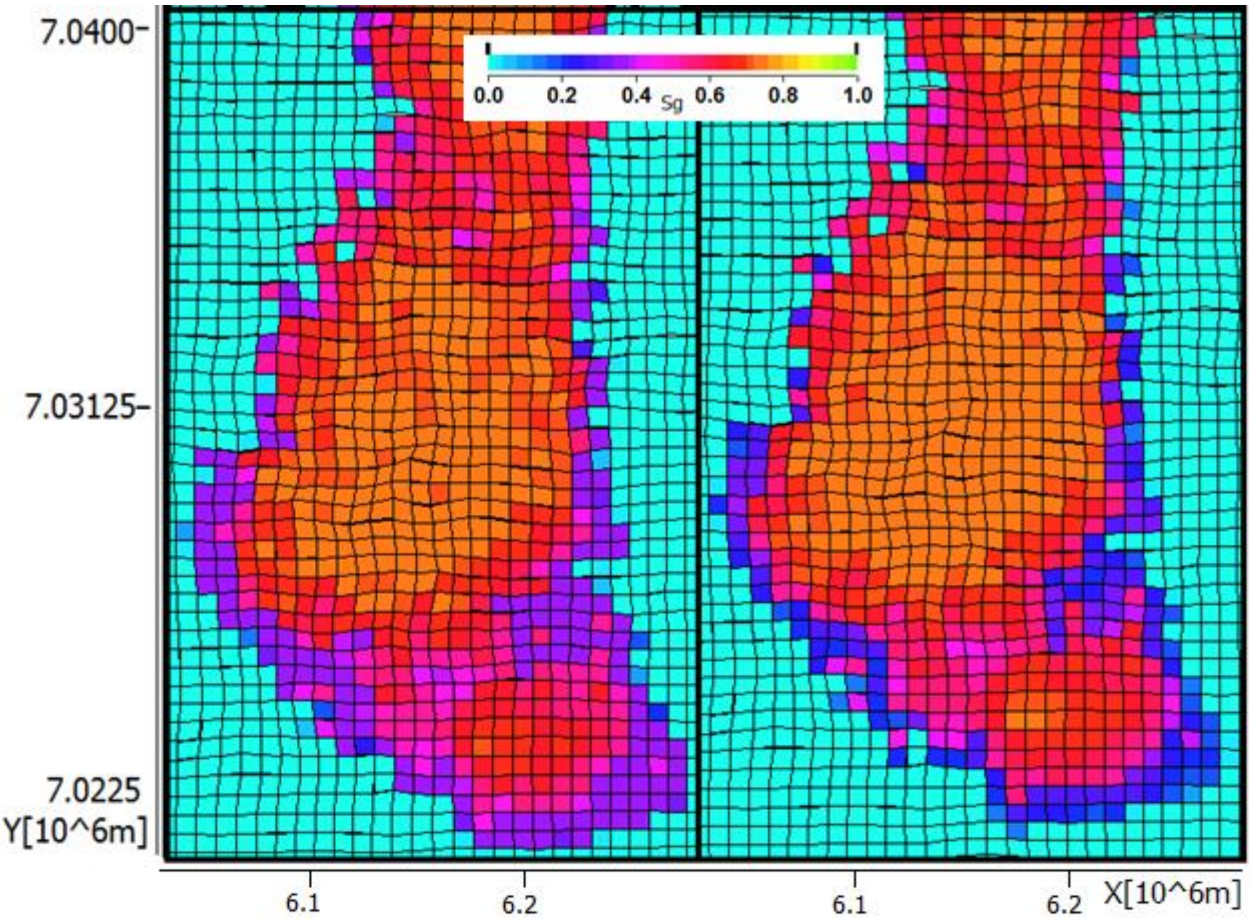

Figure 29 Comparison of gas-saturation after initialization with (right) and without (left) use of scanning-curves.

Table 4 provides the distribution of total GIIP for both methods. The difference in residual gas volume is significant in Segment 4 and 5, where 12Bcm additional gas is trapped when the scanning-curves are disregarded. The initial gas saturation in segment 1, 2 and 3 is close or equal to 1-Swc, hence the effect of using scanning-curves is much smaller in these segments.

Segment	Bounding Curves Only (X)		Scanning Curves Included (Y)		Difference (X-Y)	
	Residual	Mobile	Residual	Mobile	Residual	Mobile
1a	8,35	5,52	7,93	6,30	0,42	-0,78
1b	6,14	6,01	5,43	7,39	0,71	-1,39
2	20,17	14,33	18,34	16,55	1,83	-2,22
3a	2,40	4,97	2,24	5,00	0,16	-0,03
3b	15,36	55,97	13,47	59,68	1,89	-3,71
3c	4,80	43,44	4,38	43,70	0,42	-0,27
4	7,38	168,78	4,24	166,75	3,14	2,02
5	24,50	100,43	15,74	111,50	8,76	-11,07
Total	**89,09**	**399,44**	**71,76**	**416,88**	**17,33**	**-17,45**

Table 4 Comparison of GIP distribution with/without scanning-curves, gas-volumes in Bcm.

6. Forward Simulation Including Sensitivities

6.1 Recovery from Residual Gas

When going from initialization of the model to production mode, in 2007, a different relative permeability model for all residual gas was implemented. A bounding secondary drainage curve is applied for all the grid-blocks that went through a full imbibition process during hydrodynamic initialization, to end up at Sgr, as explained in chapter 4.3.3. The grid-blocks with higher gas-saturation than Sgr from bounding imbibition will retrace the bounding imbibition curve for drainage.

6.1.1 Residual gas saturation 0.35 from Bounding Imbibition (I3)

After the initialization Case I3 (Sgr=0.35) in chapter 5.2.1, four cases have been run in forecast. The critical gas-saturation was varied from 0.35 to 0.45 in three increments, see Table 5. In all cases the relative permeability for water and gas is 0.1 and 0.7 respectively while Corey exponents are kept the same. A graphical representation of the 4 relative permeability models is shown in Figure 30.

Secondary Drainage RelPerm in Forecast for Sgr 0.35					
Case	krg	krw	Ng	Nw	CGS
F1	0.7	0.1	2.4	4.0	0.35
F2	0.7	0.1	2.4	4.0	0.38
F3	0.7	0.1	2.4	4.0	0.40
F4	0.7	0.1	2.4	4.0	0.45

Table 5 Four different cases for Sgr equals 0.35 in *production mode/forecast*

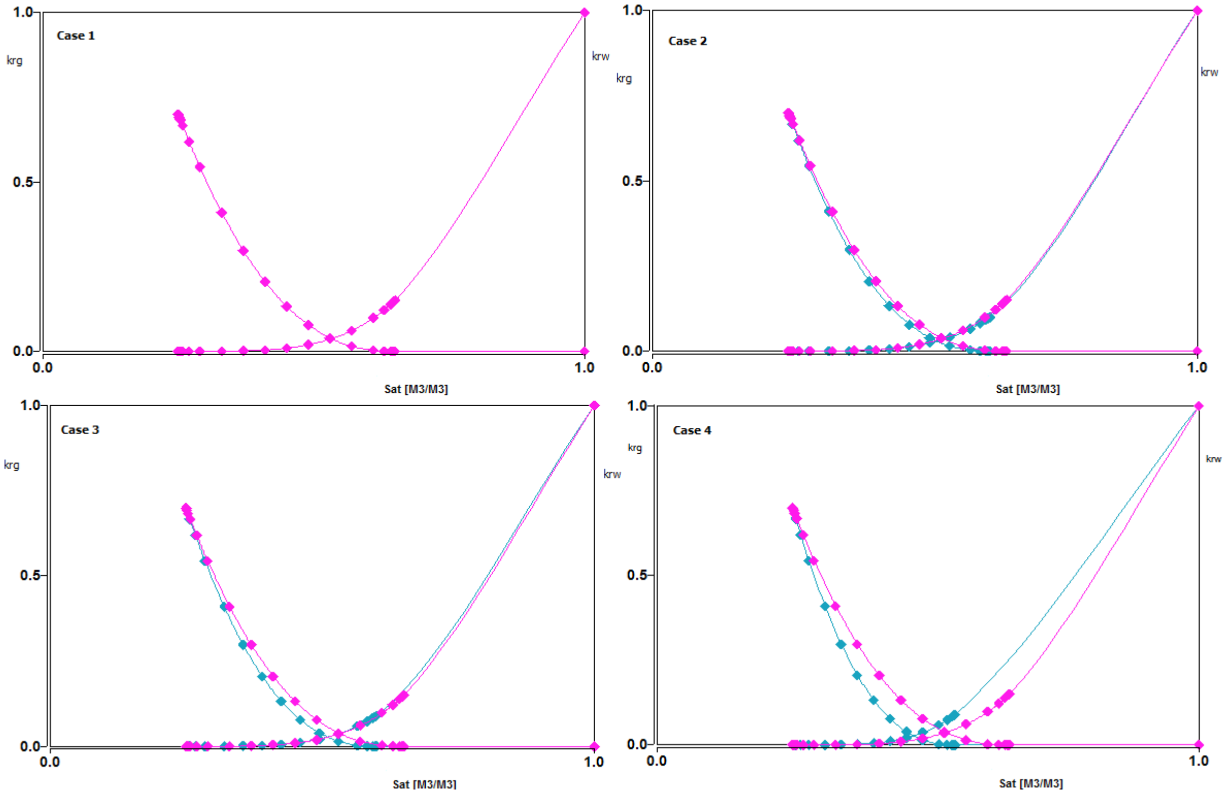

Figure 30 Relative permeability curves under initialization F1(upper left)-F4 (lower right)

The recovery factors in 2040 for Case F1 (CGS=Sgr) for all segments are summarized in Table 6. There is no recovery from Segment 1, and very limited recovery in segment 2. Pressure depletion in the Northern area (segment 1-2) is limited and therefore limited mobilization of residual gas occurs in this area. Extensive baffling across the northern part of the field limits the communication with the main producing areas which again limits the pressure depletion in this area. Sensitivities on fault transmissibility within the established history matching range have very little impact on the recovery of residual gas in segment 1 and 2. The recovery from residual gas in segment 3 and 4 is much higher as the main off-take in the field occurs in this area thus resulting in high pressure depletion throughout the whole area. Total recovery from residual gas is 18%. The overall recovery, both mobile and residual gas, is 64%.

Segment	Subegga		Egga		Total	
	Residual	Mobile	Residual	Mobile	Residual	Mobile
1a	0 %	0 %	0 %	0 %	0 %	0 %
1b	0 %	0 %	0 %	0 %	0 %	0 %
2	0 %	1 %	4 %	42 %	2 %	33 %
3a	0 %	6 %	52 %	84 %	17 %	81 %
3b	13 %	61 %	54 %	84 %	27 %	80 %
3c	31 %	78 %	73 %	86 %	42 %	84 %
4	36 %	74 %	52 %	87 %	46 %	85 %
5	0 %	0 %	22 %	64 %	22 %	64 %
Sum	11 %	65 %	21 %	76 %	18 %	75 %
Total	47 %		68 %		64 %	

Table 6 Recovery Factors @1.1.2040 Case F1

The recovery factors for all cases (F1-F4) are shown in Table 7. Total recovery from the field is almost not affected by the implementation of a mobility threshold for residual gas. The critical gas saturation in case F4 is 0.10PV higher than the residual gas saturation, which means that the residual gas needs to expand at least 28% in order to remobilize. Although this is a high, pessimistic CGS, it only reduces the recovery from residuals with 4%, showing how important the rapid expansion of gas during depletion is for the recovery of residual gas. Total recovery from residual gas is 14%, and overall recovery decreases with only 0.8% compared to the case with no mobility threshold.

Segment	**CGS**			
	0.35	0.38	0.40	0.45
1a	0 %	0 %	0 %	0 %
1b	0 %	0 %	0 %	0 %
2	2 %	2 %	2 %	2 %
3a	17 %	17 %	16 %	16 %
3b	27 %	24 %	22 %	18 %
3c	42 %	44 %	40 %	33 %
4	46 %	45 %	43 %	39 %
5	22 %	21 %	20 %	18 %
Total	18 %	17 %	16 %	14 %

Table 7 Recovery Factors Residual Gas Total Field @1.1.2040 Case F1-F4

6.1.2 Residual gas saturation 0.30 from Bounding Imbibition (I2)

For the new base case, Sgr=0.3, the effect on total recovery from residual gas by implementing a mobility threshold above residual gas saturation is shown in Figure 31.

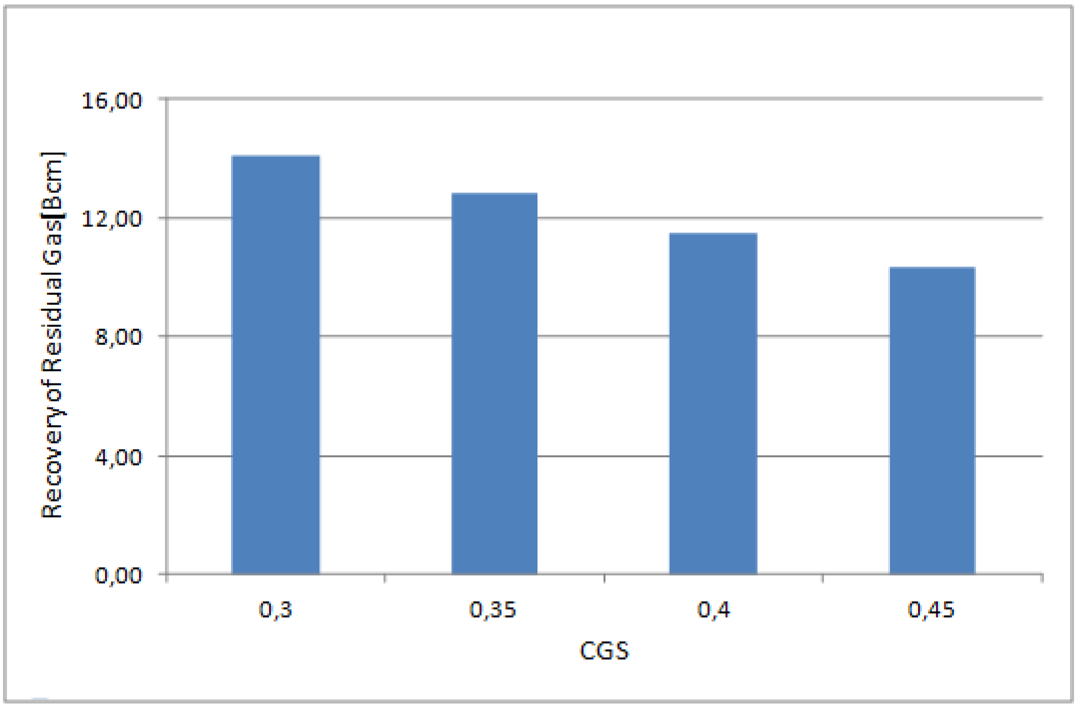

Figure 31 Recovery from residual gas (Sgr = 0.30) vs critical gas-saturation

Figure 32 illustrates the decrease in residual gas recovery per segment when CGS is 0.40 compared to when no mobility threshold above Sgr is implemented (Sgr=CGS=0.3). The difference in segment 4 and 5 is limited. Before water-breakthrough the pressure-decline in this area is steep, and the residual gas will expand and reach critical gas saturation almost independent of its value. Figure 32 shows that the implementation of the mobility threshold has greatest impact on segment 3b. The reason is the abandonment pressure and the depletion rate towards the end of production. With smaller differences in pressure towards the end of field life, gas is expanding at lower rate, hence getting more sensitive to the critical gas saturation.

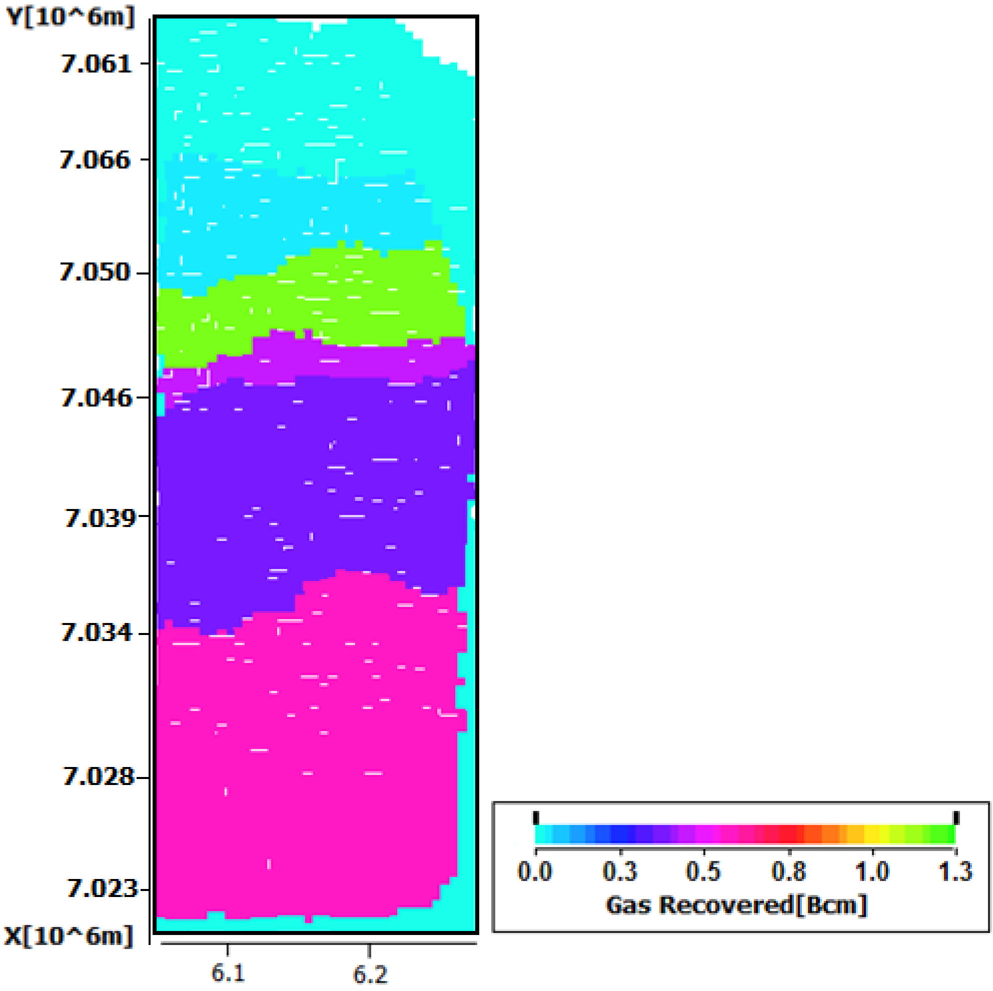

Figure 32 Difference map of gas recovery per segment: the difference between CGS = Sgr = 0.30 and CGS = 0.4 is shown.

6.2 Residual Gas Physics – Discussion of Results

In this chapter results from initialization with case I3 (Sgr=0.35, chapter 5.1) followed by forecasting case F1 (CGS=0.45, chapter 6.1) are discussed.

6.2.1 Location in the Reservoir versus Saturation Change

To understand the process and physics behind expansion and remobilization of residual gas during depletion, and to be able to check whether the different grid-blocks are following the right relative permeability curve for the different processes, some grid blocks have been tracked through the production period, from 2007 to 2040. Grid-block tracking enables checking of current pressure, saturation, relative permeability, accumulated gas and accumulated water for all time steps. This is very useful in order to understand the mechanisms of the residual gas production in different parts of the reservoir. Saturation and GIP for each grid-block will change depending on location.

A grid-block that initially contains *residual gas* has the following opportunities for saturation change during depletion in order to reach critical saturation:

I. A grid-block that is isolated from other grid-blocks containing mobile gas will increase in saturation due to expansion only. As it will not experience any gas-inflow, there will be no mass change before it reaches critical gas saturation. A typical location for such a grid-block will be on the edge of the reservoir, in well depleted areas (see the white square in Figure 33). Further discussion of saturation change for this grid-block can be found in chapter 6.2.2.

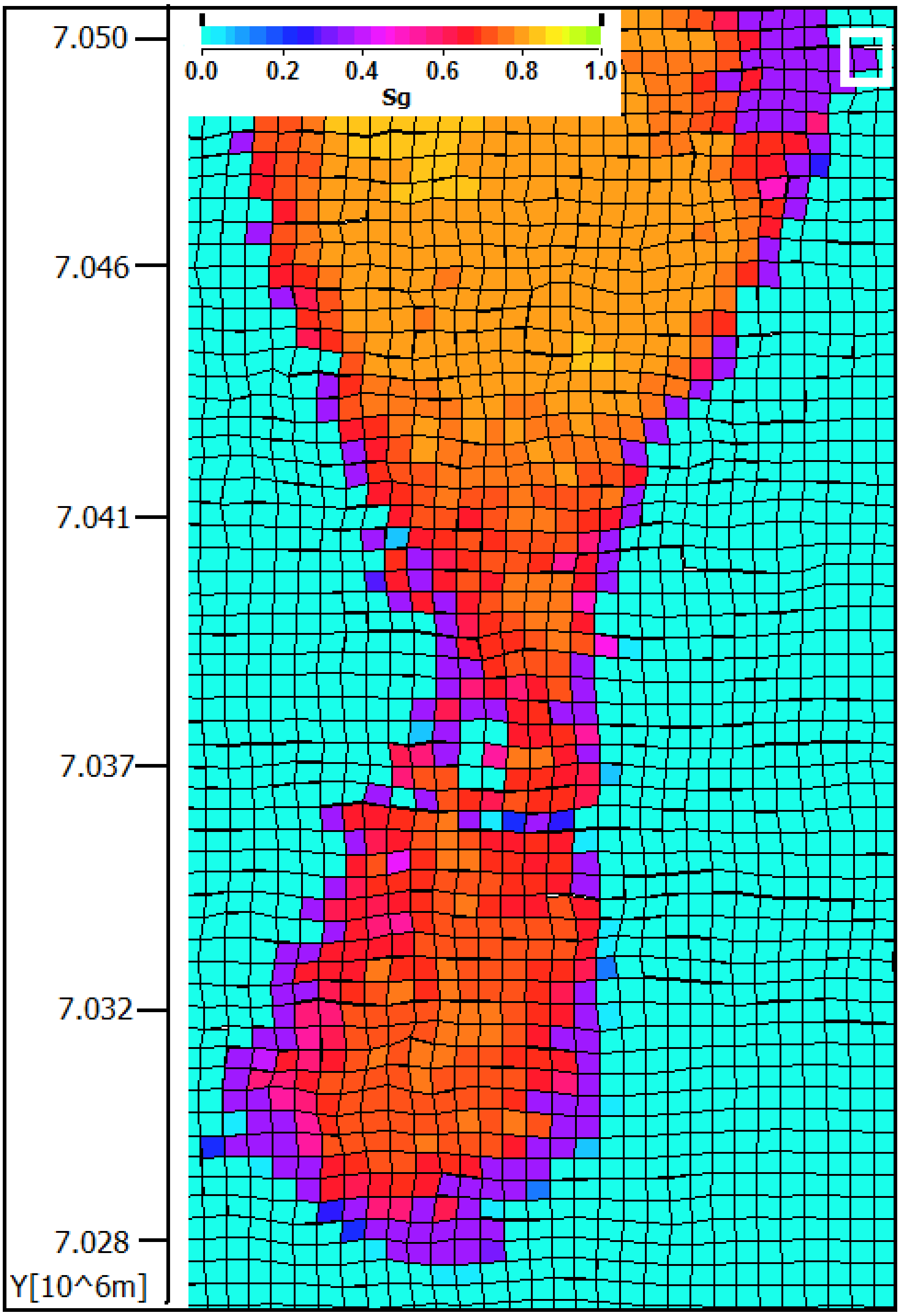

Figure 33 Saturationmap@2007, location of grid-block 35.72.3 → no potential gas-inflow from surrounding grid-blocks containing mobile gas

II. A grid-block sitting in the center of the reservoir will typically experience gas-inflow from surrounding grid-blocks, reaching critical gas saturation faster than blocks being isolated from surrounding mobile gas. Typical location of such grid-blocks is shown by the white squares in Figure 34. As gas is flowing in, the mass of gas in the grid-block will increase until remobilization. Further discussion of saturation change for these grid-blocks in chapter 6.2.3.

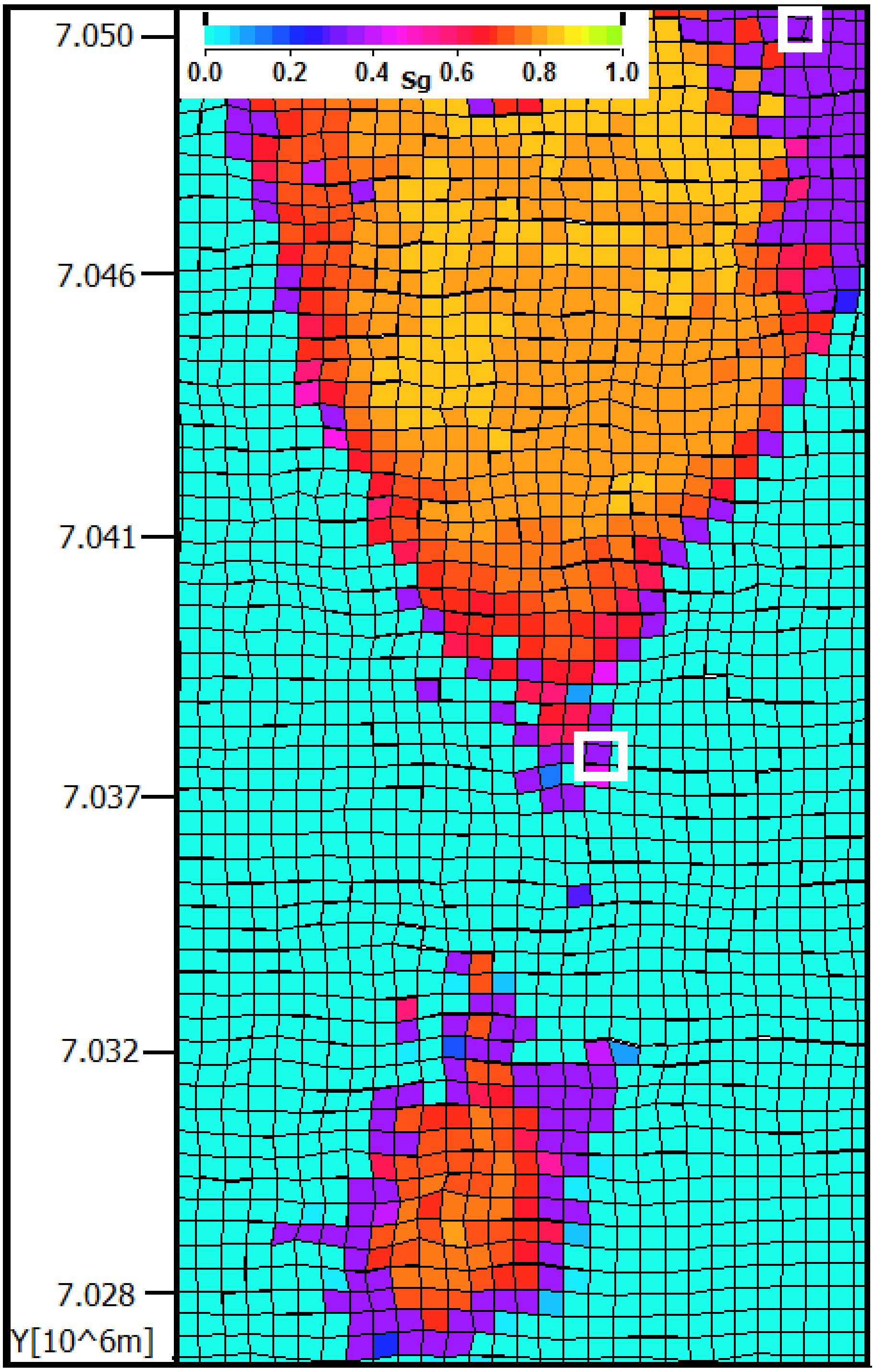

Figure 34 Saturationmap@2007, location of grid-blocks (30.78.3 and 22.46.5) → potential gas-inflow from surrounding grid-block containing mobile gas

III. A grid block that is totally isolated from depleted areas will not experience any change as the pressure will remain constant. Because of very bad communication with the rest of the field, the grid-blocks in the northern part will stay the same in terms of GIP and saturation. Pressure maps before and after production are provided in Figure 35, showing no or limited depletion in the North.

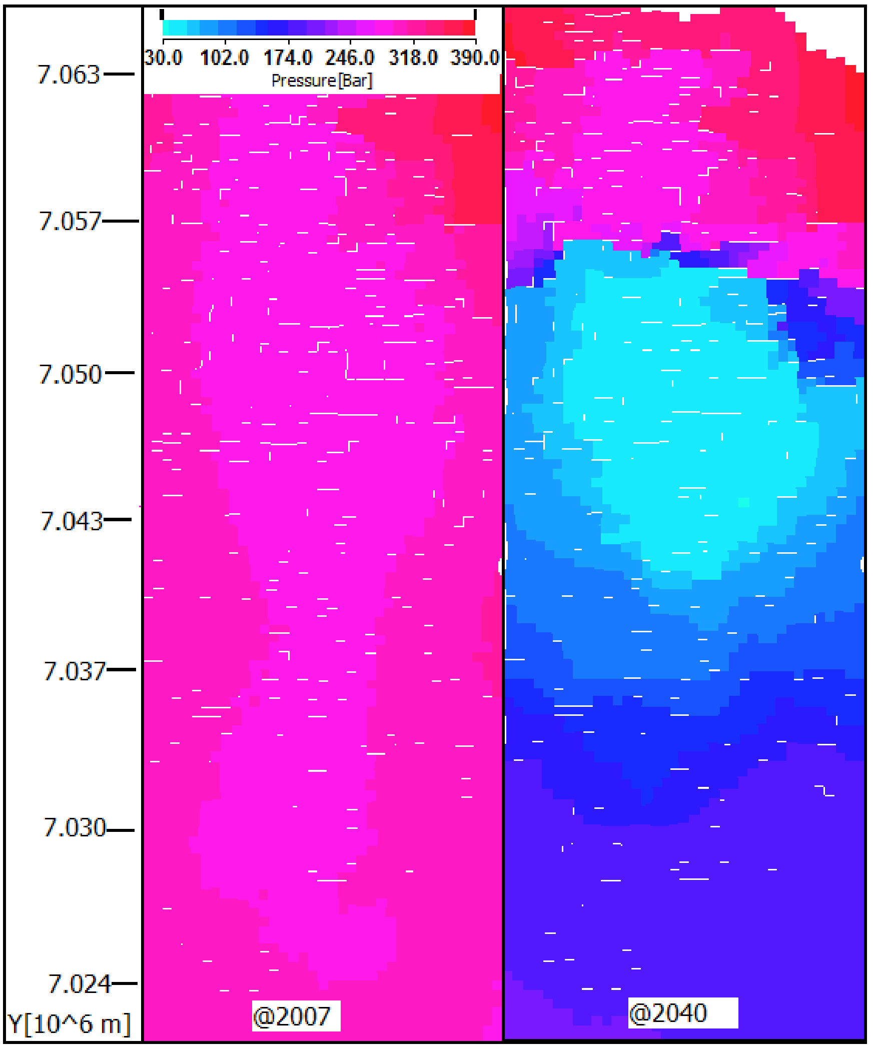

Figure 35 Pressure maps Ormen Lange before and after production (2007→2040)

Initial pressure on the left picture in Figure 35 is compared with the pressure in 2040 on the right side picture. As can be seen the reservoir pressure after production in 2040 in the North (Segment 1 and 2) is very high. This part of the reservoir experiences no or very limited depletion as a result of a fault with low transmissibility crossing the reservoir in segment 2. Consequently the pressure in 2040 is low, and residual gas recovery is very good in these segments (segment 3 and 4). Aquifer influx in the South during production makes further depletion impossible due to waterproduction, ending up on around 120bar in 2040.

Remaining GIP per km2 before (2007) and after (2040) production is provided in Figure 36. There is a great amount of gas volume left behind in the Northern part of the field, from the figure it looks like the GIIP remains constant throughout the production-period in this area. In the South higher GIP density remains as a result of water-breakthrough. The local structural height in the south-east gets partly "cut off" by the encroaching aquifer.

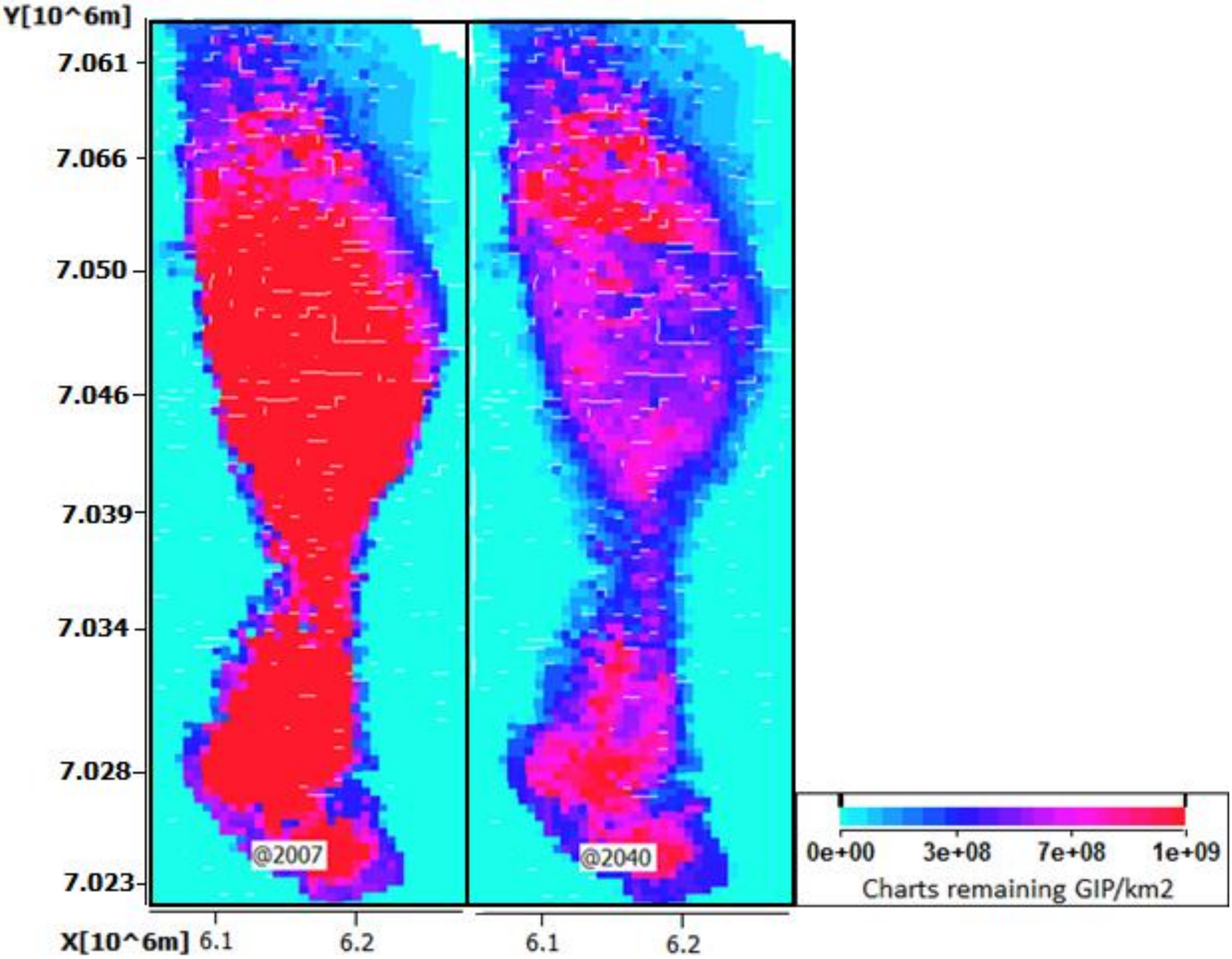
Y[10^6m]
7.061
7.066
7.050
7.046
7.039
7.034
7.028
7.023
@2007
@2040
X[10^6m] 6.1
6.2
6.1
6.2
0e+00
3e+08
7e+08
1e+09
Charts remaining GIP/km2

Figure 36 OL charts remaining GIP/km2 before and after production (2007→2040)

6.2.2 Tracking Grid-block 35.72.3

Grid-block 35.72.3, isolated from surrounding mobile gas has been tracked, see chapter 6.1.1. Gas saturation after initialization of the aquifer for this block was 0.3415, so from relative permeability data under production (Chapter 4.3) it should follow the specified secondary drainage curve for residual gas shown in blue in Figure 37. To check this, the relative permeability for this specific grid-block during production was plotted together with the secondary drainage curve. Figure 38 is a blown up version of the secondary drainage gas relative permeability curve in Figure 37, including the gas relative permeability for grid-block 35.72.3. Since the orange curve in Figure 38 is tracing the blue curve the implementation of a different secondary drainage curve for residual gas succeeded.

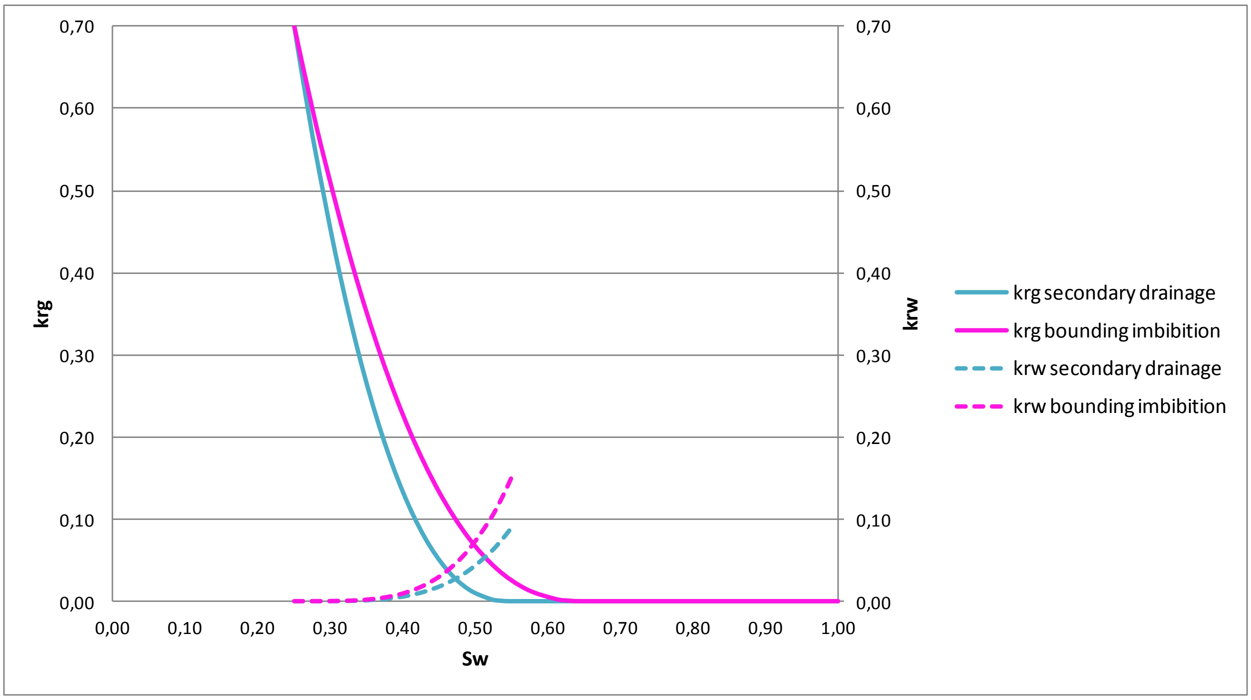

Figure 37 Bounding Imbibition and Secondary Drainage Sgr = 0.35, CGS= 0.45

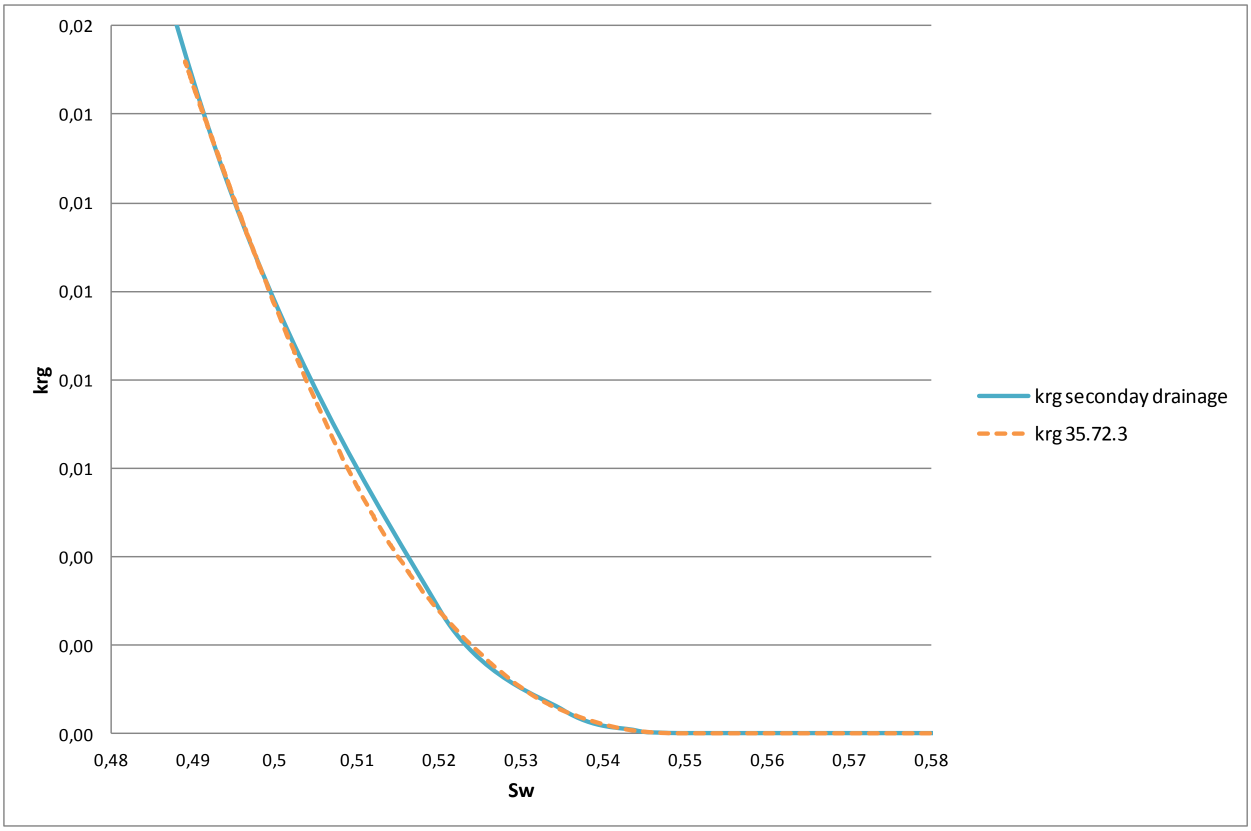

Figure 38 Secondary drainage gas relative permeability for grid block 35.72.3 CGS=0.45

Figure 39 provides gas-saturation, CGS and pressure versus time for the grid-block. A continued build-up of the gas saturation after reaching critical saturation is observed. It is expected, due to high mobility of gas that the saturation will remain close to the critical saturation. However, the continued build up above critical saturation is still thought to be dominated by mobility effects, i.e. the saturation of the hydrocarbon network increases above critical saturation in order to facilitate transport of mobile gas[8]. A.E. Zweers et al.[2] suggest that this gas-saturation increase above critical saturation means that some not yet connected clusters are still growing and more gas is developing at sites where in the end it could be trapped.

The gas saturation will, after reaching a certain point, remain constant (depending on whether it experience water-influx or not). The latter is the result of hysteresis effects; a once developed saturation will not reduce in the future[2] (assuming no water-influx). The continuous build-up of the gas saturation above critical gas saturation is observed for all grid-blocks with initial gas saturation around residual.

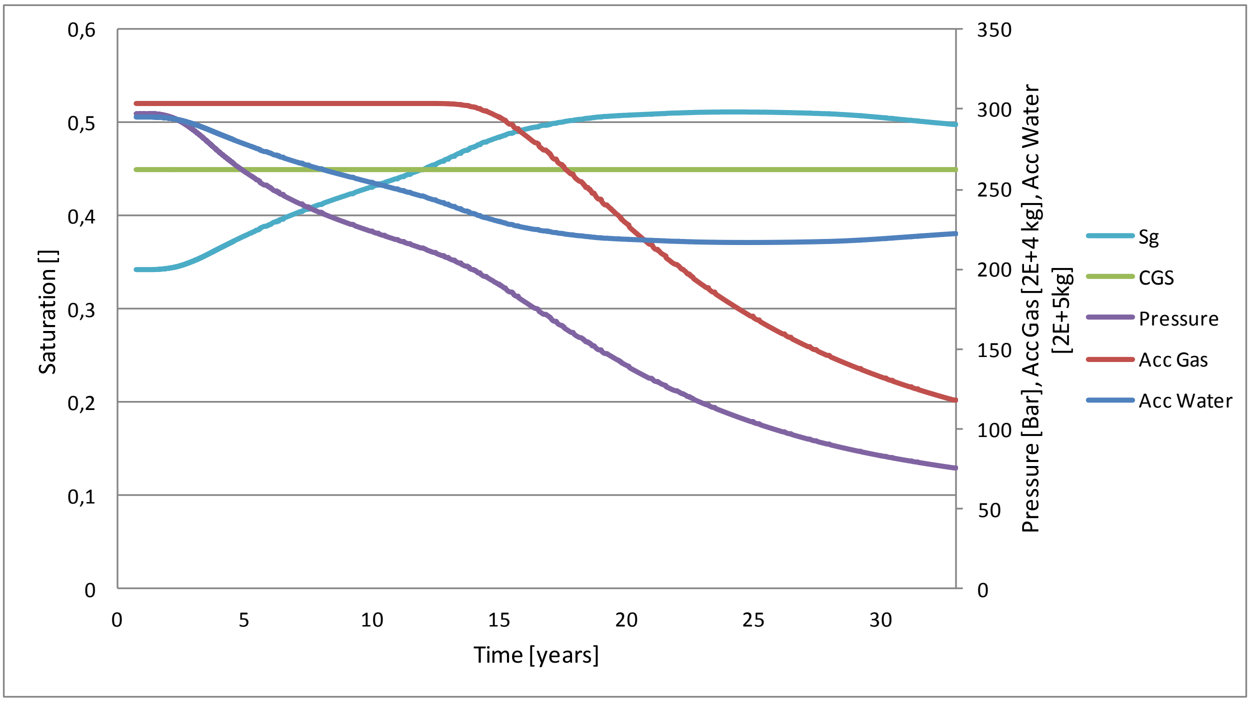

Figure 39 CGS, Sgr, pressure, accumulation of gas and accumulation of water versus time for grid-block 35.72.3

Accumulated gas and accumulated water for this specific grid-block are also plotted in Figure 39. The water-phase is mobile and will flow out of the grid block as long as the gas-phase is expanding. There is no change in accumulated gas during the first 14 years. Since the increase in gas-volume is proportional to the pressure-drop during this period a PV/Z plot versus time for the gas-phase should display a horizontal straight line, see Figure 40. The gas remobilizes after 14 years @210bar. Once the gas is remobilized, the production of water from the grid-block decreases and accumulated water remains almost constant until water breaks through in 2034 (after 27 years). Water breakthrough can also be seen in the saturation plot where the gas-saturation slightly starts to decrease after 27 years. Recovery of GIIP in 2040 for this grid-block is 61%.

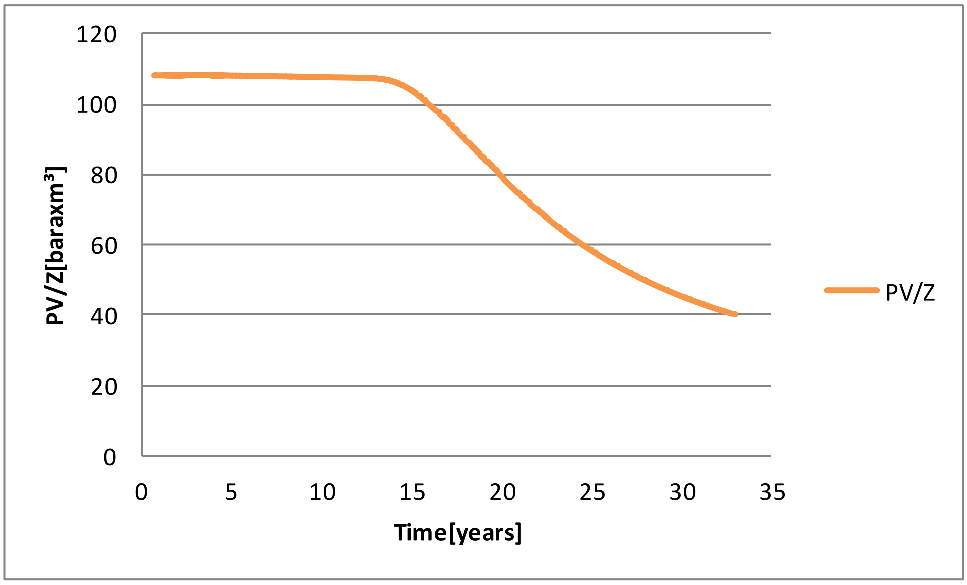

Figure 40 PV/Z versus time for grid-block 35.72.3

6.2.3 Tracking Grid-block 30.78.3 and 22.46.5

Two grid-blocks that experience inflow of gas from surrounding grid-blocks containing mobile gas are tracked, see chapter 6.1.1. The location of the grid-blocks is shown in Figure 34, one in layer 3 and one in layer 5. The gas relative permeability for the two grid-blocks is shown in Figure 41, being a blown up picture of the blue secondary drainage curve in Figure 37.

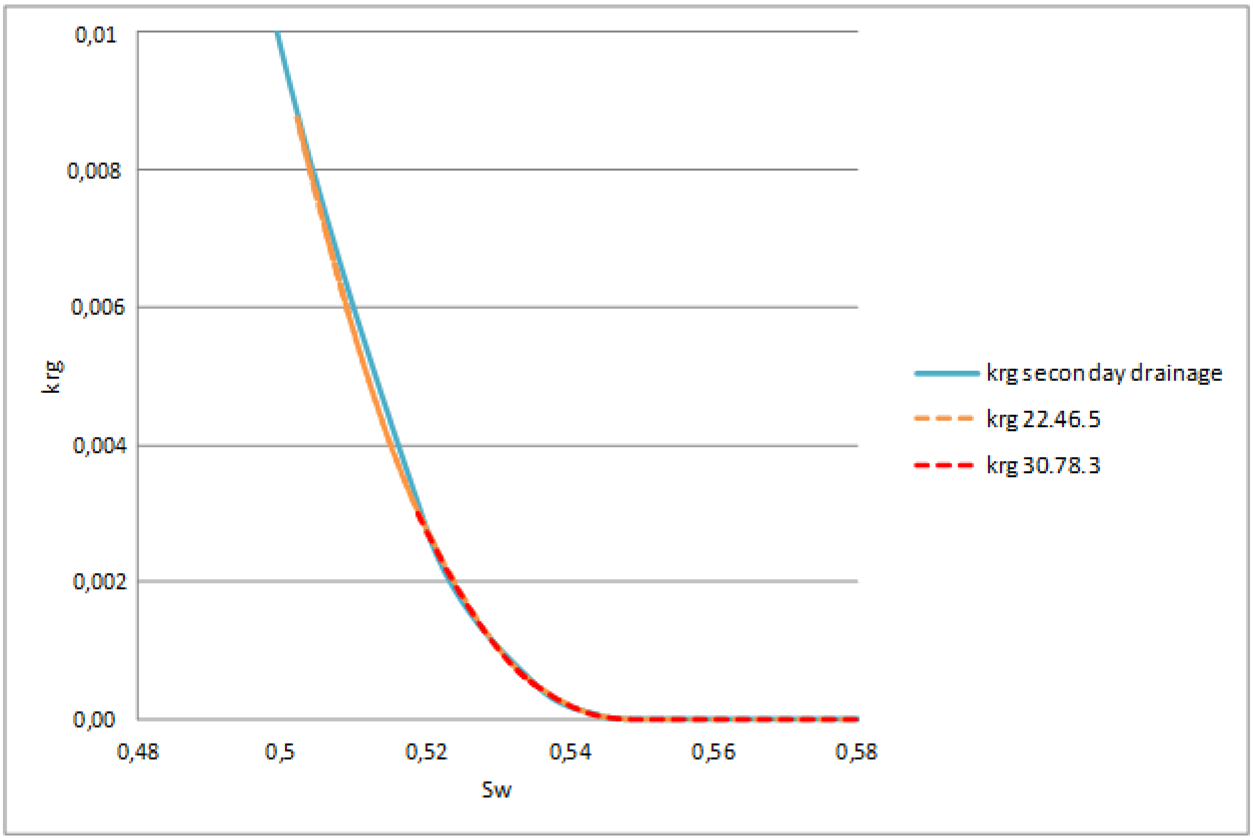

Figure 41 Secondary drainage gas relative permeability for grid-block 30.78.3 and 22.45.6

Grid-block 22.46.5 is surrounded by mobile gas from all sides in the horizontal direction, and experiences fast decrease in pressure, see Figure 42. Gas from the surrounding grid-blocks immediately starts to flow into the grid-block (see Figure 44) and critical gas saturation is reached in short time as shown in Figure 42. After remobilization, gas starts to flow out of the grid-block, and the gas saturation remains constant for almost 20 years until water is starting to break through after 25 years in 2032. The starting water-breakthrough can be seen in Figure 44. In the end 54% of the GIIP in this block is recovered (@2040).

Grid-block 30.78.3 is only surrounded by mobile gas on the west side in horizontal direction. The pressure decrease in the beginning is limited, see Figure 42. The grid-block experiences a fast increase in gas-saturation after 5 years when surrounding gas starts to enter the grid-block, see solid blue line in Figure 42. Once the critical gas saturation is reached gas starts to flow out of the block. A significant decrease in accumulated gas is observed once depletion starts, due to higher pressure decline in this period, see Figure 42 and Figure 45. Once the pressure decline decreases, production of gas from the grid-block takes off, and the gas saturation is slightly increasing. Recovery of GIIP for grid-block 30.78.3 is 5% only (@2040). From the PV/Z plots in Figure 43 it can be seen that the PV/Z curve has the same shape as the accumulated gas until remobilization of the gas. The reason why the plots in Figure 44 and Figure 45 are not merged in one plot only is the difference in accumulated gas and water-volume. For grid-block 22.46.5 the volumes are 10 times greater than for grid-block 30.78.3.

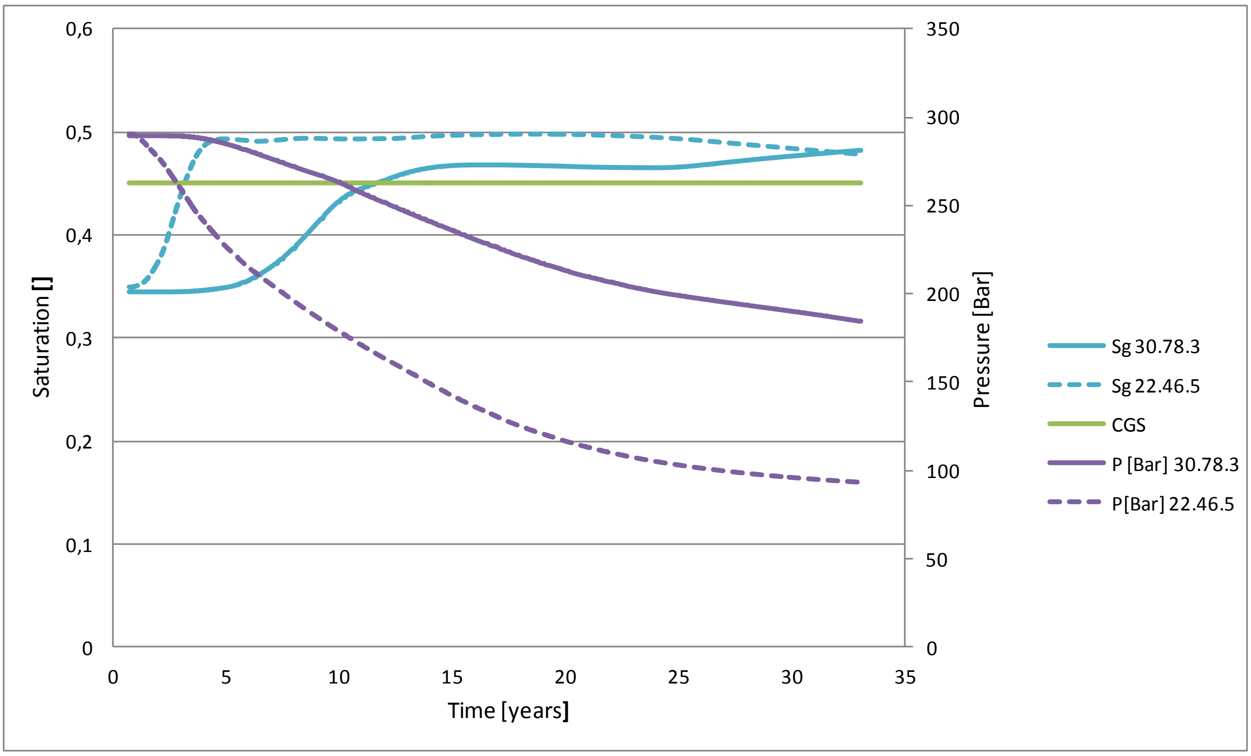

Figure 42 Pressure and Sgr versus time for grid-block 30.78.3 and 22.46.5

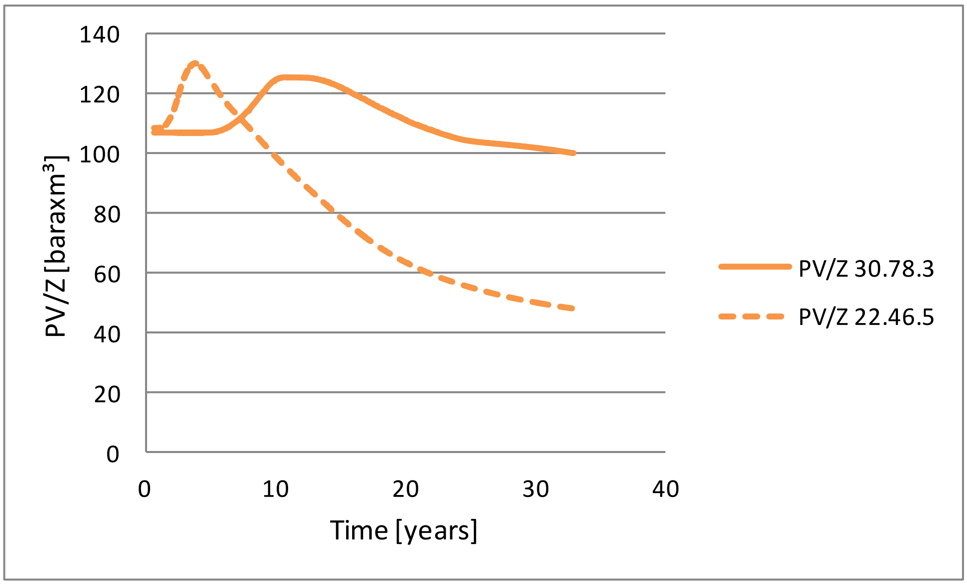

Figure 43 PV/Z versus time for grid-block 30.78.3 and 22.46.5

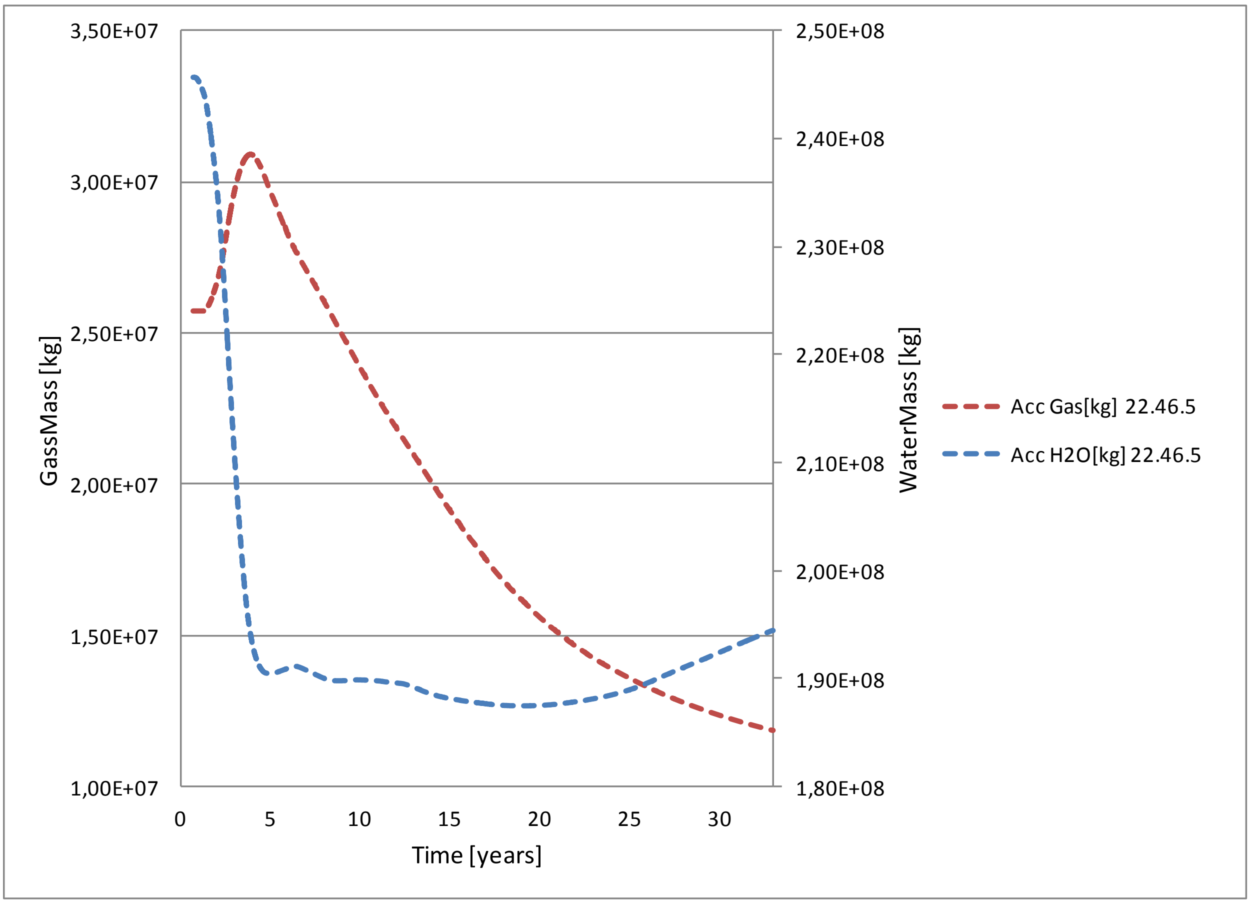

Figure 44 Accumulation of gas and water versus time for grid-block 22.46.5

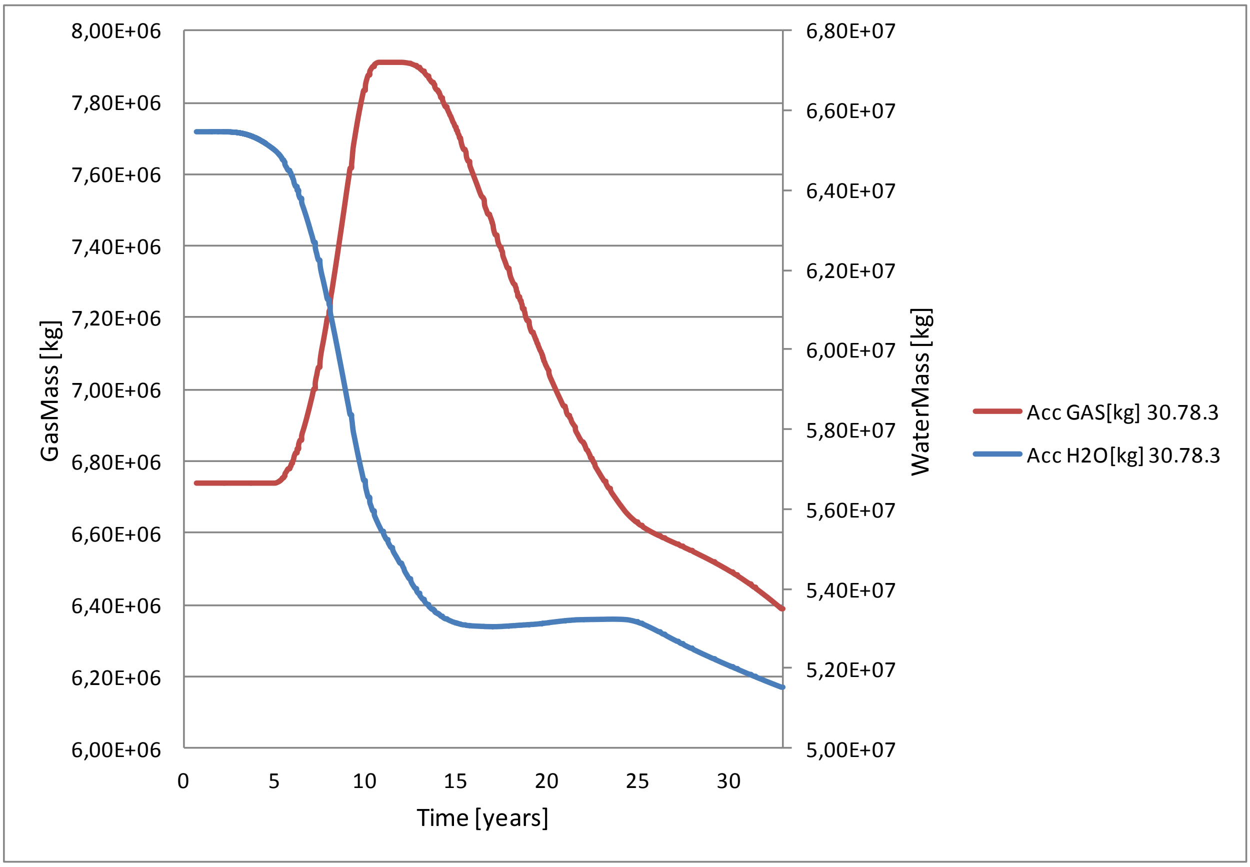

Figure 45 Accumulation of gas and water versus time for grid-block 30.78.3

6.2.4 Grid-block 29.8.1 and 29.9.1

Two grid-blocks that are sitting next to each other in the South with initial gas-saturation 0.3501 and 0.316 have been tracked. The behavior of the gas in the two grid-blocks has been compared. Since the initial gas-saturation in block 29.9.1 is greater than 0.35, the gas in this grid-block will retrace the bounding imbibition relative permeability curve used for initialization when going into secondary drainage (see red curve in Figure 47). In grid-block 29.8.1 the initial gas-saturation is 0.316, so for this block the specified secondary drainage curve for residual gas will be used (see orange curve in Figure 47). The location of the grid-blocks is shown in Figure 46 (white squares), and the gas relative permeability for the two grid-blocks is shown in Figure 47.

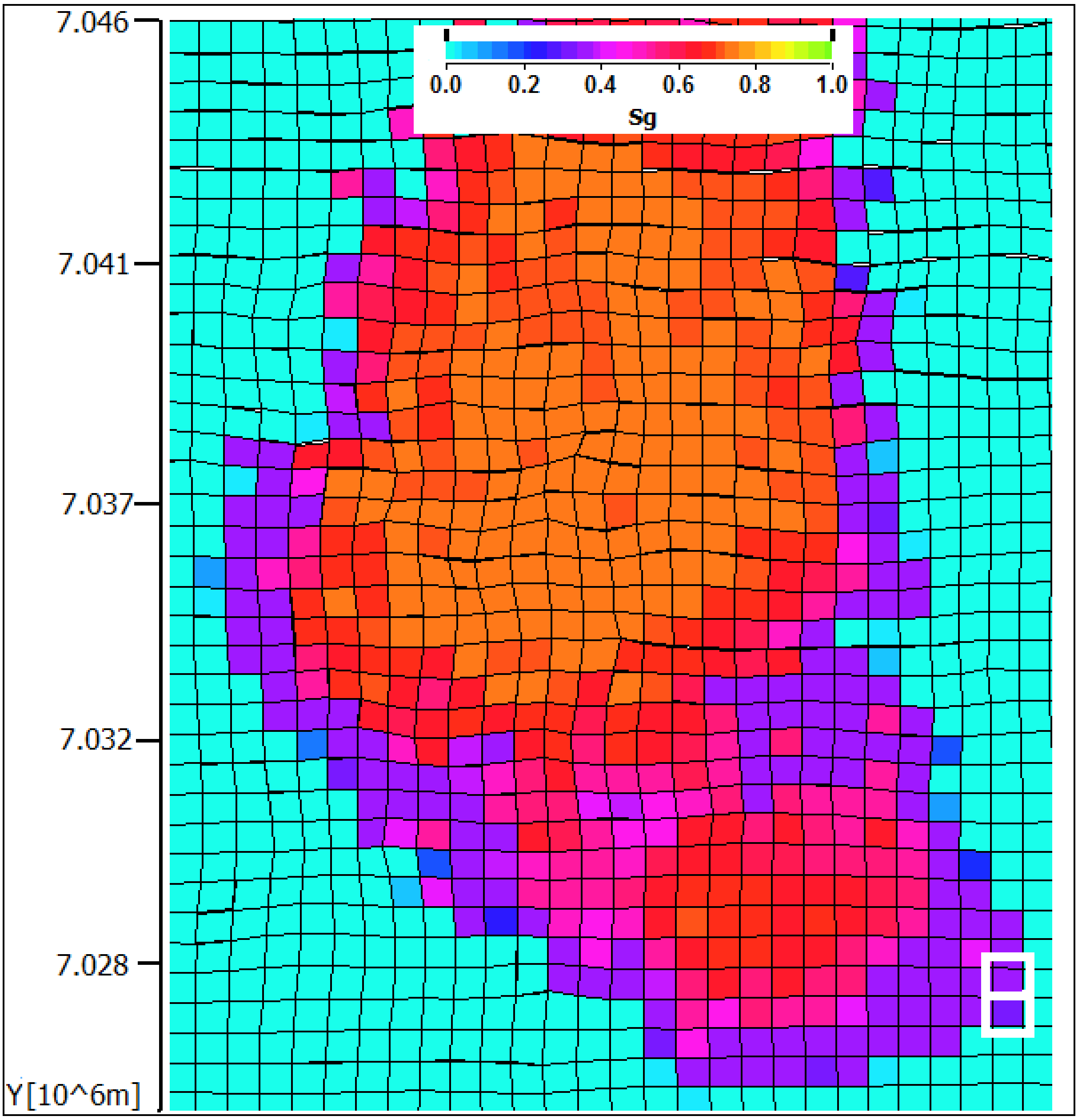

Figure 46 Location of grid-block 29.8.1 and 29.9.1 in the South

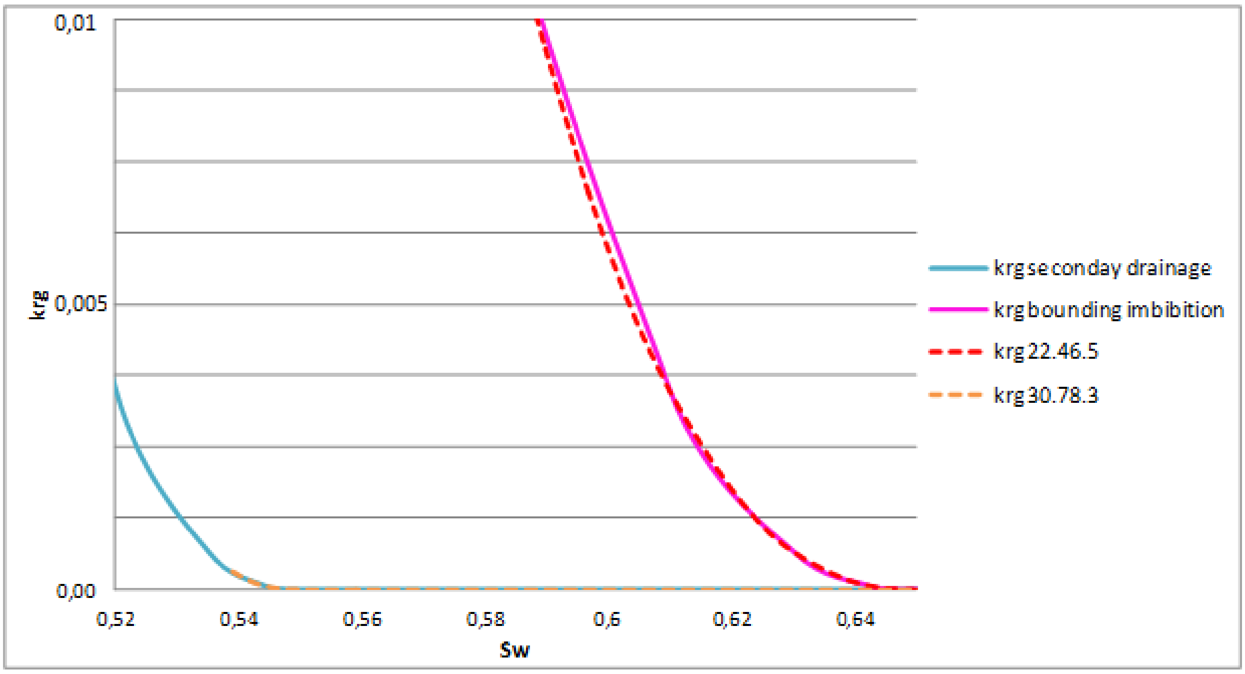

Figure 47 Secondary drainage gas relative permeability for grid-block 29.9.1 and 29.8.1

Since the grid-blocks are neighbors, have the same reservoir and fluid-properties (except for relative permeability and saturation), and are in the same distance from off-take the pressure develops in the same manner for both, see Figure 48.

By comparing the production of gas from these two grid-blocks we understand the effect of implementing a mobility threshold above residual gas saturation (when the critical gas saturation implemented is high enough). Once pressure starts to decline the gas in grid-block 29.9.1 remobilizes because of expansion, and gas starts to flow out from the grid-block, see Figure 48 and Figure 49. The gas-saturation increases around 5% saturation units above residual, gaining relative permeability in order to facilitate transport of the gas. Under the same pressure decline, the gas in grid-block 29.8.1 is still immobile. Gas from grid-block 29.9.1 will not flow into grid-block 29.8.1 because of location and direction of gas-flow towards lower pressure. The gas in grid-block 29.8.1 is still expanding towards the critical gas saturation of 0.45. By the end of the production period (@2040) the CGS is reached, see Figure 48, but the gas has not remobilized yet. So in this area where the pressure-drop is around 100 bar, the use of a different secondary drainage curve for residual gas impacts the recovery more than in zones with greater pressure-drop. For the grid-block where no mobility threshold is utilized, the recovery of residual gas is 19%. For the grid-block with initial gas saturation of 0.316, and a critical gas saturation of 0.45, no gas is recovered.

These numbers can be compared to two neighboring grid-blocks in the same layer in segment 4; grid-block 29.57.1 and 30.58.1.The latter grid-block has a residual gas saturation of 0.3451 after initialization, thus using the orange secondary drainage curve in Figure 47 under depletion. Grid-block 29.57.1 has a residual saturation of 0.3518, thus retracing the pink bounding imbibition curve when going into secondary drainage. The grid-blocks are sitting close to production area (A-template), and the pressure drop is 220bar (70bar@2040) for both. The ultimate recovery is 66% for 30.58.1 and 73% for 29.57.1, showing that for higher pressure drops the impact on recovery of a mobility threshold for residual gas is less significant.

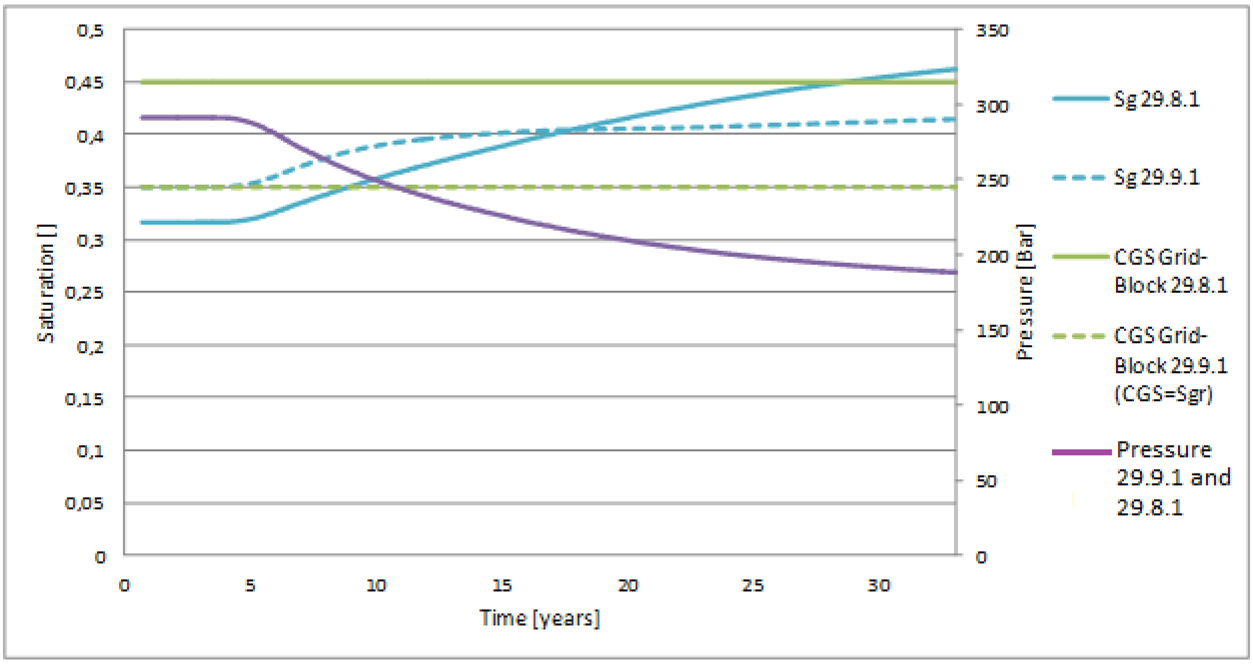

Figure 48 Sgr and pressure versus time for two different grid-blocks (29.8.1 and 29.9.1)

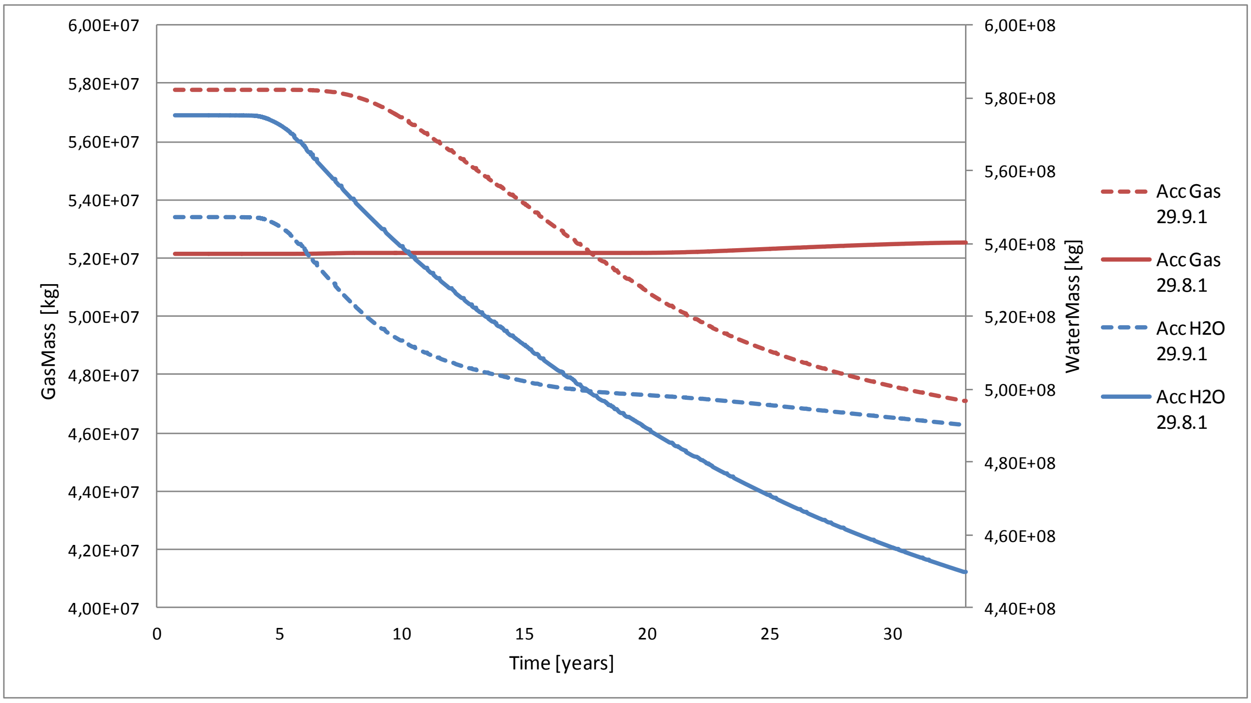

Figure 49 Accumulation of gas and water versus time for two different grid-blocks (29.8.1 and 29.9.1)

6.3 Effect of krg and Ng on Recovery of Residual Gas

The effect on residual gas recovery of changing the krg and the Ng value (Corey-correlation for gas) during secondary drainage was assessed. The new base case for Sgr, 0.30 (I2 from chapter 5.1), was applied in this study. Increasing krg (in both primary drainage and secondary drainage) without changing the other parameters implies that the residual gas during expansion and reconnection will gain relative permeability faster tracing a steeper relative permeability curve. The opposite applies for Ng; when Ng is increased the residual gas will gain relative permeability slower since the relative permeability curve will be less steep (more curved).

The krg was implemented in line with the new range established from SCAL (chapter 4.1), and the new value was applied for both bounding and secondary drainage. See Figure 50 for illustration of the relative permeability curves used. Ng was decreased from 4.0 (measured value for bounding imbibition, see chapter 4.1) to 2.4 (for secondary drainage only) in 3 steps, see Figure 51 for illustration of the different relative permeability curves. The mobility threshold is zero (Sgr=CGS=0.3) in both models. Note that it is strictly incorrect to apply primary drainage parameters for secondary drainage. It is expected that the secondary drainage curve is close to the primary drainage curve, especially at low water saturations. Since no experimental data was available for secondary drainage, primary drainage parameters were used instead.

Increasing or decreasing krg is expected to have quite an effect on recovery since both the shape (automatically changed as krg is modified) of the relative permeability curve and the end-point value is changed. For all gas-saturations the krg will vary greatly within the three different models, see Figure 50. Changing the Corey-correlation (in secondary drainage only) within the range showed in Figure 51 is not expected to have a huge effect on recovery of residual gas. This is due to lower mobility ratio of water relative to gas (methane ca 80 times less viscous than water), which makes the gas capable of moving much faster than water under a given pressure differential. Hence, when krg is constant, modifying the slope of the relative permeability curves by increasing the Corey-correlation is expected to have smaller effect on recovery than when krg is changed (for the specific range of Ng studied). The difference in gas relative permeability curves is less pronounced in Figure 51 than in Figure 50.

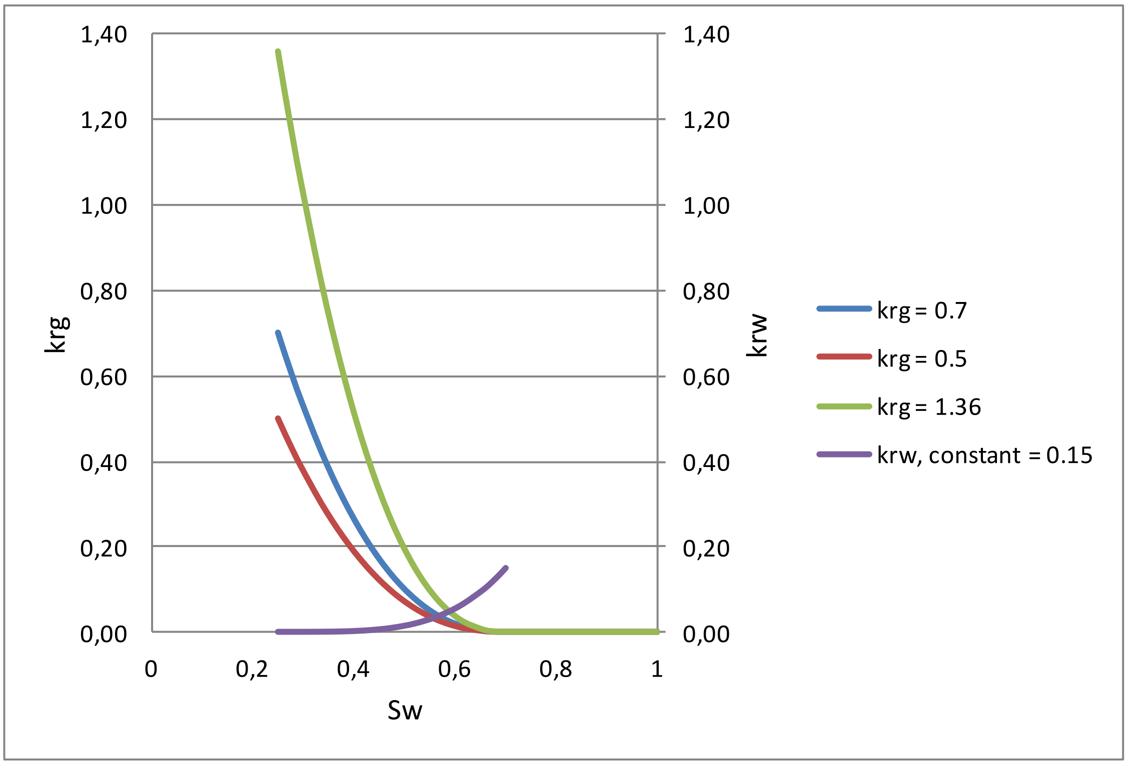

Figure 50 Relative permeability bounding imbibition and secondary drainage, Sgr=CGS=0.30, changing krg

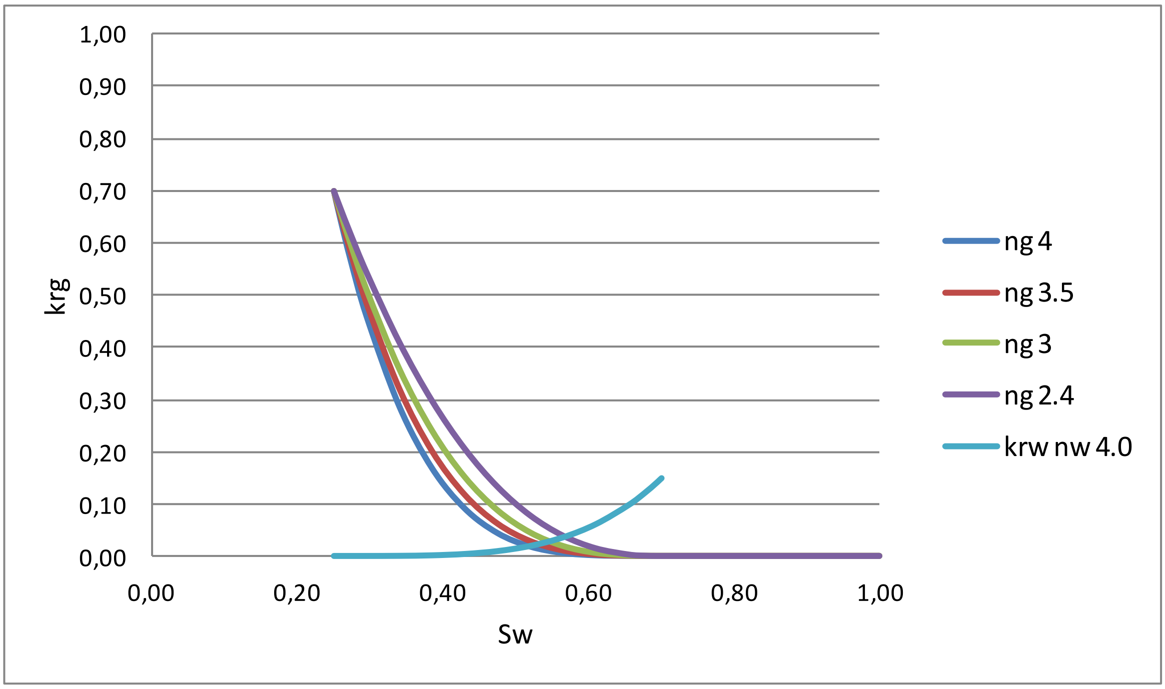

Figure 51 Relative permeability secondary drainage, Sgr=CGS=0.30, changing Ng

A random grid-block (32.70.10) initially containing residual gas was tracked. Figure 52 shows how the pressure and accumulation of gas changes throughout the time of production. The solid lines are for the high krg case, and the dotted lines are for the low krg case. Gas-flow out of the grid block occurs at a later stage when krg = 0.5 compared to krg = 1.36, and the pressure also develops in a different manner. As can be seen, the recovery of gas after 30 years is lower for lower krg. The difference in gas recovery from this specific grid-block for the two cases is 22%.

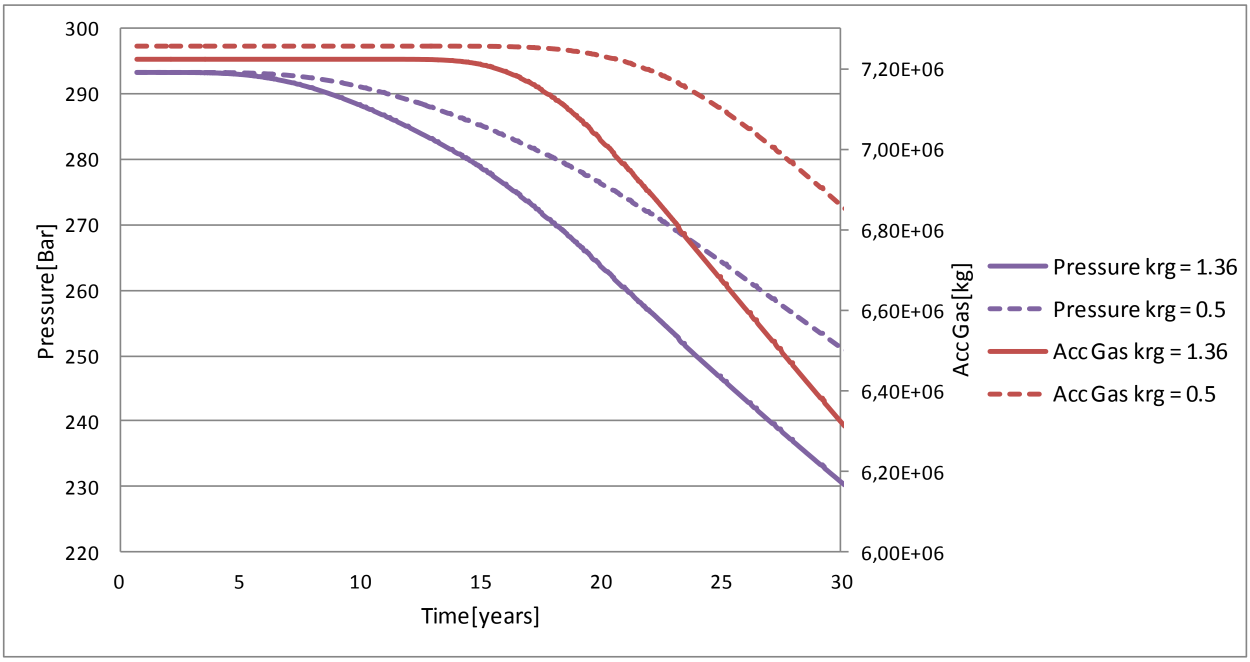

Figure 52 Pressure and accumulation of gas for grid-block 32.70.10 for two different values of krg

Total recovery from residual gas for the different krg values is shown in Figure 53. The difference in residual gas recovery between krg = 0.5 and krg = 0.7 is 4%, and the difference in residual gas recovery between krg = 0.5 and krg = 1.36 is 9%.

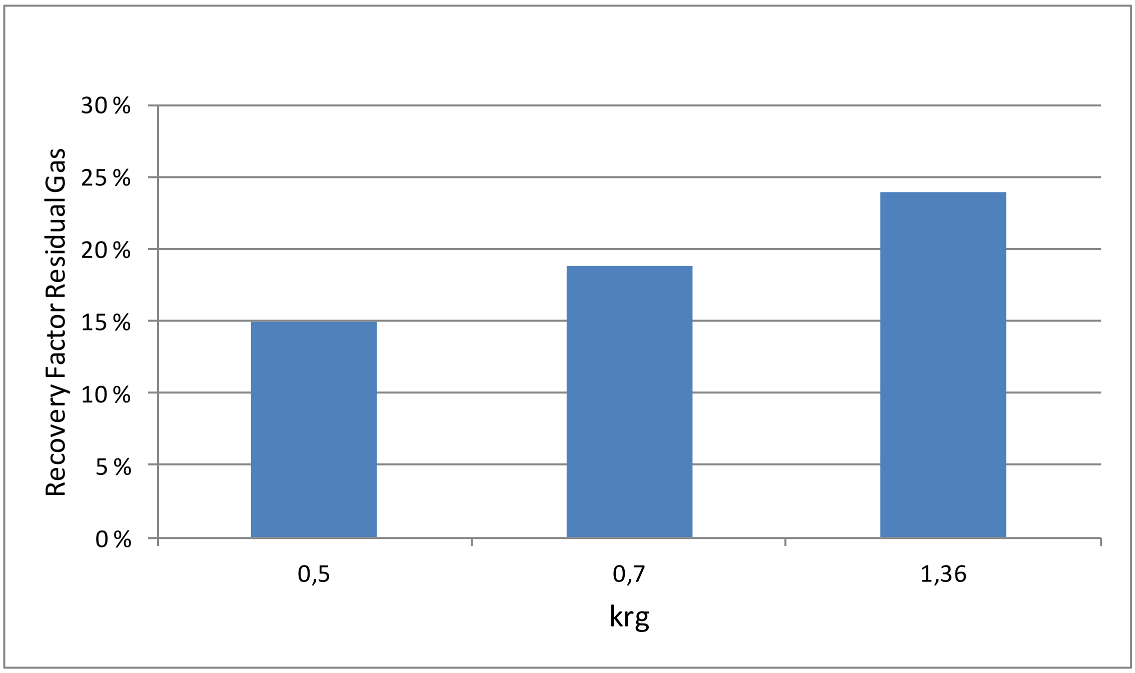

Figure 53 Recovery of residual gas versus krg

The same grid-block as in Figure 52 was tracked to assess the impact on gas-flow of changing Ng. As can be seen in Figure 53 the gas starts to flow out from the grid-block earlier for Ng = 2.4 than for Ng = 4.0. However, the difference in gas recovery from this specific grid-block for the two cases with different Ng is 2% only.

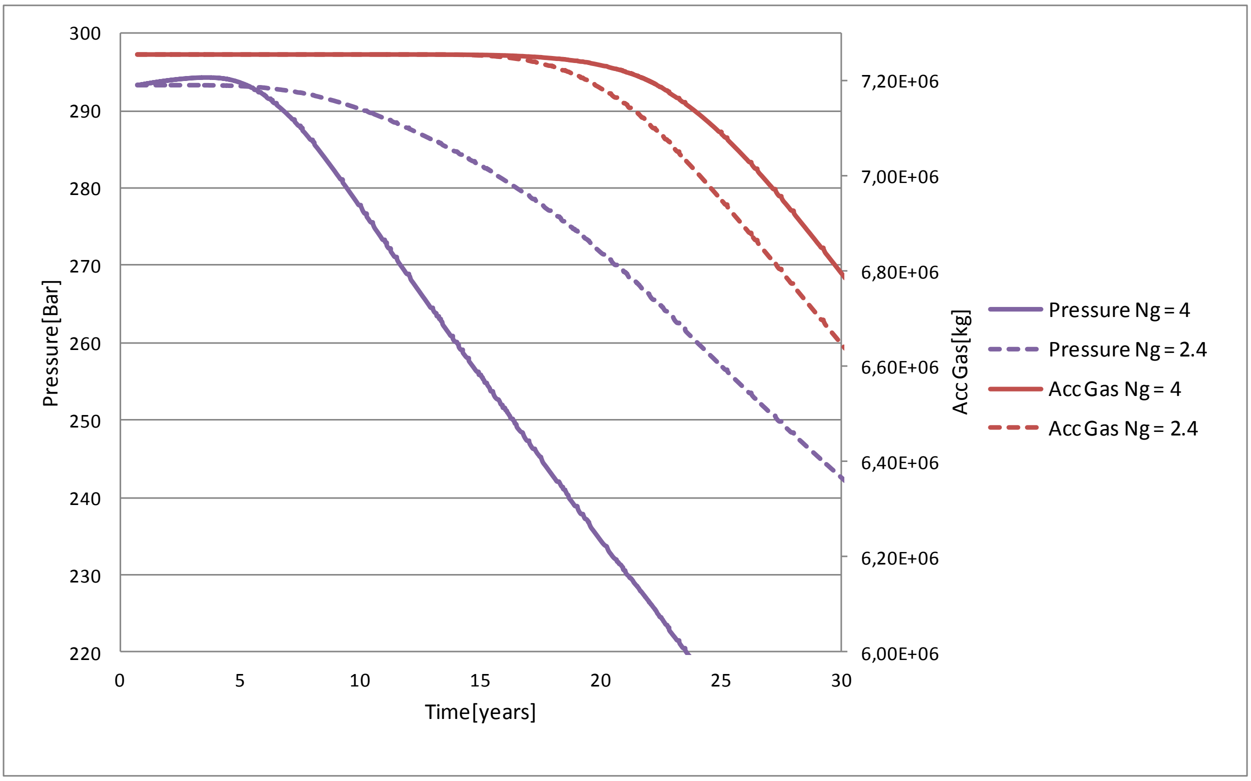

Figure 54 Pressure and accumulation of gas for grid-block 32.70.10 for two different values of Ng

Total recovery from residual gas for the different Ng values is shown in Figure 55. The difference in residual gas recovery between Ng = 4 and Ng = 3 is 1.5%, and the difference in residual gas recovery between Ng = 4 and Ng = 2.4 is 2.5%.

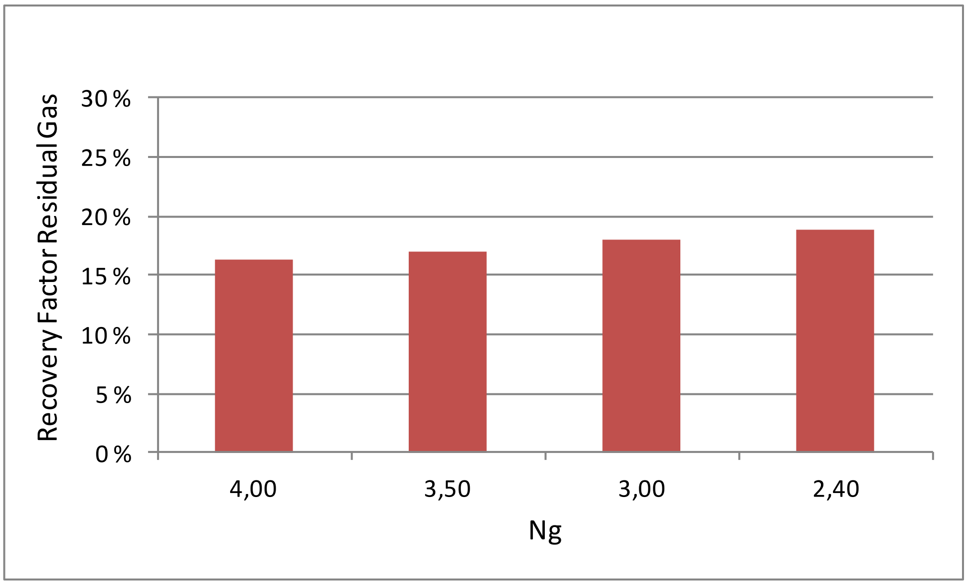

Figure 55 Recovery of residual gas versus Ng

7. Aquifer Strength Sensitivity

Aquifer support is able to provide sweep. Sweep efficiency depends on factors such as production rate, formation dip, porosity and heterogeneity. Sweep efficiency also depends largely on the aquifer properties like size and water permeability. Pressure support from an underlying aquifer may be an advantage during production. However, generally aquifer in a gas field is bad news as it tends to trap gas at high pressures resulting in large volumes of residual gas.

As the pressure in the area where water breaks through will increase, the gas will be compressed and occupy a saturation less than residual. In this case the pressure must be lowered below the previous minimum before any gas can remobilize. Thus, for enhanced recovery by coproduction from the gas in the water-invaded areas, one must be prepared to produce large volumes of water before any gas production starts. Ormen Lange facilities cannot handle large amounts of produced water, hence gas in areas subsequently waterflooded during production has to be considered lost. The entrapment pressure determines how much gas is left behind and is therefore a very important parameter, directly dependent on the aquifer strength. The following chapter quantifies the impact on residual gas recovery of altering the aquifer-strength. In all scenarios the mobility threshold above Sgr is zero, hence residual and mobile gas will retrace the imbibition curve during secondary drainage.

7.1 Stronger Analytical Aquifer

The size of the analytical aquifer in the fully initialized hydrodynamic aquifer model was increased; in the Strong Aquifer case the length of the aquifer in the East, West, South and Northeast is doubled compared to the base case, the maximum absolute permeability is increased from 700mD to 1000mD, and the water relative permeability end point is increased to 0.3 for both Egga and Subegga. The saturation and the pressure are plotted in Figure 56 for the two cases. A grid-block that experiences water-breakthrough, 13.23.6, is tracked. The grid-block is located close to the production wells in the South (D2), in the 6th layer (Egga). Initial gas saturation is 0.3502 implying immediately remobilizing as the pressure drops since Sg>Sgrmax (0.35 from bounding imbibition).

As can be seen from Figure 56 and Figure 57 there is a rapid increase in gas-saturation after 4 years of production, as a function of large pressure drop. After ten years, as more water is imbibing the grid-block the pressure-decline decreases for the base case, whilst the pressure starts to increase for the strong aquifer case. The water-influx in the strong aquifer case is heavier and occurs at higher pressure due to greater pressure support. When water is breaking through it displaces the gas-phase and gas-production from the grid-block continues until the block is fully swept by water. The peaks in the accumulated water curve is due to early water-inflow followed by some production of water from the grid-block before water is totally sweeping the grid-block, taking the gas-saturation to low values. The entrapment pressure for the normal aquifer is 155bar. For the strong aquifer the entrapment pressure is 195bar. The pressure in the grid-block is increasing after break-through as more water is flowing, compressing the gas to lower saturation. By looking at Figure 57 we can see the effect on recovery from this specific grid-block by increasing the aquifer strength. The recovery factor decreases from 39% to 25%. In the strong aquifer case the influx of water towards the end is going down, water starts to flow out again, and the pressure is slightly decreasing. Further blowdown below the minimum pressure (190bar), by producing water, could potentially lead to enhanced recovery from this grid-block. Coproduction from the block in the case with weaker aquifer has less potential, due to its lower minimum pressure and higher primary recovery.

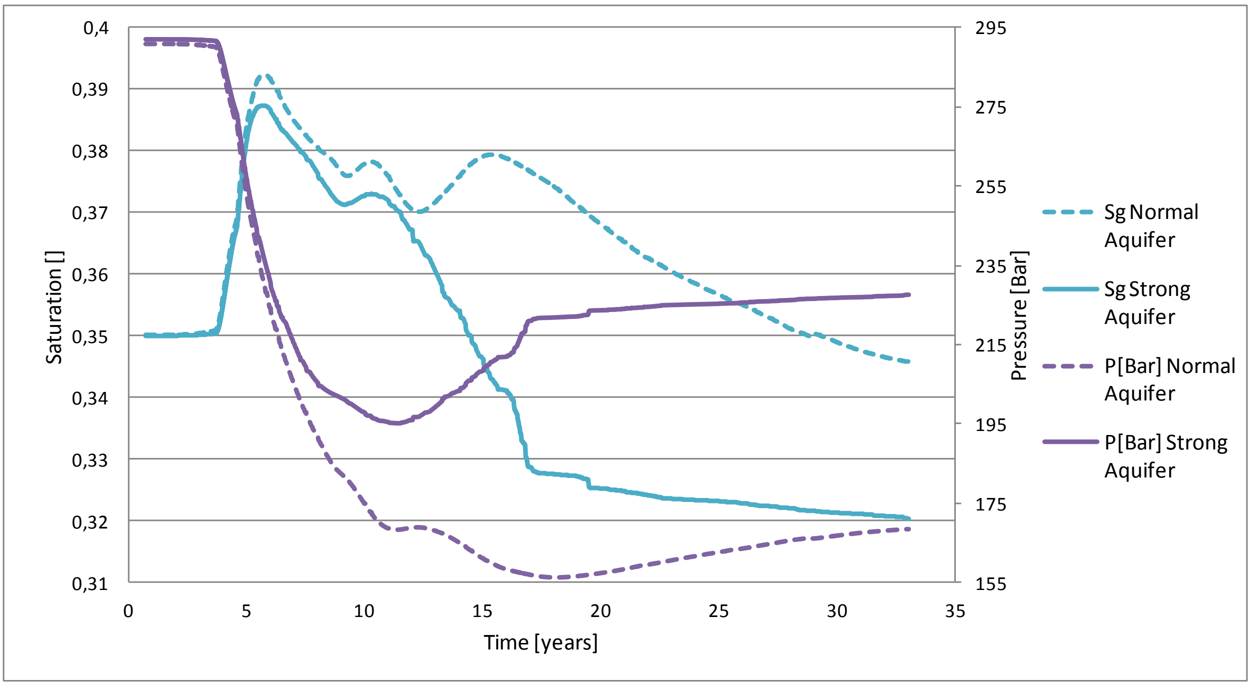

Figure 56 Saturation and pressure versus time for grid-block 13.23.6

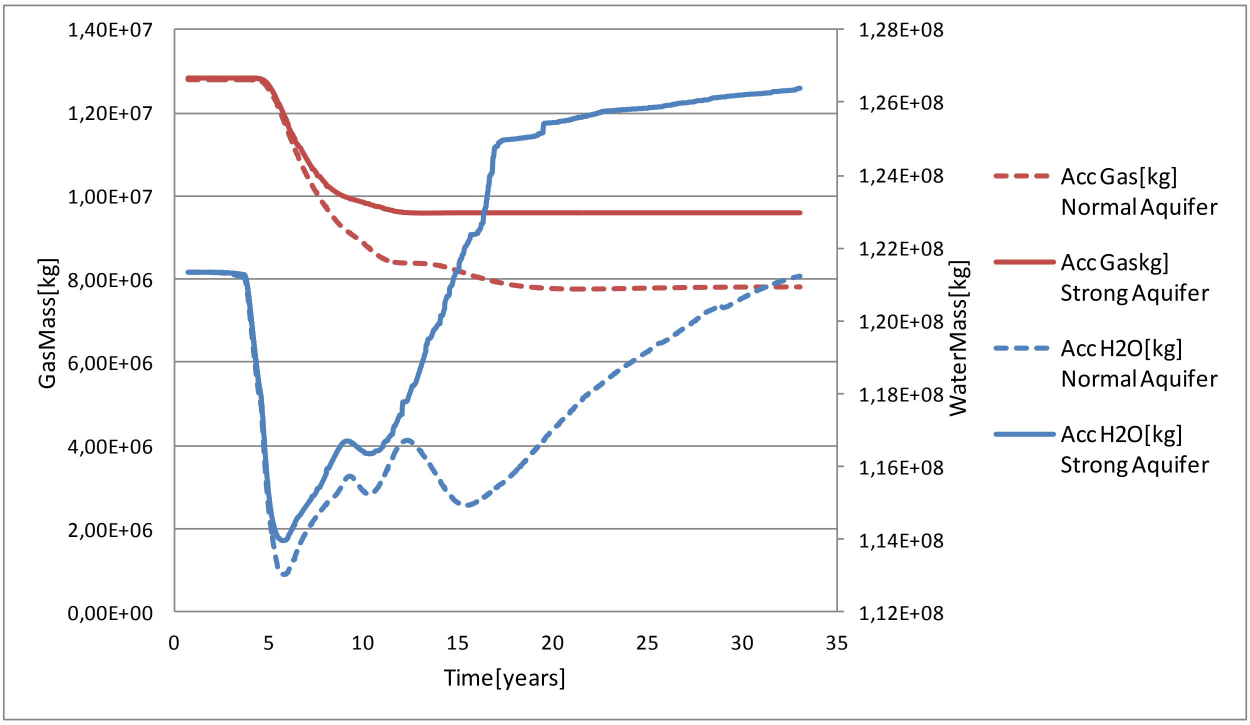

Figure 57 Accumulation of gas and water for grid-block 13.23.6

Figure 63 provides cumulative gas-production and average gas pressure in segment 5. When the aquifer is stronger the residual gas recovery in segment 5 decreases from 22% to 10% as an effect of higher abandonment pressure, see Figure 62 and Figure 63. Recovery from mobile gas in segment 5 is decreased from 64% to 54%. The recovery factors from the other segments cannot be directly compared since the initial residual volumes are very different. The flushing-effect when krw is increased results in lower residual gas volumes in segment 1-3. In segment 5 the residual gas zone is created by gas receding as the hydrodynamic aquifer strength is slowing down after Storegga slide, hence increasing krw does not have great effect on the residual gas volume. With equal initial residual gas volumes in segment 5 the recovery factors can be compared and analyzed with respect to pressure.

The impact on gas-recovery of implementing a critical gas saturation of 10%PV above residual value of 35% for the strong aquifer case is not greater than in the normal-sized aquifer (see chapter 6.1). The recovery from residuals is only reduced by 3%, from 16% to 13%. Theoretically the effect of a mobility threshold for residual gas under depletion is expected to be greater when increasing the size and strength of the aquifer. However, the residual volume after initialization of the hydrodynamic aquifer is lower in the strong aquifer case (flushing-effect of increasing krw). In the strong aquifer case 79Bcm residual gas (Sgr=0.35) is resided in the reservoir initially, compared to 89Bcm in the normal case. Therefore we cannot really compare the effect of implementing a CGS for the two different cases.

7.1.1 Sensitivity of Krw for the Strong Aquifer case

The water relative permeability under production in the strong aquifer case was decreased from 0.3 to 0.03, implying lower aquifer strength. See Figure 58.

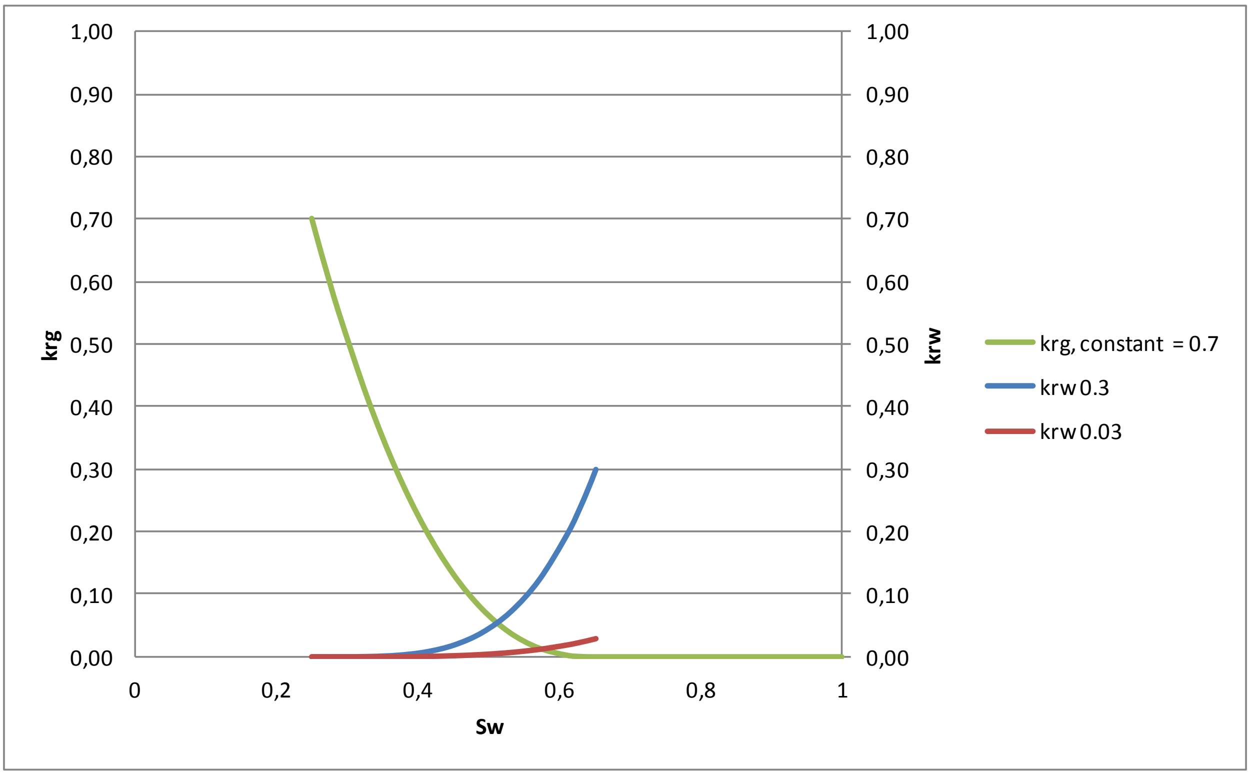

Figure 58 Relative permeability curves used under production. High (0.3) krw in blue, low (0.03) krw in red, krg remains constant

Decreasing the krw value has very limited effect on total recovery from residual gas (ΔRF=0.15%), however recovery of residual gas from segment 5 is 5% higher as an effect of later water breakthrough when krw is low, hence lower abandonment pressure. This also effects the recovery of mobile gas in segment 5 (13% increase), see Figure 62. Total gas recovery is increased by 2.5% (from 62.7% to 65.2% for Sgr=0.35). The gas-saturations in the South for the two different cases are shown in Figure 60 and Figure 61. The initial gas saturation in the same area is shown in Figure 59. Figure 61 illustrates that the reservoir is better swept when krw is low. This can be seen by looking at the colour-scale: for the lowest krw value (0.03) abandoned gas saturations are as low as 18% close to off-take, compared to

35% when krw equals 0.3. The low gas-saturation is an effect of the gas being compressed as the pressure increases after water-breakthrough (pressure increases above entrapment-pressure), hence the saturations becomes lower than residual.

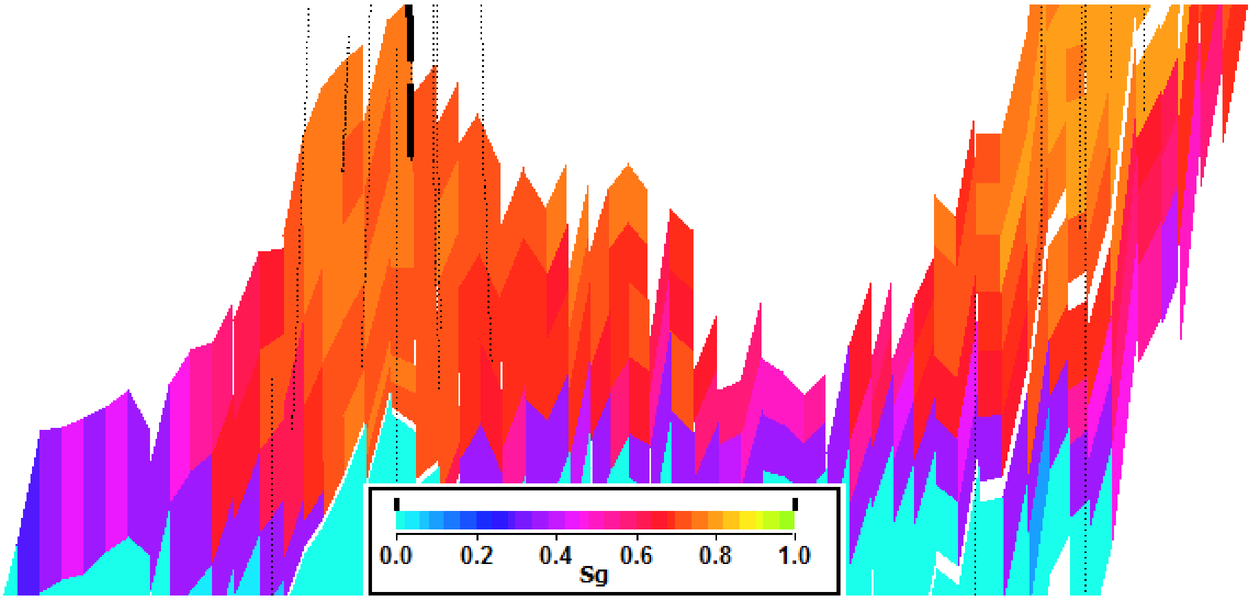

Figure 59 Initial (@2007) gas saturations in the South

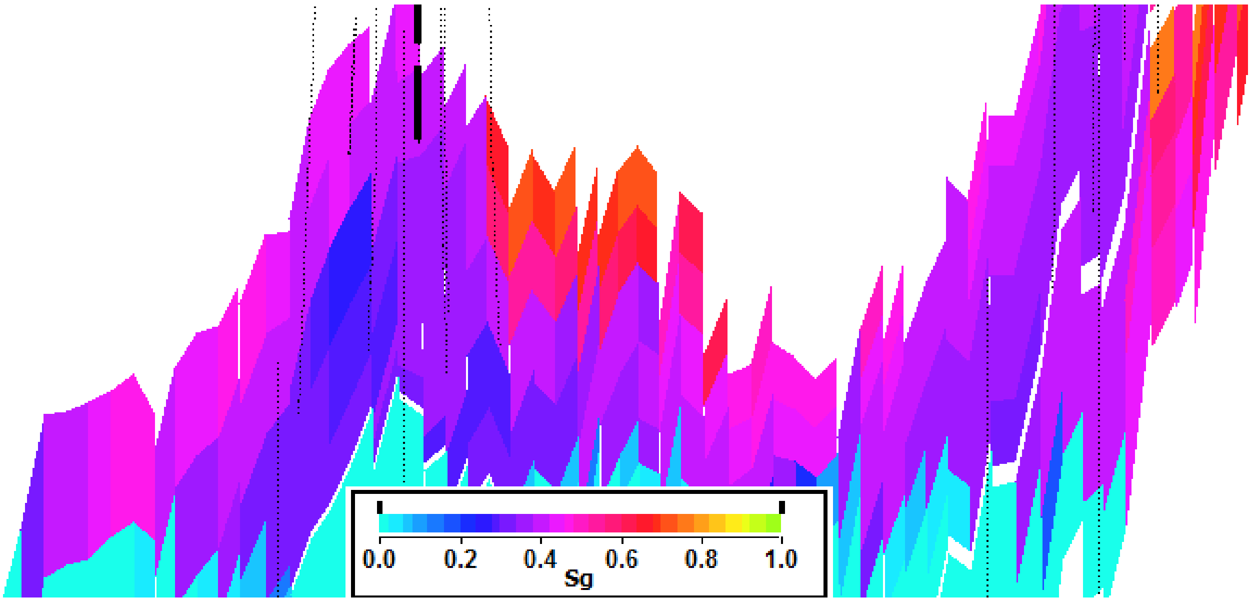

Figure 60 Gas saturation @2040 extra strong aquifer krw=0.3

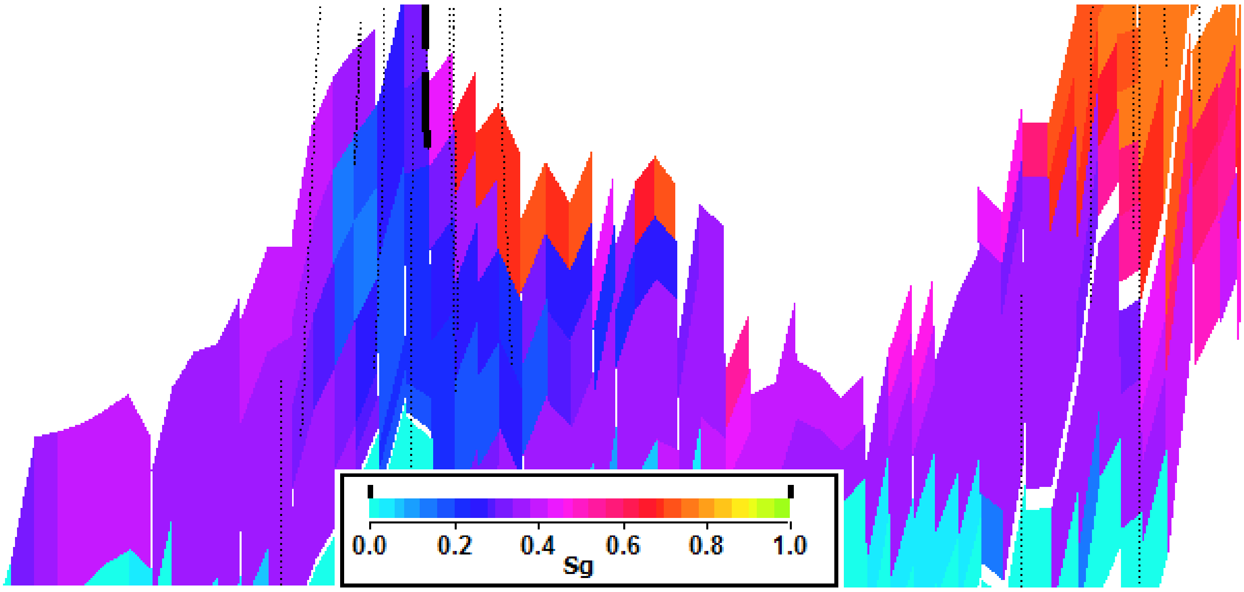

Figure 61 Gas saturation @2040 extra strong aquifer krw=0.03

7.2 Zero Analytical Aquifer

The model was run without the analytical aquifer. The advantage of a zero aquifer realization is the delaying of water-influx, hence being able to deplete the reservoir pressure further and produce more of the residual gas. The disadvantage is the lowering in pressure-support which could possibly decrease total recovery. Figure 62 provides the recovery-factors for segment 5. Due to lower abandonment pressure with zero analytical aquifer, see Figure 63, the recovery of residual gas in segment 5 is increased with 23% compared to the strong aquifer case. Compared to the normal aquifer case the recovery from residual gas in segment 5 is increased with 11%, see Figure 62.

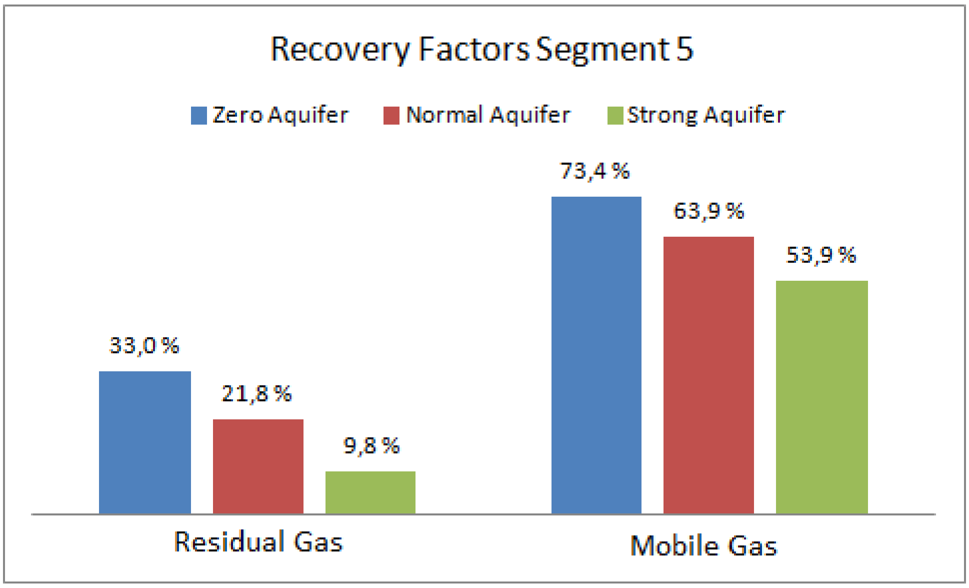

Figure 62 RF @2040 Segment 5 Sgr=0.35 for 3 different scenarios (Zero, normal, strong aquifer)

Figure 63 shows the average gas pressure in segment 5 and field cumulative production for the three different scenarios; zero, strong and normal aquifer.

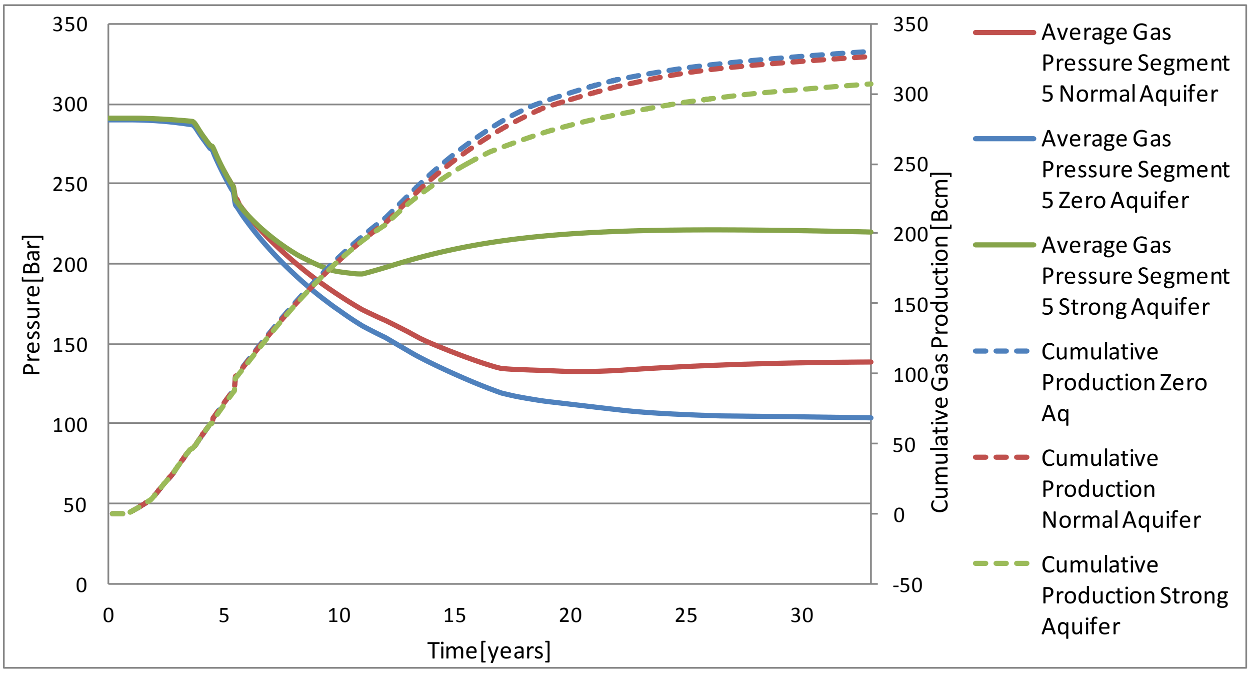

Figure 63 Cumulative gas production and average gas pressure segment 5 Sgr = 0.35

The same grid-block, 13.23.6, as in chapter 7.1 is tracked. Figure 64 and Figure 65 illustrate saturation, pressure, accumulated gas and accumulated water versus time for the case with the normal aquifer compared to the case without aquifer. The saturation changes are quite different in the case without aquifer as less water is breaking through. Water-influx occurs at the same time in the grid-block for both cases, but since the aquifer influx is lower when no analytical aquifer is present (there will still be water in the system from the hydrodynamic aquifer), pressure is still declining and gas is flowing out of the grid-block until 2040. Abandonment pressure is 70bar lower in zero aquifer case, compared to the normal aquifer, thus increasing the recovery factor, see Figure 62. The recovery factor in segment 4 is only to a small degree affected by strength in the aquifer influx from the south.

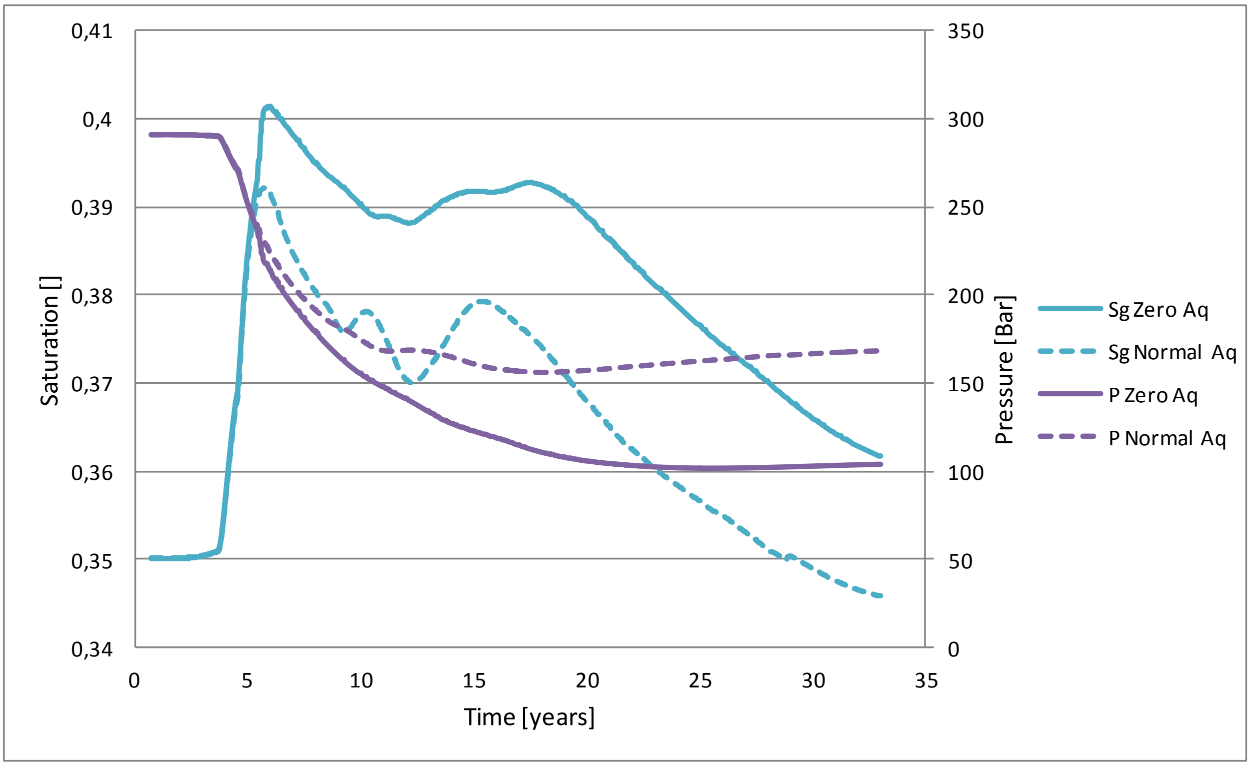

Figure 64 Saturation and pressures versus time for grid-block 13.23.6

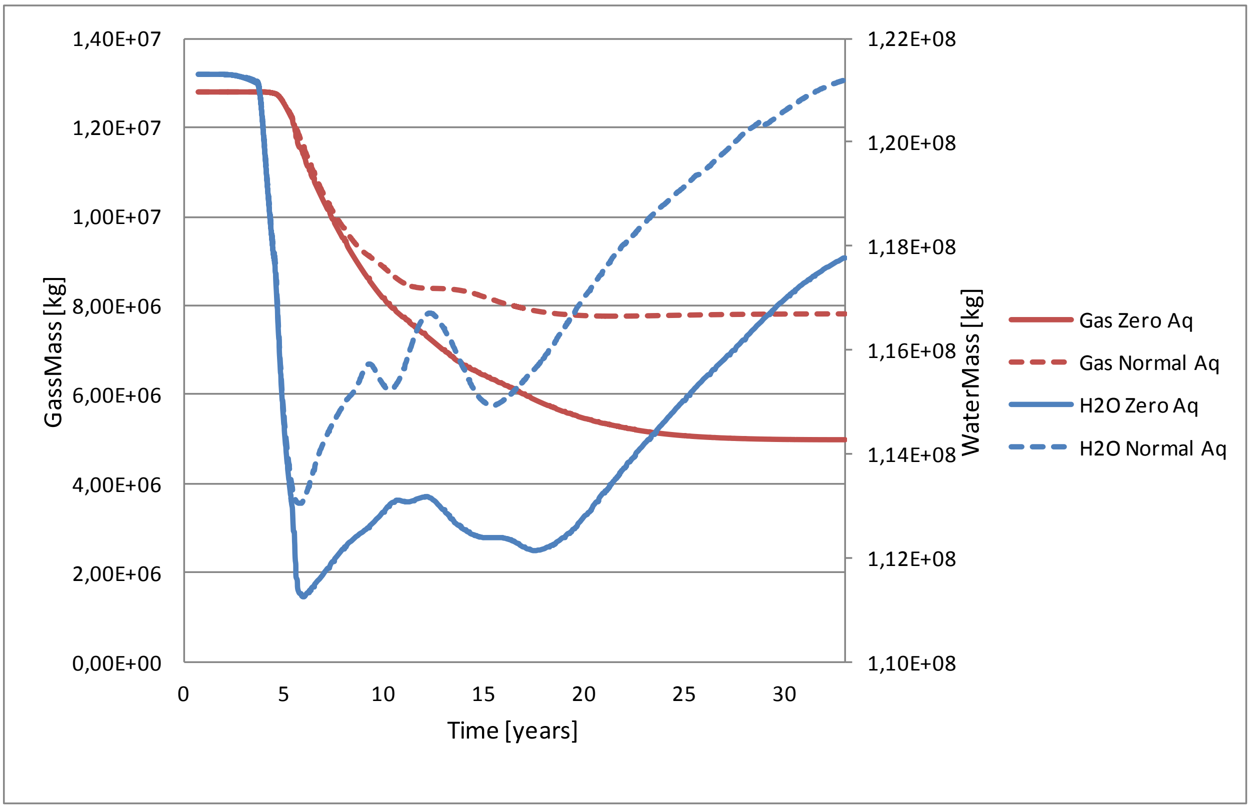

Figure 65 Accumulation of gas and water versus time for grid-block 13.23.6

Figure 66 shows gas-saturation maps for the reservoir in 2040. Difference in water-influx from the South towards the saddle can be seen for the three scenarios. It is clear that for the zero-aquifer case the water-influx is small compared to the strong aquifer case. Cyan equals 100% water, and blue area is where water has imbibed, bringing the gas-saturation down to residual. In the south water break-through is limiting the recovery of residual gas.

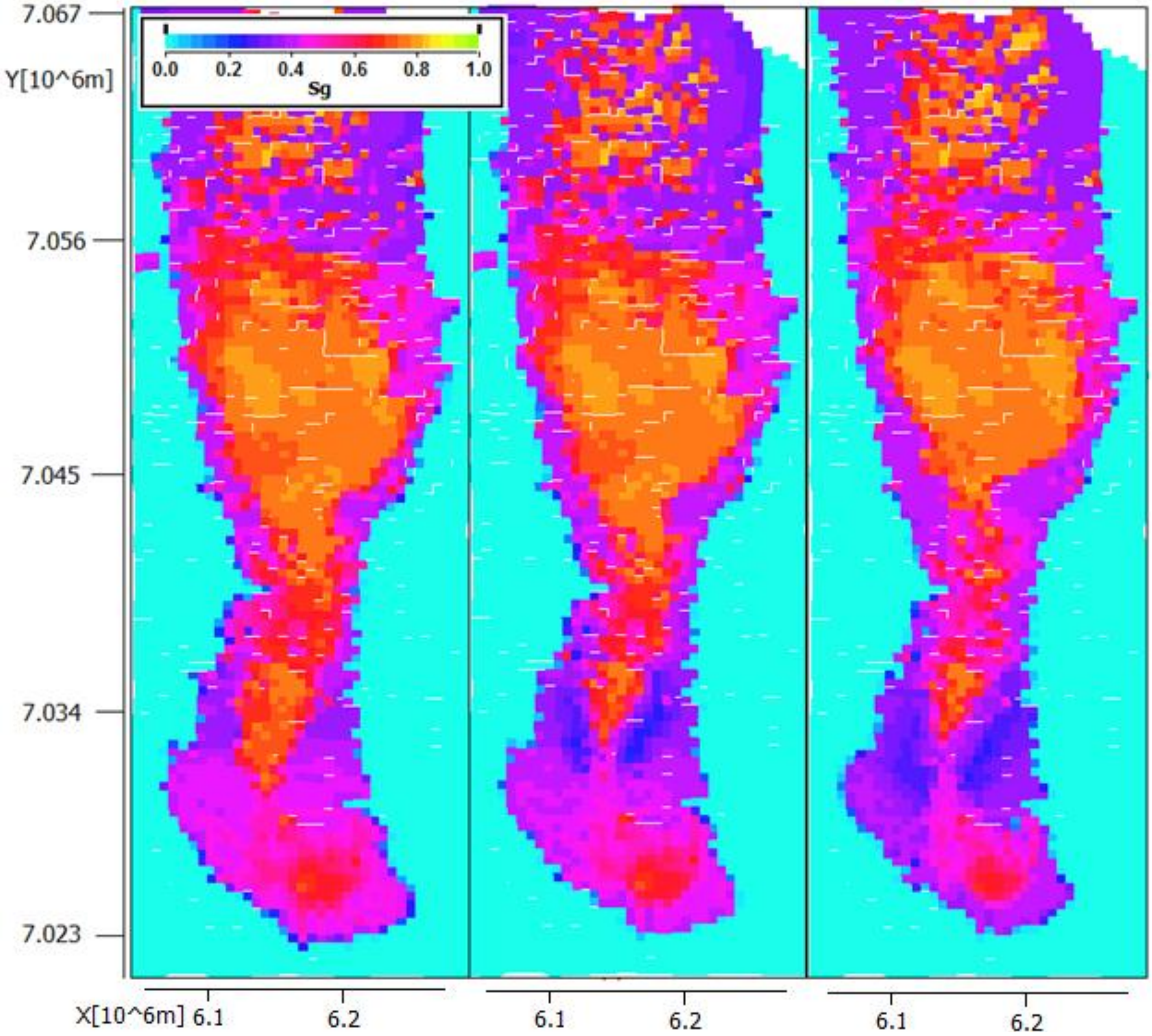
7.067
Y[10^6m]
7.056
7.045
7.034
7.023
0.0
0.2
0.4
0.6
0.8
1.0
Sg
X[10^6m] 6.1
6.2
6.1
6.2
6.1
6.2

Figure 66 Gas-saturation@2040; left figure no analytical aquifer, mid figure normal, right side strong aquifer

7.3 Impact of Sgr on water-breakthrough

Water break through is controlled by aquifer size, permeability, gas production rate and residual gas saturation. For constant krw, higher residual gas saturation results in earlier breakthrough. However, higher residual gas saturation results in less available pore-volume for the water to flow, hence lower krw. The following chapter addresses the sensitivity of Sgr on water-breakthrough in the South when Sgr and krw are treated independently and when they are treated as a function of each other.

7.3.1 Sgr and krw treated independently

The relative permeability curves for the gas and water phase when Sgr and krw are treated independently are illustrated in Figure 67. Notice that the end point relative permeability for water is the same in all scenarios. This is not necessarily physically correct, as higher trapped gas saturation causes lower relative permeability for water.

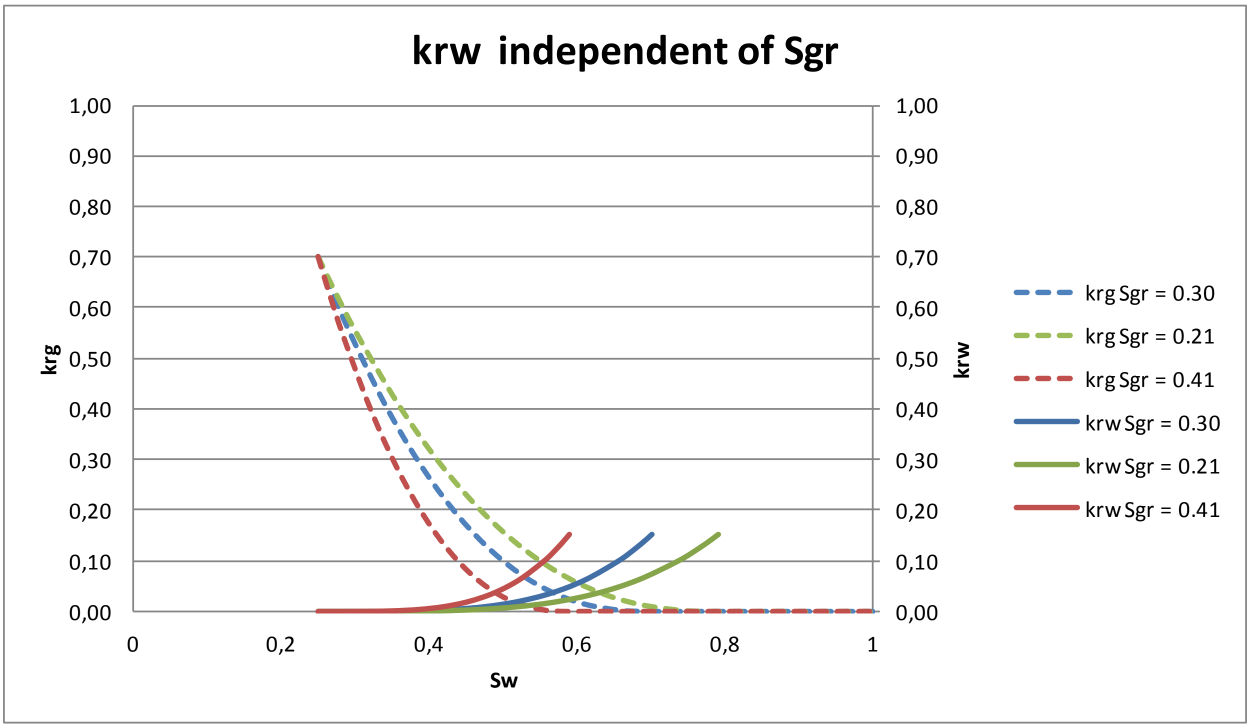

Figure 67 Imbibition relative permeability for constant krw, Sgr = 0.21→0.41

Figure 70 shows the abandonment pressure for the different Sgr values in Figure 67. Figure 68 shows the recovery factors for segment 3-5 for the different Sgr values. When Sgr is increasing, see Figure 67, the aquifer is flowing faster (rapid increase in krw), reaching the producers in the south earlier. Hence the abandonment pressure in the South is increasing, limiting expansion and recovery of residual gas. Only 13% of the residual gas in segment 5 is recovered when Sgr= 0.41 compared to 44% when Sgr is 0.21, see Figure 68.

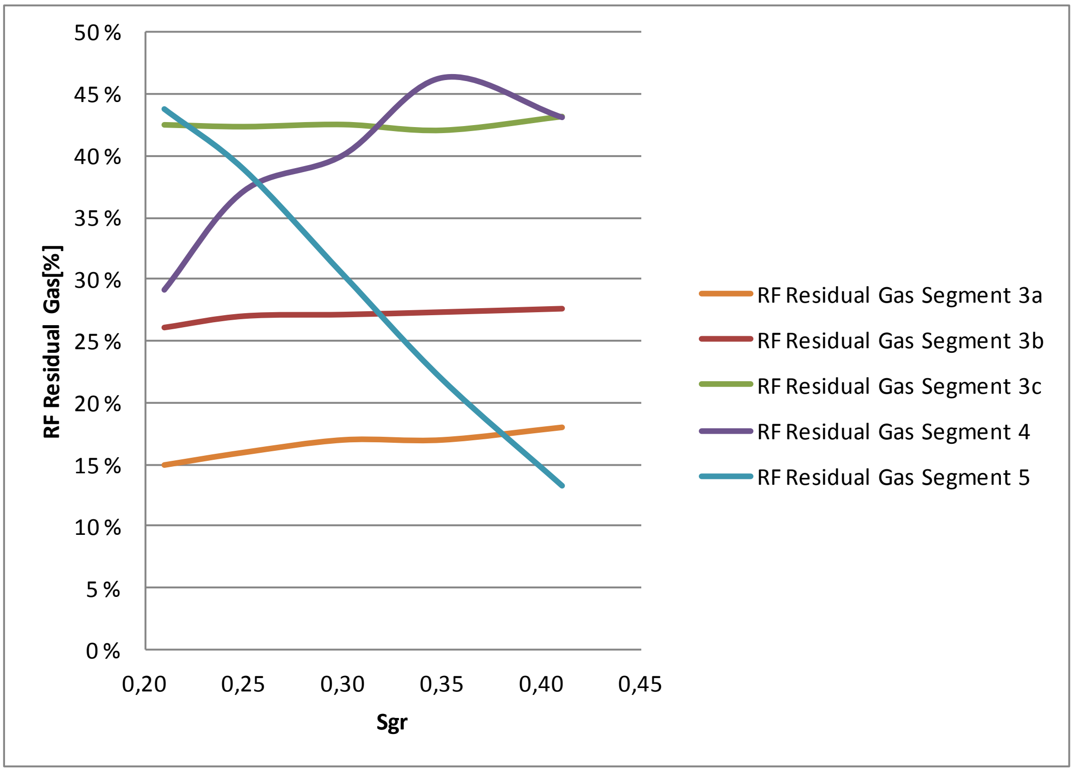

Figure 68 Recovery factor of residual gas from segment 3-5 versus residual gas versus Sgr for segment 3, 4 and 5, krw independent of Sgr

Figure 70 shows that the abandonment pressure in the other segments is less sensitive to Sgr (since there is no water-breakthrough) and the recovery- factors from residual gas in these segments (segment 1-3) are more or less constant. Segment 1 and 2 is excluded in Figure 68 due to limited recovery. From Figure 68 it seems like the recovery factors from segment 4 is increasing as Sgr increases. This has been investigated and the reason why the recovery factor increases is not 100% clear yet. A possible reason is that since capillary pressure hysteresis is ignored, there will be a different distribution of residual gas in the reservoir as Sgr increases. For higher Sgr there will be a thicker transition zone since the same capillary pressure curve is used, see Figure 69. Since there is a greater amount of neighbouring grid-blocks containing residual gas when Sgr is high, in both vertical and horizontal direction, the residual gas may reconnect earlier.

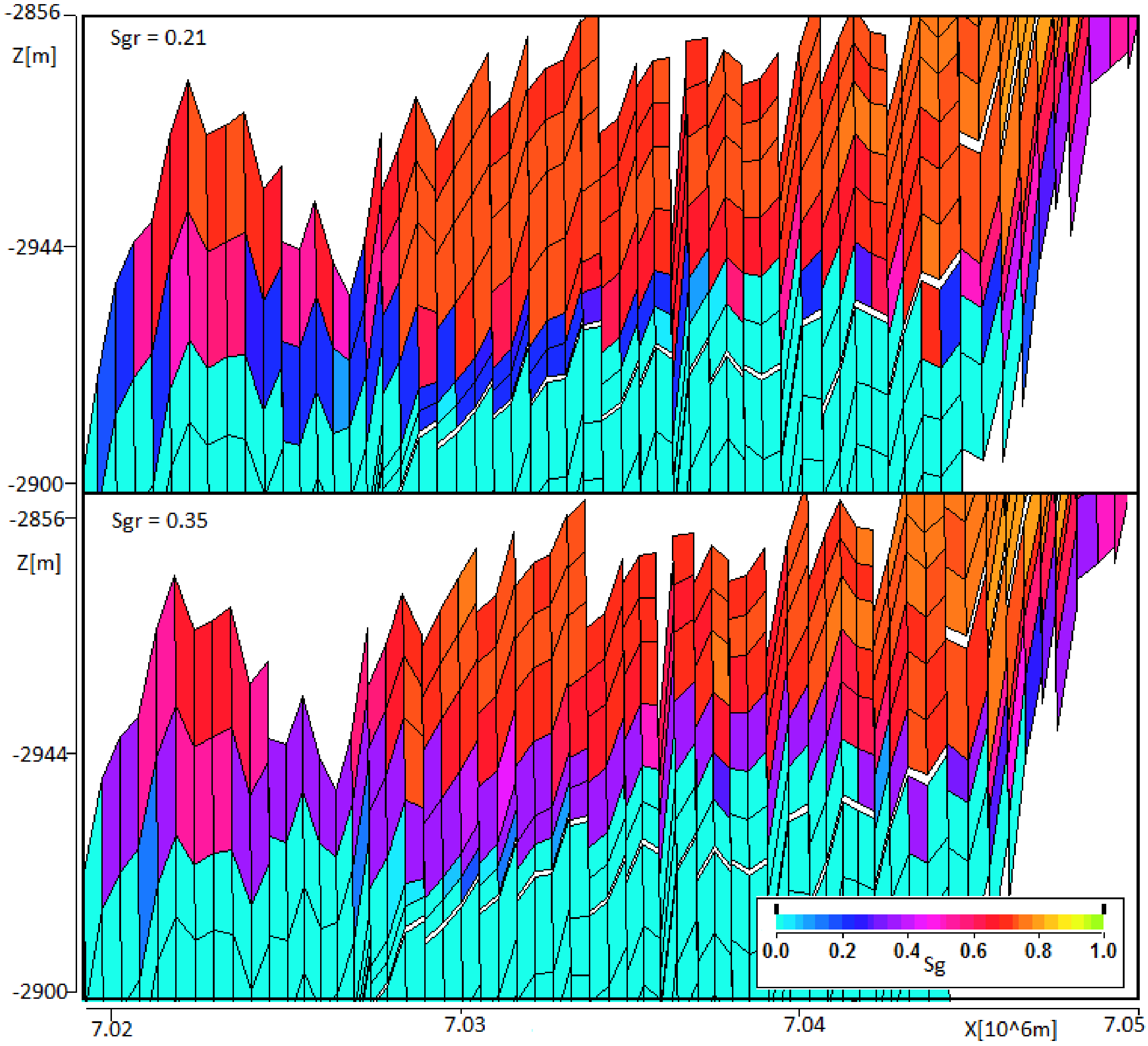

Figure 69 Sg @2007 in segment 4 and 5 (transition zone) for 2 different Sgr cases

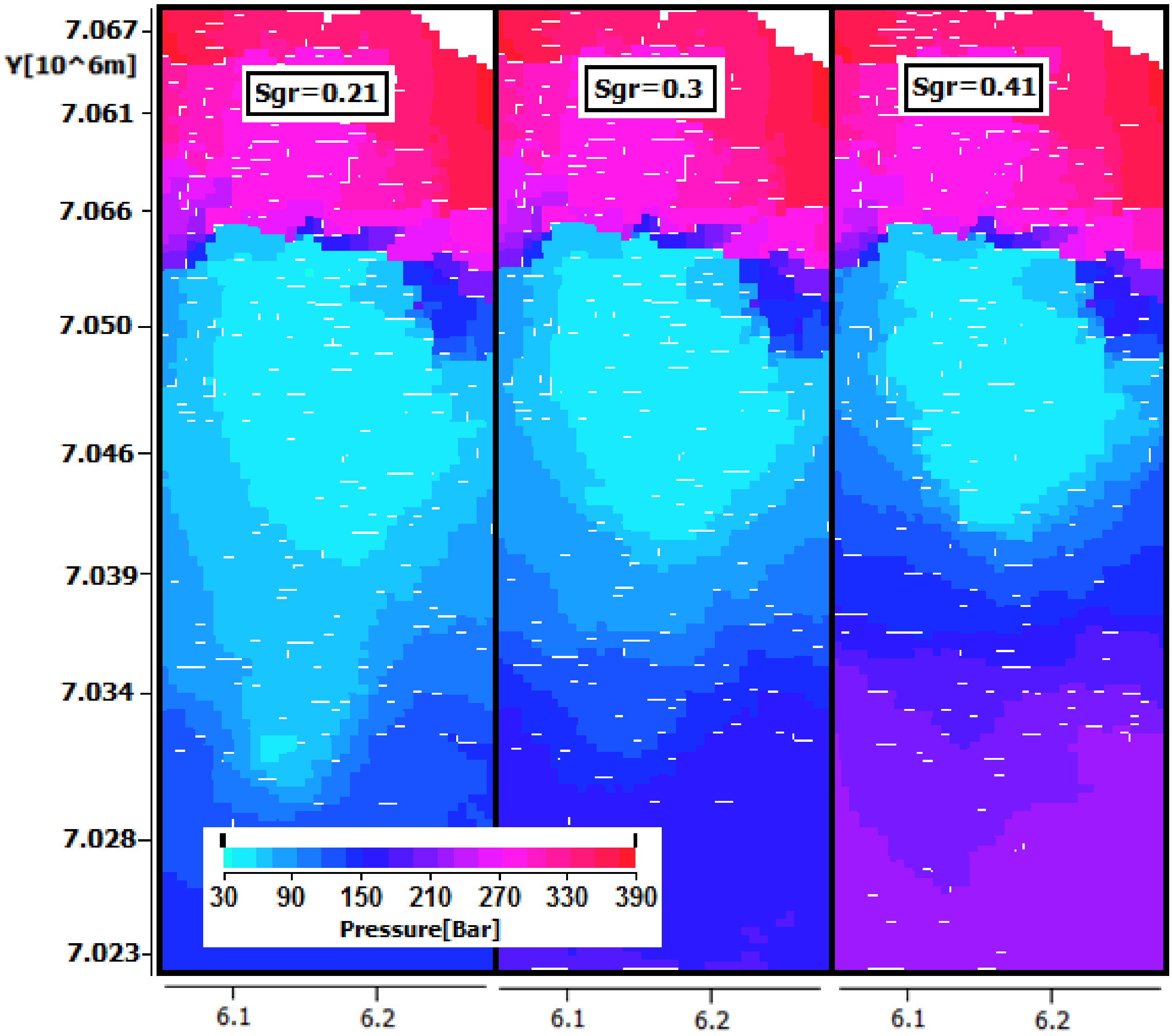

Figure 70 Abandonment pressure for the 3 different Sgr-cases (0.21→0.41) independent krw

Figure 71 provides remaining GIP/km2 in 2040. Due to higher abandonment pressure more gas is abandoned in the reservoir as Sgr increases.

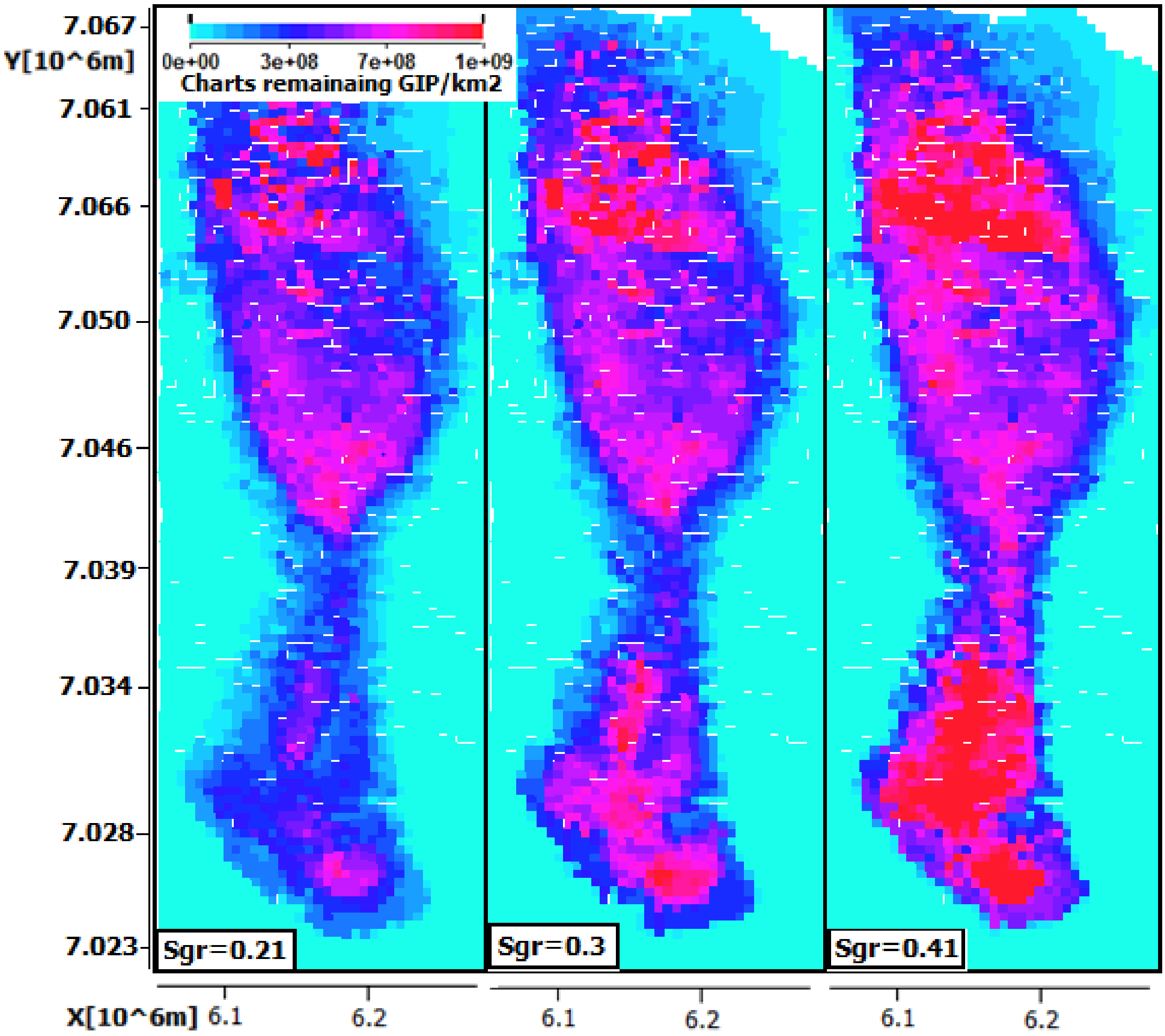
7.067
Y[10^6m]
7.061
7.066
7.050
7.046
7.039
7.034
7.028
7.023
0e+00
3e+08
7e+08
1e+09
Charts remainaing GIP/km2
Sgr=0.21
Sgr=0.3
Sgr=0.41
X[10^6m]
6.1
6.2
6.1
6.2
6.1
6.2

Figure 71 Charts remaining GIP/km2 @2040 for the 3 different cases (Sgr 0.21→0.41) krw independent

7.3.2 Krw treated dependent on Sgr

The relative permeability curves for the gas and water phase when krw is treated as a function of Sgr are provided in Figure 72. This relative permeability model provides a dependency between Sgr and krw, and the values are based on recent SCAL performed on plug material from well 6305/7-D-7H[18] as described in Chapter 4.1. Figure 73 shows the measured krw values from the latest and from previous lab experiments. Based on the latest data set (green in Figure 73 a relationship can be inferred between Sgr and krw; where a higher Sgr coincides with a lower krw. The Corey correlations of the relative permeability of water is modified in order to line up the end point relative permeabilities for water on the same curve for all Sgr. Sgr=0.3(krw=0.07) and Nw=4 is used as a reference (see chapter 4.1).

Figure 74 and Figure 75 shows water-breakthrough in 6305/7-D3 and 6305/7-D2 for the two different relative permeability models. Water-breakthrough is not that sensitive to Sgr when krw is dependent on Sgr as for the other model, when krw is constant.

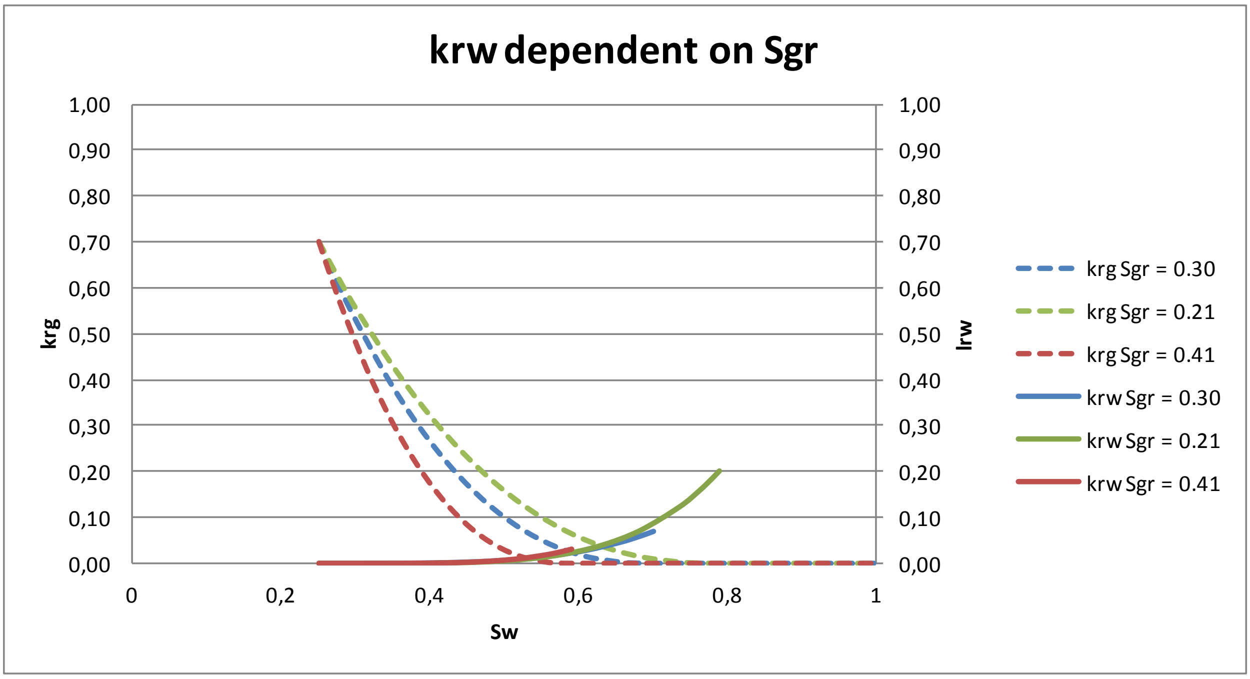

Figure 72 Imbibition relative permeability for dependent krw, Sgr = 0.21→0.41

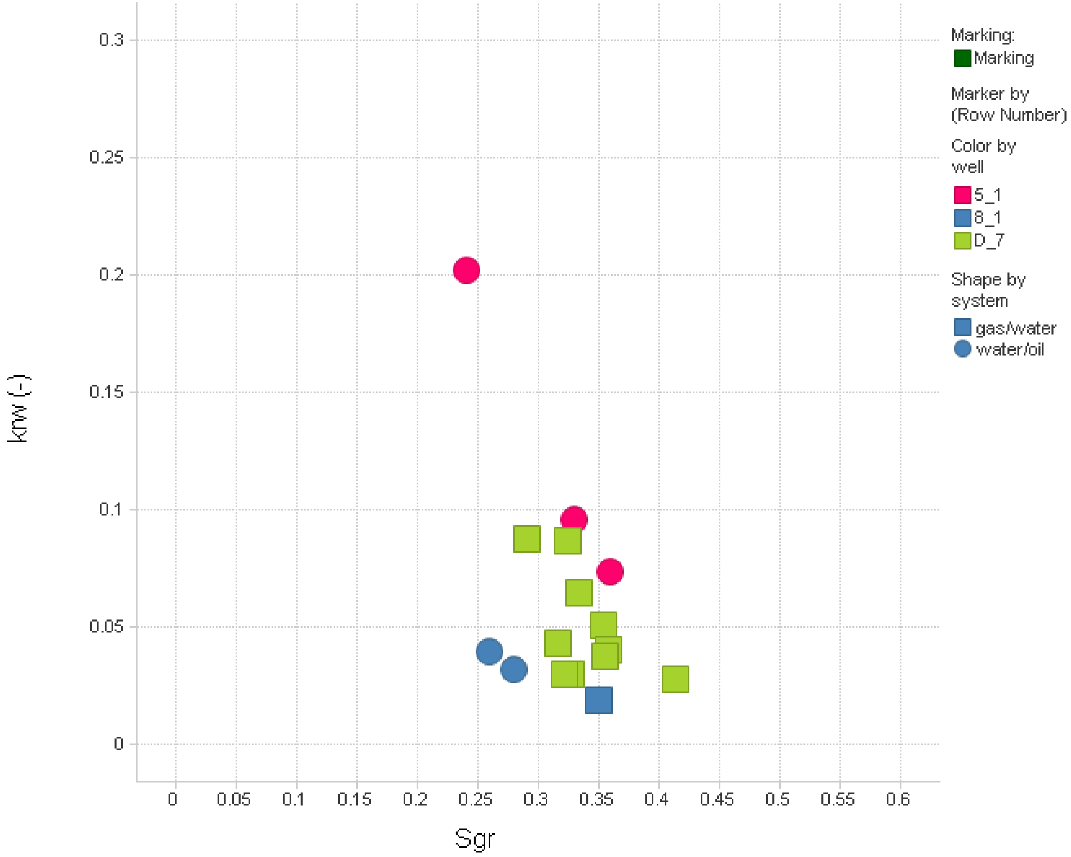

Figure 73 Water relative permeability end point, green dots from recent SCAL on D7.

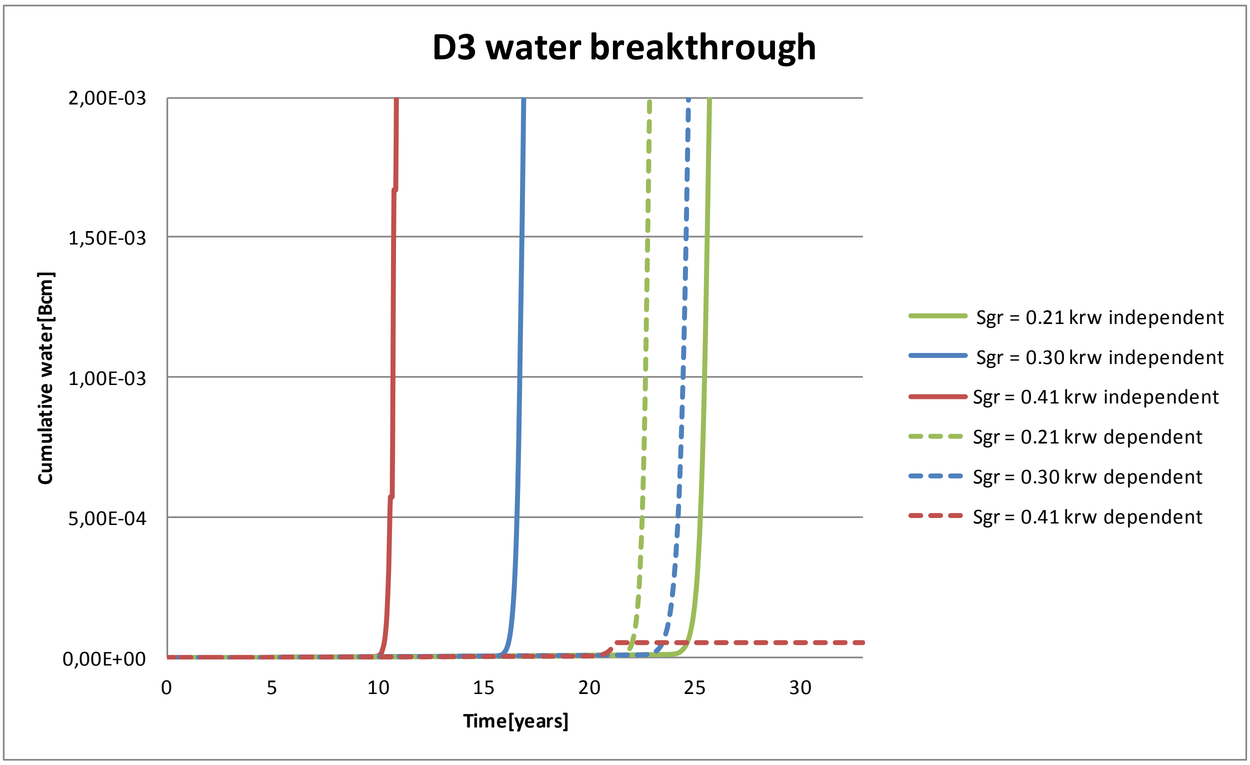

Figure 74 Water-breakthrough in 6305/7-D3 for the two models in chapter 7.3.1 and 7.3.2

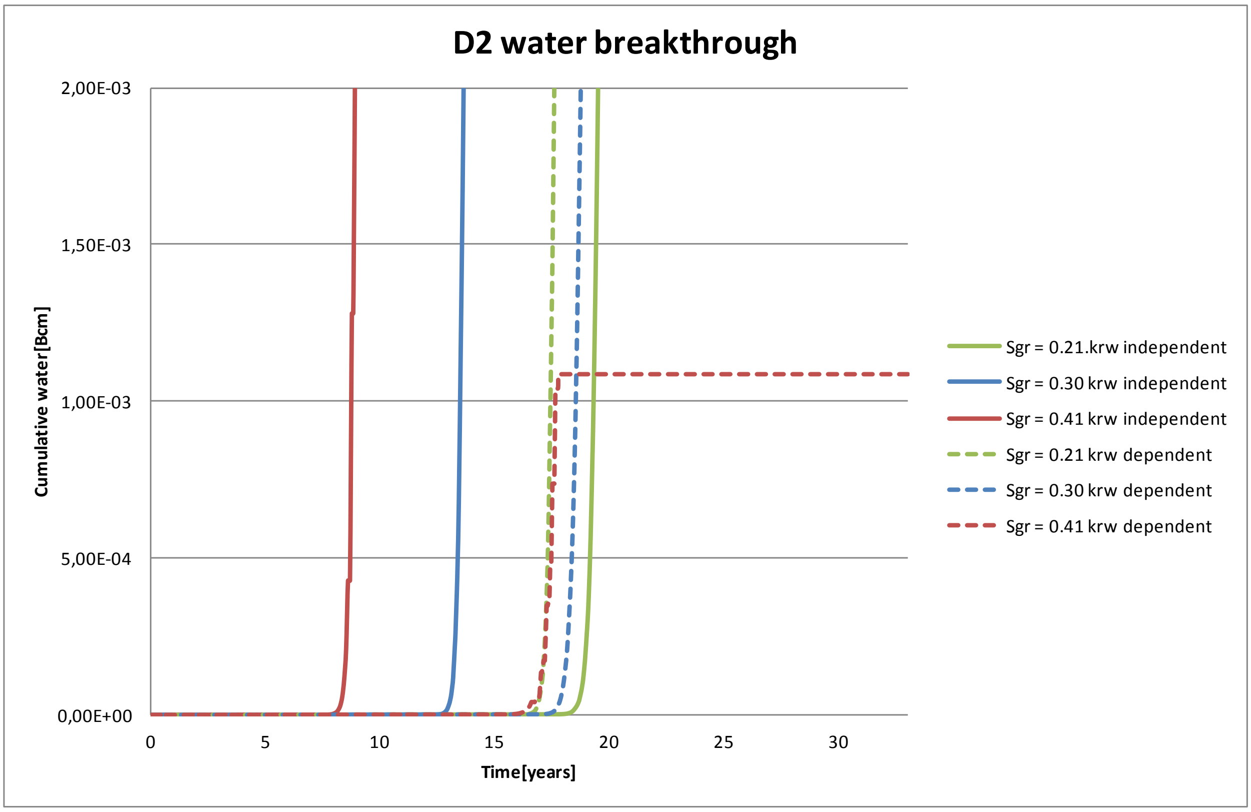

Figure 75 Water-breakthrough in 6305/7-D2 for the two models in chapter 7.3.1 and 7.3.2

When krw is independent of Sgr, the early shut-in of the wells when Sgr increases is the main reason for lower recovery of residual gas in segment 5. When krw is treated dependent of Sgr krw will decrease as Sgr increases, see Figure 72. When krw is lowered break-through occurs later, hence the abandonment pressures decreases and recovery of residual gas increases; see Figure 76 and Figure 77.

Since low residual gas saturation implies more pore-volume available for water to flow, krw is increased for Sgr=0.21 in the relative permeability model in Figure 72. Therefore the water-breakthrough will occur earlier than when krw is kept constant, hence recovery of residual gas decreases, see Figure 77.

Figure 78 and Figure 79 displays maps of abandonment pressure and remaining GIP/km2 for the relative permeability model in Figure 72. It is clear that abandonment pressure and remaining GIP at time of abandonment is lower compared to the case where krw is independent of Sgr as summarized Figure 70 and Figure 71.

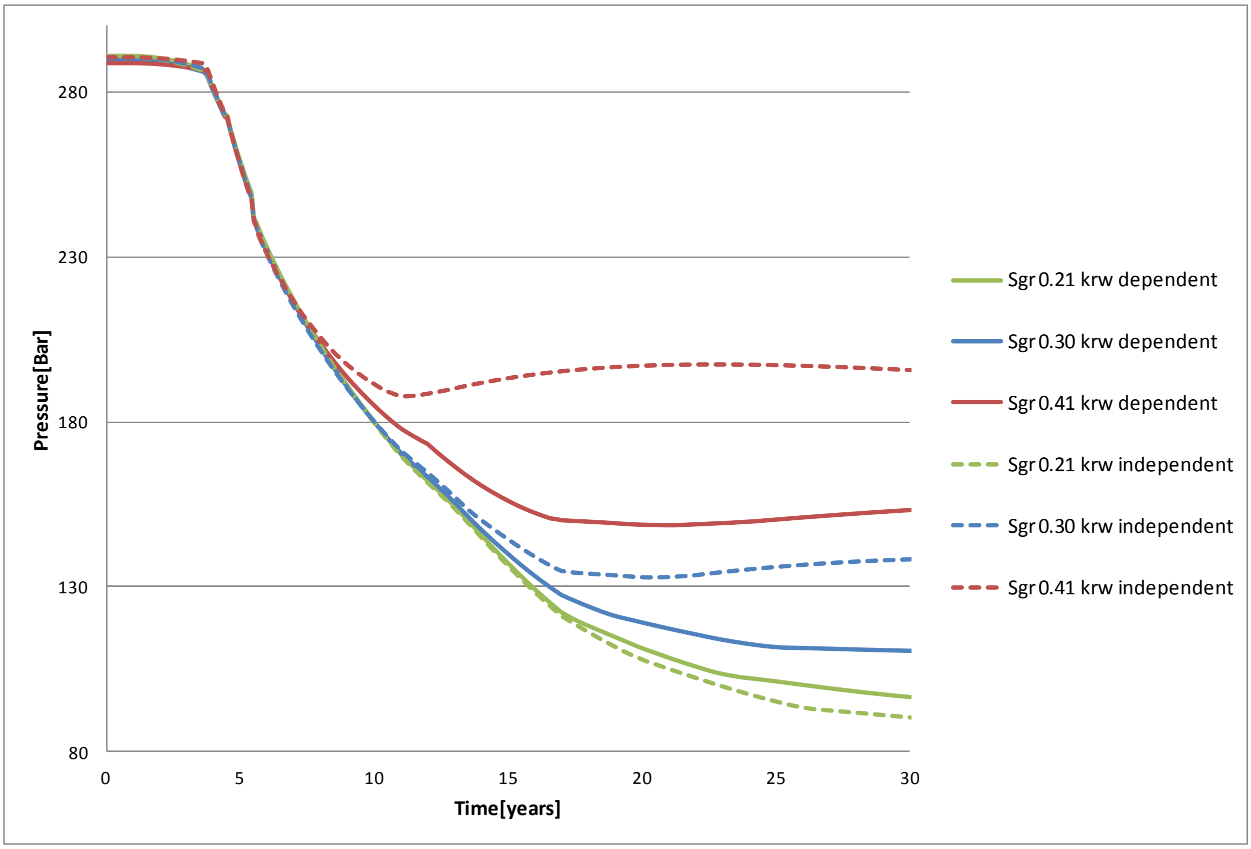

Figure 76 Average gas pressure segment 5 for the two relative permeability models in chapter 7.3.1 and 7.3.2

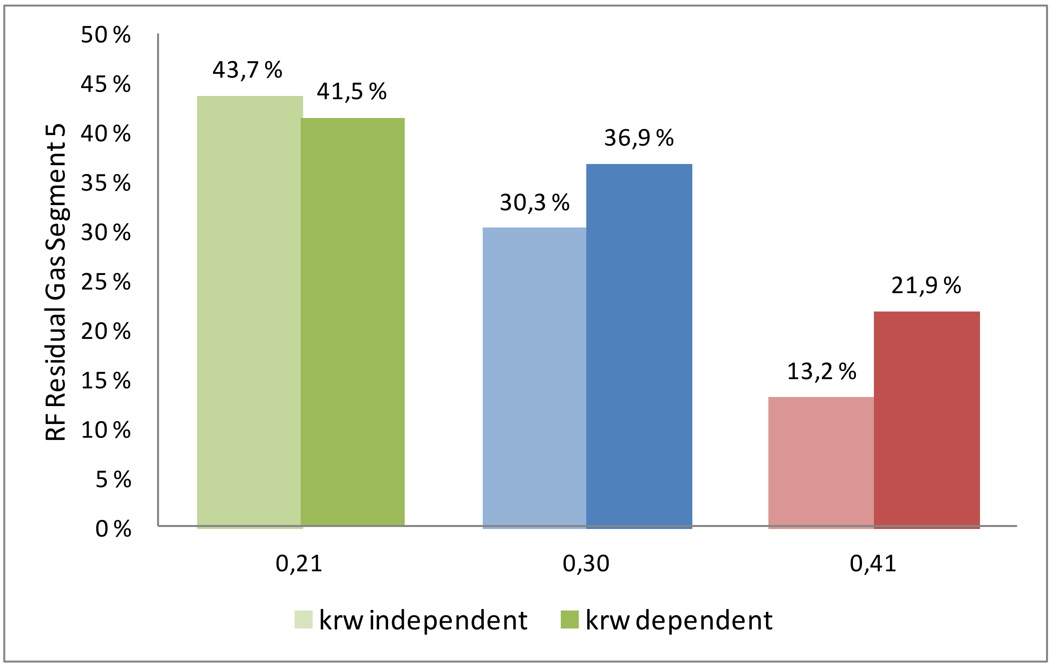

Figure 77 RF residual gas @2040 in segment 5 when Sgr is independent (weak color)/dependent (strong color) of Sgr

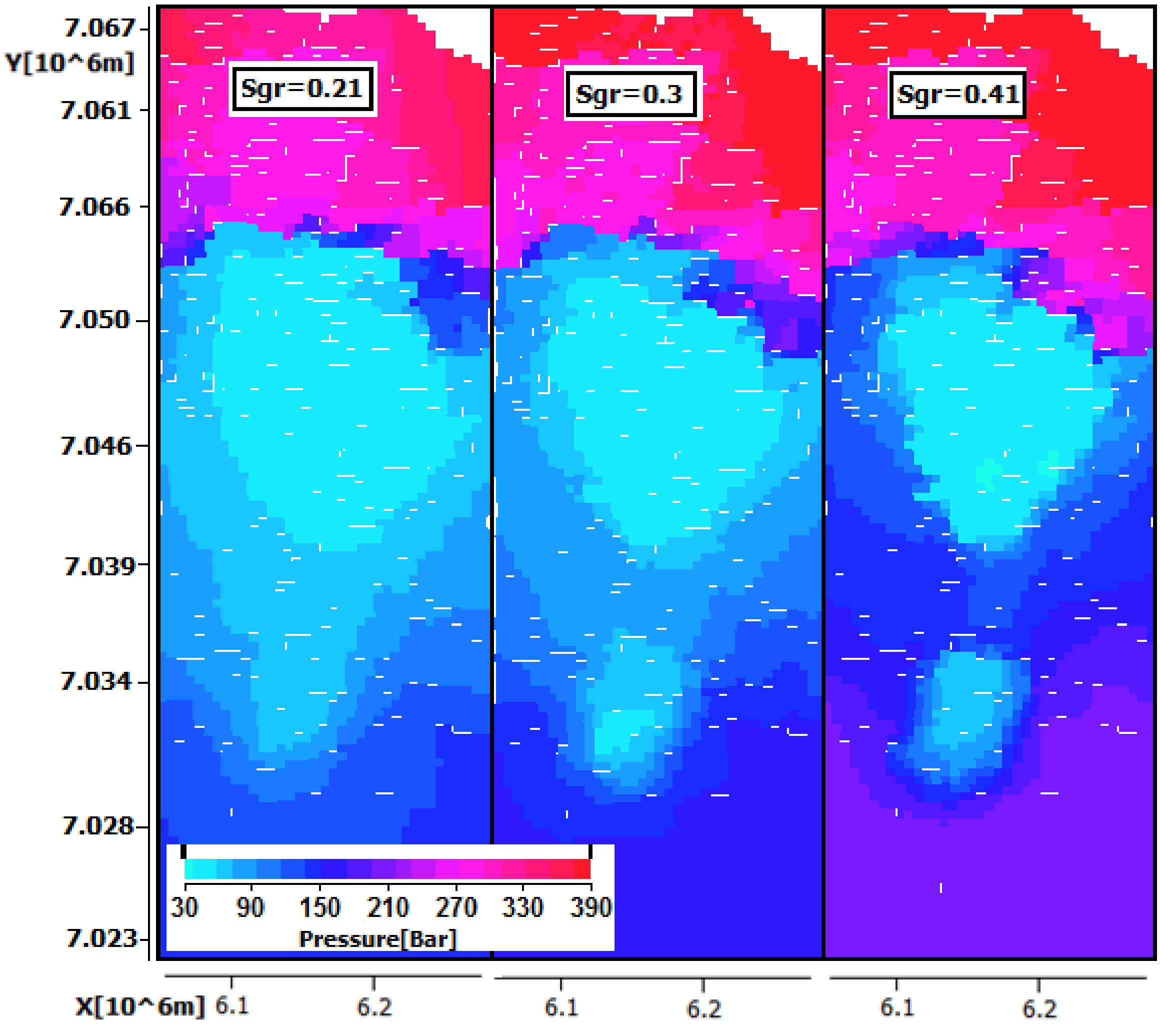
7.067
Y[10^6m]
7.061
7.066
7.050
7.046
7.039
7.034
7.028
7.023
Sgr=0.21
Sgr=0.3
Sgr=0.41
30
90
150
210
270
330
390
Pressure[Bar]
X[10^6m]
6.1
6.2
6.1
6.2
6.1
6.2

Figure 78 Abandonment pressure @2040 for the 3 different cases (Sgr 0.21→0.41) dependent on krw

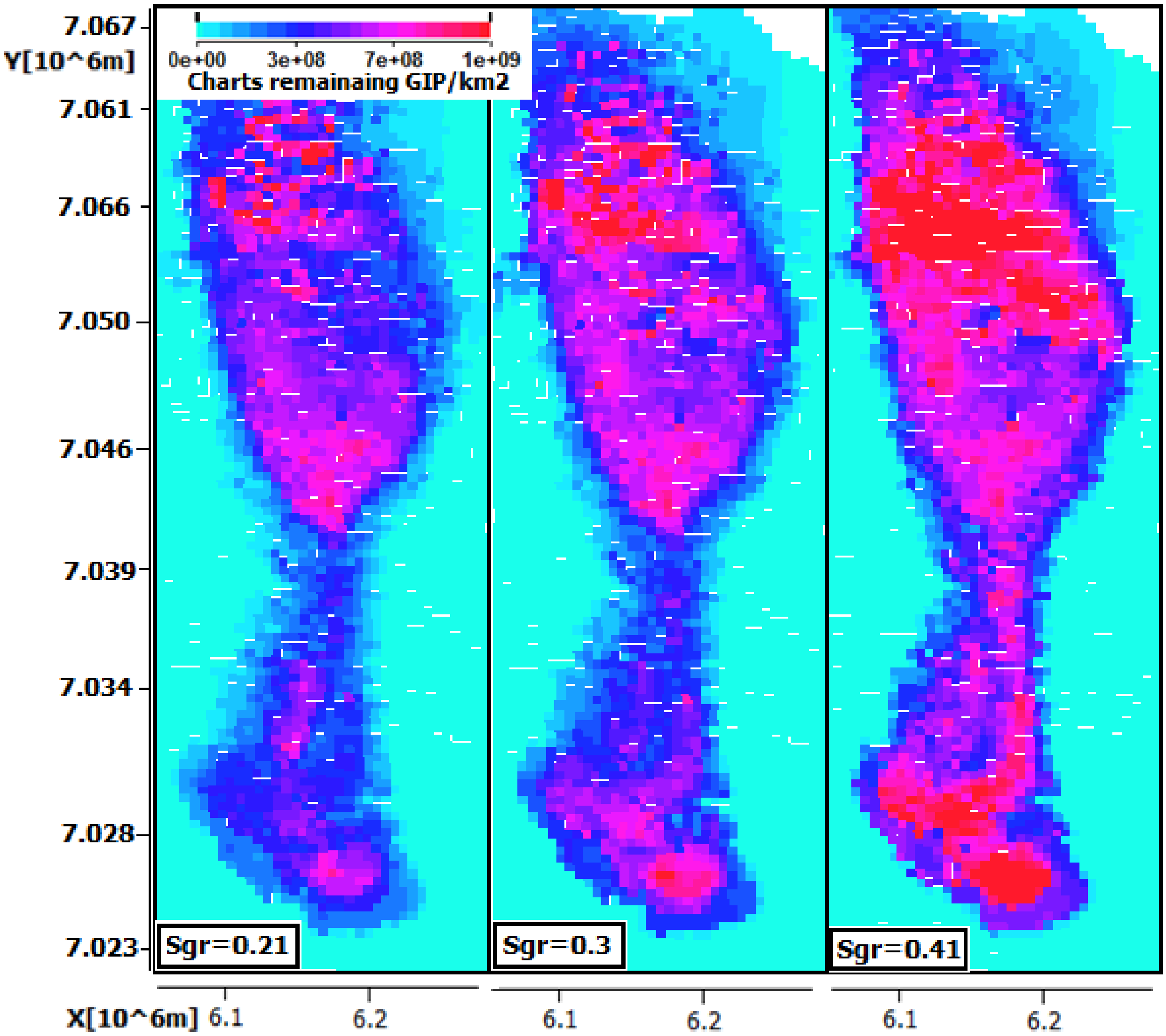
7.067
Y[10^6m]
7.061
7.066
7.050
7.046
7.039
7.034
7.028
7.023
0e+00
3e+08
7e+08
1e+09
Charts remainaing GIP/km2
Sgr=0.21
Sgr=0.3
Sgr=0.41
X[10^6m]
6.1
6.2
6.1
6.2
6.1
6.2

Figure 79 Charts remaining GIP/km2 @2040 for the 3 different cases (Sgr 0.21→0.41) dependent on krw

8. Conclusions

8.1 Literature

- Whenever the fluid saturations in the reservoir undergo a cyclic process, relative permeabilities display hysteresis effects. The main mechanism for hysteresis is trapping of the non-wetting phase during an imbibition process, as a function of the initial saturation.

- The residual gas saturation is dependent on rock type and reservoir quality. Residual gas saturations decrease as sandstones becomes cleaner, better sorted, and less cemented. For a given rock-type, higher initial gas saturation results in higher residual gas saturation.

- Most literature indicates that residual gas requires approximately 5% increase of gas saturation units to reach critical gas saturation (CGS) prior to gas remobilization and production, and that use of conventional (gas-injection) relative permeability in residual gas zones may result in over-prediction of gas-recovery.

- The magnitude of differences between gas injection and gas-expansion secondary drainage relative permeabilities is dependent on rock-type. Some results in the literature support the view that differences are larger for more permeable rocks.

- It is reported that the critical gas saturation in gas-reservoirs is independent on depletion rate, although this is not supported by data. In depressurization experiments with live oil, the nucleation sites are activated below the bubble pressure and their number and spreading is directly dependent on the depletion rate. In the process considered in this work, they are already existing and active sites during blowdown of trapped gas, therefore the kinetics of the gas growth should not be dependent on the manner the pressure is decreased (depletion rate).

8.2 Simulation

- Total residual gas volume in 2007 is 80±30 Bcm gas depending on the residual gas saturation. Depending on scenario 15±6 Bcm of the residual gas is recovered in 2040, and the recovery factor of residual gas is 15±5%.

- The total residual gas volume after initialization of the hydrodynamic aquifer with scanning curves between the bounding imbibition and drainage curve is approximately 20% lower compared to initialization using the bounding imbibition curve only.

- A critical gas saturation 5% higher than the residual gas saturation, reduces recovery from the residual gas zones with 2%, independent of the Sgr value.

- Pressure depletion and gas-expansion is driving the remobilization of trapped gas. Future development plans will increase recovery of residual gas as the pressure will be further depleted.

- Earlier breakthrough of water in the south with a stronger acting aquifer case results in earlier shut-in of the wells, hence higher abandonment pressure and 12% lower recovery of residual gas in segment 5.

- Water-breakthrough and recovery of residual gas in Segment 5 highly depends on Sgr when krw is chosen independent of Sgr. However, the latest SCAL measurements suggest that there is a correlation between Sgr and krw. The latter implies a lower dependency of Sgr on residual gas recovery as krw will be lower for higher Sgr values.

- The recovery factor of residual gas is 9% higher for krg = 1.36 compared to krg = 0.5. When the Corey-exponent to the gas relative permeability is increased for the secondary drainage cycle from the measured bounding imbibition value of 2.4 to 4 the recovery of residual gas decreases with 2.5%.

9. Recommendations

9.1 Laboratory

- Perform secondary drainage relative permeability experiments to validate assumptions made in this work.

9.2 Simulation

- Implement Sgr values dependent on initial gas saturation and rock type in the reservoir model.

- Implement hysteresis also in the capillary pressure curves.

- Include residual gas volumes in the asset reservoir model. When the residual gas value is increased the total GIIP has to be increased to obtain the same conditions (in order to get the same history match on production and be able to match the pressures).

- Investigate a possible water pump off solution to lower pressure in the residual gas area of segment 1 and 2 in order to enhance recovery of both residual and mobile gas from these segments.

- Further study the behavior of the residual gas in segment 4, attempting to explain better why the recovery factor of the residual gas in this segment develops in a different manner than segment 3 as the residual gas saturation increases.

10. Nomenclature

Sgr = Residual Gas Saturation
Sgi = Initial Gas Saturation
Swc = Connate Water Saturation
CGS = Critical Gas Saturation
SCAL = Special Core Analysis
MoReS = Modular Reservoir Simulation, Shell reservoir simulation tool
Krg = Relative Permeability Gas
Krw = Relative Permeability Water
HDA = Hydrodynamic Aquifer
DHI = Direct Hydrocarbon Indicator
RF = Recovery Factor
Nw = The Corey correlations of the relative permeability of water
Ng = The Corey correlations of the relative permeability of gas
TD = True Depth
TVSS = True Vertical Depth Subsea
FWL = Free Water Level

11. References

1. Norske Hydro, 2003, Reservoir Engineering Report, Ormen Lange Project
2. A.E. Zweers, F. van Poelgeest and K.Wit, May 1991, Approach for theoretical modeling of the development of critical gas saturation during pressure decline.
3. Drummond, Marathon Oil UK Ltd.; T. Fishlock, P. Naylor, AEA Technology; B. Rothkopf, iReservoir.com , October 2001, Relative Permeability Measurements for Post-Waterflood Depressurization of the Miller Field, North Sea.
4. E.M. Braun, SPE, and R.F. Holland, Exxon Production Research Co, 1995, Relative Permeability Hysteresis: Laboraory Measurements and a Conceptual Model, SPE 28615
5. KILLOUGH, J.E., EXXON PRODUCTION RESEARCH CO., February 1976, Reservoir Simulation with History-Dependent Saturation Functions.
6. Carlson F.M 1981. Simulation of Relative Permeability Hysteresis to the Nonwetting Phase. Paper SPE 10157 presented at the Annual Technical Conference and Exhibition, San Antonio, Texas, 5-7 October.
7. A. Cable et al. 2004. Mobilization of Trapped Gas from Below the Gas-Water Contact, Paper SCA 2004-29 presented at the Society of Core Analysts Symposium, Abu Dhabi, 5-9 October.
8. P.Egermann, T.Schaaf, and B.Bréfort, 2009, A modified Hysteresis Relative Permeability Including a Gas Remobilzation Threshold for Better Production Forecasts of Gas Storages.
9. A/S Norske Shell E&P Ormen Lange, 2011, Ormen Lange Field Hydrodynamic Simulation Modeling Study.
10. C. R. Holmgren and R. A. Morse, Stanolind Oil and Gas Co., 1951, Effect of free gas saturation on oil recovery by water flooding.
11. J.R. Kyte, R.J. Stanclift Jr., S.C. Stephan Jr., and L.A. Rapoport, The Carter Oil Co., 1956, Mechanism of waterflooding in the presence of free gas.
12. KILLOUGH, J.E., EXXON PRODUCTION RESEARCH CO., February 1976, Reservoir Simulation with History-Dependent Saturation Functions.
13. R.J. Lenhard and M. Oostrom, January 1998, A parametric model for predicting relativepermeability-saturation-capillary pressure relationships of oil-water systems in porous media with mixed wettability.
14. Norske Hydro, 2003, Ormen Lange Project , Reservoir Engineering Report.
15. KILLOUGH, J.E., EXXON PRODUCTION RESEARCH CO., February 1976, Reservoir Simulation with History-Dependent Saturation Functions.
16. R.J. Lenhard and M. Oostrom, January 1998, A parametric model for predicting relativepermeability-saturation-capillary pressure relationships of oil-water systems in porous media with mixed wettability.
17. A/S Norske Shell, October 2010, 2010 Ormen Lange Field Development Review report 37-1E-NS-K15-00014.
18. Weatherford laboratories, January 2012, SCAL Ormen Lange, Well: 6305/7-D-7 H
19. Fishlock, T.P., U.K. Atomic Energy Authority; Smith, R.A., U.K. Atomic Energy Authority; Soper, B.M., U.K. Atomic Energy Authority; Wood, R.W., U.K. Atomic Energy Authority, May 1998, Experimental Studies on the Waterflood Residual Gas Saturation and Its Production by Blowdown.
20. A.N. Nyre, CIPR and IFT/University of Bergen; S.R. McDougall, Heriot-Watt University; and A. Skauge, CIPR/University of Bergen, 2008, Effect of Depressurization on Trapped Saturations and Fluid Flow Functions
21. E. Undeland, Residual Gas Mobility, December 2011.
22. M.H. Holtz, The University of Texas, Austin, 30 April-2 May 2002, Residual Gas Saturation to Aquifer Influx: A Calculation Method for 3-D Computer Reservoir Model Construction

23. G.D. Henderson, A.Danesh, J.M.Peden, August 1991, “An experimental investigation of waterflooding of gas condensate reservoirs and their subsequent blowdown”.
24. A/S Norske Shell EP Ormen Lange, Dec 2011, 2011 Ormen Lange Field Development Review
25. Norske Hydro, October 2003, Ormen Lange Plan for Development and Operation, Report nr. 37-00-NH-X01-00001
26. S. Price, M. Grecula, M. Boyaferrero, U. Klein-Helmkamp, G. de Bruijn, A/S Norske Shell, 2011, 2011 Ormen Lange GIIP Determination Report, Note-for-File. EP201104200599
27. S.Price, M. Boya Ferrero, A/S Norske Shell, 2010, Ormen Lange Hydrodynamic Fluid-Fill Model - Isopotential mapping, Note-for-File. EP201102200473
28. S. Price, A/S Norske Shell, 2011, Ormen Lange Hydrodynamic Fluid-Fill Model - Isopotential mapping post-6305/4-2 update, Note-for-File. EP201102200474.
29. F. Riis, A. Solltvedt, NGF, Geological Society of Norway, No 4, 2010, Pore pressure regimes of the Norwegian continental shelf: Can information from pressure data be better integrated in reservoir models?
30. G.L. Chierici, G.M. Ciucci, G. Long, 1963, Experimental research on gas saturation behind the water front in gas reservoir subjected to water drive.
31. G. Løvoll, Y. Méheust, K. J. Måløy, E. Aker, J. Schmittbuhl, 2005, Competition of gravity, capillary and viscous forces during drainage in a two-dimensional porous medium, a pore scale study.
32. Weatherford Laboratories AS, January 2012, Final Report SCAL Ormen Lange Well: 6305/7-D-7-H